UNIVERSITA' DEGLI STUDI DI PADOVA

SEDE AMMINISTRATIVA: UNIVERSITA’ DEGLI STUDI DI PADOVA
DIPARTIMENTO DI SCIENZE FARMACEUTICHE

SCUOLA DI DOTTORATO DI RICERCA IN SCIENZE MOLECOLARI
INDIRIZZO IN SCIENZE FARMACEUTICHE
XX CICLO

NEW PENTA- AND HEXACYCLIC DERIVATIVES OF QUINOLIZINIUM ION: DNA-BINDING AND DNA-PHOTOCLEAVAGING PROPERTIES

Direttore della Scuola: Ch.mo Prof. Maurizio Casarin

Supervisore: Ch.mo Prof. Francesco Dall’Acqua

Dottoranda : Anita Faccio

31 GENNAIO 2008

Ai miei genitori

e a Massimo

INDEX

Abstract V

Riassunto IX

1. INTRODUCTION 1
    - 1.1 CANCER THERAPY 3
    - 1.2 INTERACTION WITH DNA 6
        - 1.2.1 Binding mode 7
        - 1.2.2 Groove binding 7
        - 1.2.3 Intercalation 8
    - 1.3 DNA 11
        - 1.3.1 B-form of DNA 12
        - 1.3.2 A-form of DNA 15
        - 1.3.3 Z-form of DNA 15
    - 1.4 ULTRAVIOLET RADIATION 17
        - 1.4.1 Photosensitized reactions 19
        - 1.4.2 Mechanism of photosensitized reactions 20
        - 1.4.3 Clinical application of phototherapy 22
    - 1.5 APOPTOSIS 24
        - 1.5.1 Morphological features of apoptosis 25
        - 1.5.2 Caspases are central initiators and executioners of apoptosis 27
        - 1.5.3 Mitochondria as central regulators of intrinsic apoptosis pathways 30
        - 1.5.4 Disease as consequence of dysregulated apoptosis 31
    - 1.6 CELL CYCLE 33
    - 1.7 TOPOISOMERASE I AND II 35
        - 1.7.1 Topoisomerase I 36
        - 1.7.2 Topoisomerase II 37

2. AIM OF THE PROJECT 41

3. DNA-BINDING PROPERTIES 47

3.1 COMPOUNDS 49

3.2 CIRCULAR DICHROISM SPECTROSCOPY 50

3.3 LINEAR DICHROISM SPECTROSCOPY 53

3.4 SPECTROPHOTOMETRIC TITRATIONS 56

3.5 SPECTROFLUORIMETRIC TITRATIONS 61

3.6 DNase I FOOTPRINTING 64

3.7 CONCLUSION ON DNA-BINDING PROPERTIES 68

4. DNA-PHOTOCLEAVAGING PROPERTIES 71

4.1 DNA PHOTOCLEAVAGE 73

4.2 DETERMINATION OF OXIDATIVE DAMAGES 76

4.3 DETERMINATION OF PROTECTION INDUCED BY SCAVENGERS 78

4.4 DNA-SEQUENCING 80

4.5 CONCLUSION ON DNA-PHOTOCLEAVAGING PROPERTIES 82

5. BIOLOGICAL ACTIVITY 83

5.1 CELLULAR CYTOTOXICITY 85

5.2 STABILITY OF THE COMPOUNDS AFTER UV-A IRRADIATION 89

5.3 CELLULAR PHOTOCYTOTOXICITY 92

5.3.1 Determination of the protection induced by scavengers 96

5.3.2 Evaluation of lipidic peroxidation 97

5.4 INTRACELLULAR LOCALIZATION 99

5.5 DETERMINATION OF MECHANISM OF CELLULAR DEATH 101
5.6 INVOLVEMENT OF MITOCHONDRIA IN CELLULAR DEATH 103
5.7 DETERMINATION OF CASPASE ACTIVATION 105
5.8 ANALYSIS OF CELL CYCLE 106
5.9 TOPOISOMERASE I AND II 109
  5.9.1 Inhibition of topoisomerase I 109
  5.9.2 Inhibition of topoisomerase II 112
5.10 CONCLUSION ON BIOLOGICAL ACTIVITY 113

6. EXPERIMENTAL PROCEDURES 115
6.1 MATERIALS 117
  6.1.1 Compounds 117
  6.1.2 Reagents and solvents 117
6.2 METHODS 119
  6.2.1 Circular dichroism spectroscopy 119
  6.2.2 Linear dichroism spectroscopy 120
  6.2.3 Spectrophotometric and spectrofluorimetric titrations 122
    6.2.3.1 Spectrophotometric titrations 122
    6.2.3.2 Spectrofluorimetric titrations 122
    6.2.3.3 Evaluation of binding constants (*K*) and binding site size (*n*) 123
  6.2.4 DNase I footprinting 124
    6.2.4.1 Preparation, radiolabeling and purification of DNA fragments 124
    6.2.4.2 DNase I footprinting and electrophoresis 124
  6.2.5 Irradiation procedures 125
  6.2.6 DNA-photocleavage 125
    6.2.6.1 Determination of oxidative damages 126
    6.2.6.2 Determination of protection induced by scavengers 127

6.2.7 DNA-sequencing 127
6.2.8 Cellular cytotoxicity and phototoxicity 128
    6.2.8.1 Determination of the protection induced by scavengers 129
6.2.9 Evaluation of lipidic peroxidation 130
6.2.10 Confocal microscopy 130
6.2.11 Flow cytometer 131
6.2.12 Determination of mechanism of cell death 133
    6.2.12.1 Externalization of phosphatidylserine (PS) 133
6.2.13 Involvement of mitochondria in cell death 134
    6.2.13.1 Determination of mitochondrial potential membrane 134
6.2.14 Determination of caspase activation 135
6.2.15 Analysis of cell cycle 135
6.2.16 Topoisomerase I and II assay 137
    6.2.16.1 Topoisomerase I relaxation and cleavable complex assay 137
    6.2.16.2 Topoisomerase II relaxation assay 137
    6.2.16.3 Topoisomerase II cleavable complex assay 138

7. REFERENCES 139

8. ACKNOWLEDGEMENTS 157

ABSTRACT

The discovery of new compounds with antitumoral activity has become one of the most important goals in medicinal chemistry. One interesting group of chemotherapeutic agents used in cancer therapy comprises molecules that interact with DNA. Research in this area has revealed a range of DNA recognizing molecules that act as antitumoral agents, including groove binders, alkylating and intercalator compounds. DNA intercalators are molecules that insert perpendicularly into DNA without forming covalent bonds. The only recognized force that maintain the stability of the DNA-intercalators complex, even more than DNA alone, are van der Waals, hydrogen bonding, hydrophobic, and/or charge transfer forces. These molecules have attracted particular attention due to their antitumoral activity. For example, a number of acridine and anthracycline derivatives are excellent DNA intercalators that are now on the market as chemotherapeutic agents. However, the clinical application of these and other compounds of the same class has encountered problems such as multidrug resistance (MDR), and secondary and /or collateral effects. These shortcoming have motivated the search of new compounds to be used either in place of, or in conjunction with, the existing molecules. Along these lines, especially important are the ligands capable of structure- or sequence-selective binding to nucleic acids, since such compounds may purposefully influence the biological functionality of genetic material in vivo.

The condensed poly(hetero)aromatic compounds are usually regarded as representative DNA intercalators, especially if they posses electron-deficiency or charged aromatic cores. However, only a few ligands are known that bind to the DNA by the intercalative mode exclusively. A vast number of ligands, which have an intercalating part endowed with a variety of substituents, bind to the DNA by a mixed mode, since the substituents occupy the DNA grooves upon binding. In view of the complexity of the ligand-DNA recognition process, a study with model compounds which posses only one DNA-binding mode is desired.

Measurement of the binding constant and biological activity of DNA-intercalator complexes in the 1970's and QSAR studies in the 1980's, leads to the conclusion that there should exist a relationship between cytotoxic activity and binding force. Otherwise, cytotoxicity is not only dependent on the ability to interact with DNA, since

there are many DNA intercalators that are incapable of working as cytotoxic agents. To be effective, a drug must first overcome many barriers, including metabolic pathways, and cytoplasmatic and nuclear membranes. Once drug is situated in the nucleus, it must be capable of interacting with DNA by intercalating, that is forming a stable complex with a relatively long half-life. Cytotoxicity could be also a consequence of the poisoning of topoisomerases, enzymes that are directly involved in DNA recognition, in the fundamental steps of cellular growth. The spatial arrangement of DNA before, during, and after replication is essential to a high-quality cell division process. In this way, DNA topology is governed by these enzymes. The enzymes can be classified into two main classes: type I, which breaks only one strand of the DNA, although both strands are involved in the interaction with the enzyme, and type II, which breaks both strands of the duplex. They are both a good leads for DNA intercalators, which induce cytotoxicity when they poison the enzymes by stabilizing the ternary, DNA–intercalator–topoisomerase complex in such a way that the enzymatic process cannot continue forward or backward. Finally, once the enzyme–DNA complexes are poisoned by intercalators, the ternary complex is detected by the cell as a damaged portion, which triggers a series of events, which induces cell apoptosis (programmed cell death).

In recent years much interest has been focused on molecules that may bind and modify genetic material. Along these lines, there has been increasing attention in the discovery and investigation of compounds that cleave DNA when irradiated with visible or UV light. These molecules are called photonucleases and they exhibit a large potential for therapeutic applications because they are often inert until activated by light and allow control of the reaction both in a spatial and temporal sense. The photonucleases operate by several distinct mechanism. One class of compounds photosensitizes the excitation of reactive intermediates that react with DNA, such as singlet oxygen, or the hydroxyl radical. In a second class, the photonuclease is bound to the nucleic acid before its activation and the DNA damage is thus localized at or near the binding site. These compounds, like any other small DNA-binding molecule, associate by intercalation or fit into the minor groove of the DNA. So, the photosensitized damage of DNA offers a promising tool to destroy DNA on purpose and may have a photobiological effects as they can be applied as phototherapeutics. The photosensitization of cells and tissue using photoactive drugs has been exploited in a variety of phototherapies for the treatment of multiple diseases. In fact in the last 20 years there was the development of dyes for photodynamic therapy, in particular porphyrins and porphyrins-based compounds, or new psoralen derivatives to apply for the well known PUVA therapy. Moreover photosensitization approaches have also been investigated for antimicrobical use, disinfections of blood products, as well as for wound closure in photochemical tissue bonding.

Among the compounds investigated along these lines are quinolizinium derivatives such as coralyne and the related molecules. Moreover was recently observed that the tri- and tetra-benzoquinolizinium derivatives and indoloquinolizinium exhibit DNA-binding and, after UV-A irradiation, DNA-photodamaging properties. However, other examples for DNA-binding quinolizinium derivatives with photonuclease activity are still rare.

The compounds analyzed in this project are a penta- and hexacyclic derivatives of quinolizinium ion, namely, diazoniapentaphene derivatives, diazoniaanthra[1,2-a]anthracenes, diazoniahexaphene and a partly saturated hydroxyl-substituted diazoniapentaphene. The investigations of these compounds allow to evaluate both the influence of the position of the positive charge and if the extension of π system may enhance the interaction between DNA base pair. Finally, biological studies are carried out, because their cytotoxic and photocytotoxic activity was never been consider before.

RIASSUNTO

La scoperta di nuovi composti ad attività antitumorale è uno dei più importanti obiettivi in campo medico. Un importante gruppo di agenti chemioterapici, utilizzati nella terapia contro i tumori, comprende molecole che interagiscono con il DNA. Molte ricerche effettuate in questo campo, hanno portato alla scoperta di composti che riconoscono ed interagiscono con il DNA quali agenti antitumorali, tra questi vi sono molecole che si legano al solco minore, molecole alchilanti e intercalatori. A quest'ultima classe appartengono quelle molecole che interagiscono inserendosi tra coppie di basi azotate senza però contrarre legami di tipo covalente. Le uniche forze che premettono la stabilizzazione del complesso sono rappresentate, oltre che dal DNA stesso, dai legami di van der Waals, legami a idrogeno e/o attrazioni di carica. Tali molecole sono di particolare interesse per le loro proprietà come farmaci antitumorali. Ad esempio, la classe dei derivati dell'acridina e dell'antraciclina è un ottimo esempio di intercalatori attualmente sul mercato come agenti chemioterapici. Tuttavia l'applicazione clinica di questi e di altri composti della stessa serie ha presentato dei problemi, tra i quali l'insorgere della resistenza (MDR) associata a effetti secondari e/o collaterali. Questi ostacoli hanno indotto ad approfondire la ricerca verso nuove molecole che possano sostituire o possano essere utilizzate in associazione con i farmaci già esistenti. Quindi sono risultati di particolare interesse quegli agenti che sono in grado di riconoscere particolari strutture o sequenze della macromolecola del DNA e di legarsi selettivamente a queste andando così ad indurre modificazioni funzionali a livello del materiale genetico *in vivo*.

I composti poli-etero-aromatici condensati sono solitamente degli agenti intercalanti, soprattutto se possiedono nella loro struttura delle carenze elettroniche o delle cariche nel nucleo aromatico. Tuttavia solo pochi agenti interagiscono con il DNA esclusivamente mediante intercalazione. Infatti la maggior parte delle molecole presenta un legame misto poiché una parte si intercala nella macromolecola mentre i sostituenti si dispongono lungo il solco minore. Data la complessità che regola l'interazione delle varie molecole con il DNA, è auspicabile lo studio di agenti che interagiscono esclusivamente mediante un unico tipo di legame.

Negli anni ’70 e ’80, la determinazione della costante di legame e dell’attività biologica del complesso intercalatore-DNA, così come lo studio dei rapporti struttura-attività hanno portato alla conclusione che esiste una relazione tra l’attività citotossica e l’affinità di legame. Si deve però sottolineare che l’attività citotossica non dipende esclusivamente dall’affinità di legame, poiché esistono molti intercalatori che non presentano attività biologica. Un composto per essere attivo deve innanzitutto superare molte barriere, quali le membrane citoplasmatica e nucleare, ed inoltre anche i vari processi metabolici intrinseci della cellula. Se riesce a raggiungere il nucleo, tale sostanza deve essere capace di interagire con il DNA tramite intercalazione portando alla formazione di un complesso stabile e con un tempo di emivita piuttosto prolungato. La citotossicità può essere anche la conseguenza di un’inibizione dell’attività di particolari enzimi quali le topoisomerasi. Tali enzimi sono direttamente implicati nel determinare la topologia del DNA in particolari passaggi della crescita cellulare. La struttura topologica del DNA prima, durante e dopo la replicazione è essenziale per una corretta divisione cellulare. La funzione di tali enzimi è infatti quella di modificare la conformazione della macromolecola. Esistono due classi principali di topoisomerasi: il tipo I, che induce la rottura di un singolo filamento, anche se entrambi i filamenti sono coinvolti nell’interazione con l’enzima, e il tipo II, che provoca la rottura di entrambi i filamenti della doppia elica. Entrambe queste proteine risultano essere degli ottimi bersagli per i composti intercalanti, che causano citotossicità agendo come veleni nei confronti dell’enzima. Infatti tali molecole portano alla stabilizzazione del complesso ternario DNA-intercalatore-topoisomerasi, bloccando quindi l’attività enzimatica della proteina. Tale complesso ternario si comporta come una potente endotossina che provoca l’attivazione di una serie di eventi che culminano nella morte cellulare programmata (apoptosi).

Negli ultimi anni è stato rivolto un notevole interesse verso quelle molecole che in seguito ad interazione con il DNA causano modificazioni a livello del materiale genetico, ed in particolare verso quei composti che inducono danno in seguito ad irradiazione con luce UV-Vis. Queste molecole, denominate fotonucleasi, possiedono un notevole potenziale terapeutico in quanto esse sono spesso inerti previa attivazione con luce UV-Vis e quindi la reazione può esser controllata sia dal punto di vista spaziale che temporale. Le fotonucleasi possono agire o in seguito ad attivazione diretta che porta alla formazione di specie reattive dell’ossigeno, quali ossigeno singoletto o radicali idrossilici, oppure mediante legame con il DNA e successiva attivazione con induzione del danno in siti limitrofi alla sequenza di legame. Questi composti interagiscono con la doppia elica o mediante intercalazione o tramite legame lungo il solco minore. Quindi le fotonucleasi rappresentano un importante classe di composti che causano danno al DNA solo in seguito ad attivazione e che possono essere sfruttati agenti fototerapici. Tale area di ricerca ha ricoperto un notevole interesse negli ultimi 20 anni, e si è focalizzata soprattutto nello sviluppo di nuovi composti da utilizzare nella terapia fotodinamica (porfirine e analoghi) e nella terapia PUVA (psoraleni e derivati). Tali molecole trovano applicazione sia come farmaci antitumorali che antimicrobici, oppure come prodotti disinfettanti per i componenti del sangue o delle ferite.

Alcuni dei composti studiati, appartenenti alla classi precedentemente descritte, sono i derivati dello ione chinolizinio come la coralina e molecole analoghe. Recentemente è stato osservato che i derivati tri- e tetraciclici del benzochinolizinio ed il relativo derivato indolico sono in grado sia di legarsi al DNA che di indurre danno in seguito ad attivazione con luce UV-A. Queste caratteristiche ricoprono un’importanza notevole se si considera che sino ad ora non erano stati ancora scoperti dei derivati del chinolizinio con attività fotonucleasica. I composti analizzati in questo progetto di ricerca sono dei derivati penta- ed esacicli dello ione chinolizinio, quindi derivati del diazoniapentafene, del diazoniantra[1,2-a]antracene, del diazoniaesafene e un derivato del diazoniapentafene parzialmente saturato e con un sostituente ossidrilico. Lo studio di tali molecole permetterà di valutare l’influenza della posizione relativa delle doppie cariche positive presenti nella struttura ed inoltre di verificare se l’estensione del sistema π porta ad un incremento dell’affinità di questi composti verso la doppia elica del DNA. Infine, saranno effettuati degli studi biologici per valutare l’eventuale citotossicità e fotocitotossicità poiché fino ad ora non è mai stata studiata.

1. INTRODUCTION

1.1 CANCER THERAPY

Many different therapeutic approaches are nowadays available for the treatment of cancer in clinical use. The surgery and radiotherapy are useful techniques to removed localized cancer, while systemic treatments, as chemotherapy, hormone-therapy and immunotherapy, have a better applications for leukaemia or metastatic tumour. In particular, chemotherapy implies the use of chemical compounds, synthetic or from natural origin, which are largely used in order to block or to decrease neoplastic cancer proliferation through cytotoxic mechanism. Much effort has been put into finding biological differences between cancer and somatic cells with the purpose to identify specific target and to preserve the physiologic system. Unfortunately, there are little differences between the two cell types; so the only use of an anticancer agent is not enough to destroy neoplastic populations without side effects. In fact, a real limit of the chemotherapy is the strong toxicity against high proliferative tissues (i.e., bone-marrow, gastro-intestinal and skin tissues) [1-3]. Another important problem is the rising of chemoresistance due to molecular changes of specific pump or particular membrane protein as, for example, P-glycoprotein (Pgp), belonging to the class of MRP (*multi drug resistance proteins*). The function of Pgp is to reduce the intracellular accumulation of drugs in the extracellular compartment, blocking the therapeutic action of the agents. So, at the moment, the main strategy is the association of a miscellaneous of agents (polychemotherapy) with different targets [4, 5].
The anticancer agents, actually in clinical use, can be classified on the basis of their different mechanism of action [6, 7], as:

- **Antimetabolic agents:** belong to this class all the compounds with a chemical structure similar to the one of the metabolites normally present in the cells. This structural analogy induces or the block of the enzymatic system, in which is involved the target, or the synthesis of inactive substance or with another function. The consequence is the stop or the destroy of the cancer proliferative apparatus. The limit is that, at the moment, there is no evidence of different biochemical pathway between cancer or “normal” cells; anyway, the relative abundance of the malignant cells, due to the intensive proliferation, gives a sort of selectivity toward them.

Some examples of these agents are the antagonist of folic acid (i.e., metotrexate) and the analogous of the purinic and pyrimidinic bases (i.e., 6-mercaphtopurine and 5-fluorouracyle, respectively).

- **Antimithotyc agents:** they are natural alkaloid or semi-synthetic compounds which interact with microtubules inducing a damage and, consequently, cell death. These molecules interfere with the normal process of polymerization-depolymerization of heterodimer α-β of the tubulin. The most important agents belonging to this class are taxol and the alkaloids of Vinca [8, 9].

Another important target for cancer therapy is DNA. The interaction of small molecules with DNA (Fig. 1.1) is classified in a varieties of way:

- **Alkylating agents:** they interact directly with DNA inducing the formation of covalent binding involving base modifications through alkylation. In alkylation chemistry, chlorine is a good leaving group that facilitates nucleophilic attack of nitrogen to form an imminium ion in a strained ring system. This readily undergoes alkylation at N7 of a guanine to form a monoalkylated adduct. This process can then be repeated to form crosslinked DNA that can occur either between two complementary strands (interstrand), as generated by chlorambucil and melphalan, or within a strand of DNA (intrastrand), as for cisplatin. All these reactions induce a permanent damage in the double helix and the induction of cell death [10-12].

- **Code-reading agents:** the agents belong to these family are able to recognize and bind specific sequence of the double helix of DNA. The interactions are usually non-covalent, so reversible, and can be specific toward particular sequence or non-specific. These compounds are further classified into intercalator and groove binding. Intercalation occurs when planar aromatic molecules insert fully between two base pairs of DNA (i.e., doxorubicin and actinomycin D), while groove binders are usually crescent shaped cationic molecules that bind in the minor or major groove of DNA (i.e., distamycin and netropsin, TFOs and PNAs, respectively) [13-15].

- **Quadruplex-interactive agents:** there are special sequences in DNA that can form secondary DNA structure, such as four-strand (parallel), two-strand (hairpin) or one-strand structures in which consecutive runs of guanines are found (G-quadruplex). Examples of DNA sequence that induce G-quadruplex are telomeres and promoters that contain a polypurine-rich strand. The equilibrium between double-strand and G-quadruplex is dependent on helicases (enzyme with unwinding function). The drugs can either inhibit helicases or facilitate formation of new quadruplex (i.e., perylene and cationic porphyrins) or can sequester newly formed G-quadruplex (i.e., telomestatin) [16, 17].

- **Protein-DNA complexes as molecular target:** DNA is not only a repository of encoded sequence information, but also the scaffold on which DNA-binding proteins assemble. These proteins are involved in packaging, transcription regulation, replication, recombination and repair, and all the processes are crucial for normal cellular growth. Blocking proteins from binding to DNA is the simplest way of interfering with protein-DNA complexes. So DNA-interactive drugs can also work by acting as a type of enzyme inactivator, for example as topoisomerase I and II poison. Some agents can bind both DNA and enzyme (i.e., doxorubicin), while others can bind only on topoisomerase (i.e., etoposide) and therefore do not interfere with other processes that occur on DNA [18-20].

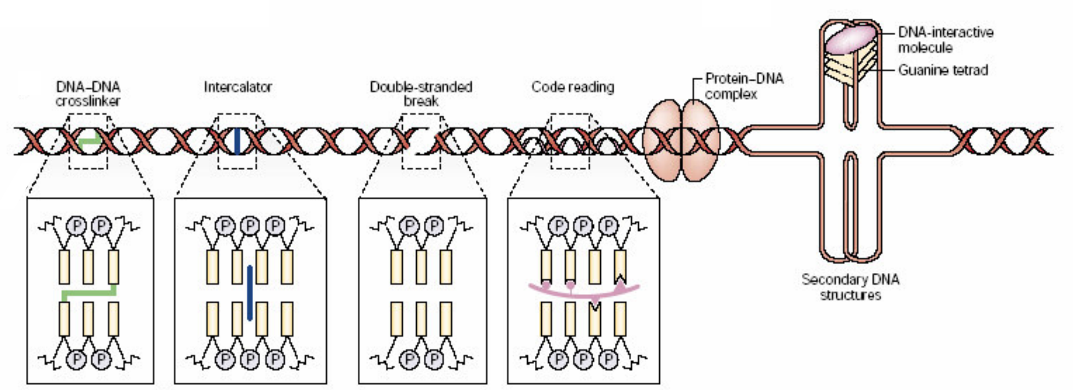

Figure 1.1 Classes of DNA-interactive agents and their molecular interactions with DNA.

1.2 INTERACTION WITH DNA

The association of external molecules with DNA has attracted considerable interest in bioorganic and medicinal chemistry [21, 22]. Such complex formation leads to significant modification of the structure of the DNA and therefore may have an important influence on the physiological function of the DNA, namely gene expression [23]. Most notably, the strong association of a molecule with DNA may lead to cell death and is not a desirable process in healthy tissue. Nevertheless, the suppression of the DNA replication and gene transcription by this association may also be used to destroy unwanted cells, such as tumour cells or other infected tissue in living systems. Therefore, one of the most challenging goals in this area of research is the design of DNA-binding molecules which selectively bind to DNA in unwanted cells and lead to cell death without damaging the healthy cells. Along these lines, many investigations have been performed to gain more insight into different aspects of the association process of large and small molecules with DNA, and several classes of DNA-binding molecule have been established and investigated in detail [24]. For example, proteins represent a group of macromolecules whose association with DNA constitutes important steps in the gene-transcription process [25]. Consequently, one promising lead structure for functional DNA-binding drugs is based on polyamide derivatives [26]. Oligosaccharides have also been shown to be important DNA-binding moieties in DNA-targeting drugs such as Calicheamycin [27]. Organometallic complexes have been shown to associate with DNA [28], and also used to investigate charge-transfer through DNA [29]. Cationic organic dyes are another important class of DNA-binding molecule. Representative examples are proflavine [30], acridine orange [31], methylene blu [32], ethidium bromide [33], thiazole orange [34], anthraquinone derivatives [35], pyrido-annelated indolinium derivatives [36], acridizinium derivatives [37], and protoberberines [38]. Such dyes have the advantage that their interaction with DNA can be easily evaluated, qualitatively and quantitatively, by absorption and emission spectroscopy, because of the significant change of their pronounced dye properties (absorption and emission) on DNA binding. These simple and straightforward spectroscopic methods are especially advantageous because organic dyes absorb and emit at wavelengths which do not interfere with the absorption of the DNA bases (λ_{max}= 260 nm).

1.2.1 Binding modes

In general, two binding modes are possible between guest molecules and the host DNA: (a) minor or major groove binding, and (b) intercalation (Fig. 1.2). A third binding mode, external binding, is also known; this results exclusively from attractive electrostatic interactions between a positively charged molecule and the negatively charged phosphate backbone of the DNA. In contrast, groove binding and intercalation can be viewed as the formation of a supramolecular assembly based on associative interactions such as π stacking, hydrogen bonding, attractive van der Waals, or hydrophobic interactions. Each binding interaction is usually initiated by hydrophobic transfer of the DNA binder from the polar aqueous solution into the less polar environment of the DNA. If the DNA binder carries a positive charge, association with DNA also leads to a release of DNA counter cations from the DNA grooves.

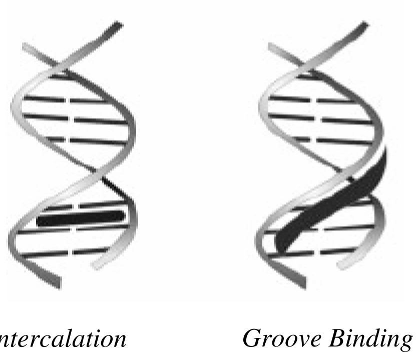

Figure 1.2 Binding modes of small molecules with DNA.

1.2.2 Groove binding

The DNA helix has two grooves of different size, the minor and the major grooves, which can serve as binding sites for guest molecules. Whereas relatively large molecules such as proteins bind preferentially to the major groove of DNA [25], the minor groove is the preferred binding site for small ligands [22-24]. The binding pocket of a DNA groove is defined by two different regions, the ‘‘bottom’’, formed by the edges of the nucleic bases that face into the groove, and the ‘‘walls’’, which are formed from the deoxyribose–phosphate backbone of the DNA. Groove binders usually consist of at least two aromatic or heteroaromatic rings whose connection allows conformational flexibility, such that a crescent-shaped conformation can be achieved and the molecule fits perfect into the groove. In addition, functional groups are required to form hydrogen bonds with the nucleic bases at the bottom of the groove. Typical minor-groove binders are Hoechst 33258 [39] and netropsin [40], distamycin A and DAPI (Fig. 1.3) [7].

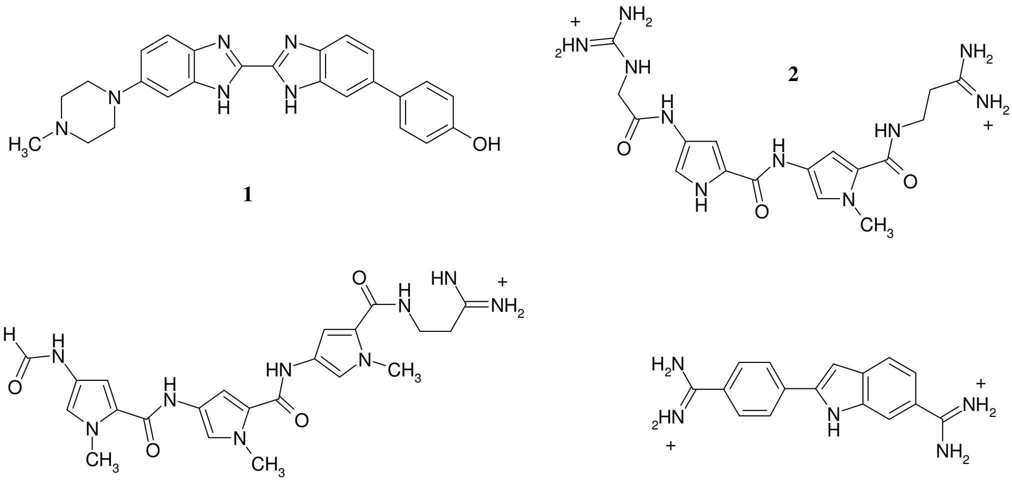

1 2 3 4

Figure 1.3 Examples of minor-groove binders: 1 = Hoechst 33258; 2 = netropsin; 3 = distamycin A; 4 = DAPI.

Most groove binders have binding selectivity toward AT-rich areas, because grooves, which consist of GC base pairs, are sterically hindered by the guanine amino functionality at C-2 and its hydrogen bond with the C-2 carbonyl functionality of cytosine. It has also been observed that in AT-rich grooves the electrostatic potential is higher than in GC-rich regions. Thus positively polarized or charged ligands also has greater affinity for the AT-rich groove, because of favourable electrostatic attraction. Nevertheless, some groove binders are known that bind preferentially in GC-rich grooves, because they are substituted with functionalities that form strong attractive interactions with the guanine amino group [40].

1.2.3 Intercalation

In a DNA helix, the nucleic bases are located in an almost coplanar arrangement. In his pioneering work Lerman showed that this arrangement enables planar polycyclic aromatic molecules to intercalate between two base pairs [30, 41]. Important driving forces for this binding mode are dipole–dipole interactions and π stacking of the guest molecule with the aromatic nucleic bases. Other than groove binding, intercalation has a significant influence on the DNA structure, because the DNA needs to unwind so that the intercalator fits between the two base pairs. This unwinding leads to a lengthening of the helix of more than 3.4 Å, along with a significant change of the deoxyribose conformation [21, 22]. It has been observed that the binding of one intercalator between two base pairs hinders access of another intercalator to the binding site next to the neighbouring intercalation pocket. This ‘‘neighbour exclusion principle’’ is well accepted and can be used as a general rule; it is, however, not fully understood. It has been proposed that structural changes of the DNA on intercalation lead to limited access to the neighbouring binding pocket for steric reasons. Also, the intercalation process can reduce the negative electrostatic potential at the intercalation site, so that attractive electrostatic interactions no longer occur close to this site.

Intercalators usually exhibit a planar structure with, at least, two annelated aromatic rings (Fig. 1.4). In most cases, a positive charge is required for an appropriate binding affinity, in order to enhance the attractive ionic interactions between the cation and the phosphate backbone [24, 25]. This cationic moiety is usually provided by a quaternary nitrogen atom, which may be generated either by simple protonation, as in the aminoacridine series (i.e., proflavine) [30], or by N-alkylation, as found in the well-know phenantridine series (i.e., ethidium bromide) [36]. As a consequence, the pH of the environment has a significant influence on the DNA-binding properties of such ligands. Alternatively, it is possible to introduce the cationic nitrogen atom as a bridgehead between two annelated rings, as the alkaloids of the protoberberine series (i.e., berberine and coralyne) [38, 42], the quinolizinium ion [36] and related derivatives, whose DNA-binding properties have already been described [37, 43-47]. In these cases the brutto charge is independent of the pH of the environment.

The compounds analyzed in this thesis are penta- and hexacyclic derivatives, belong to the family of quinolizinium ions.

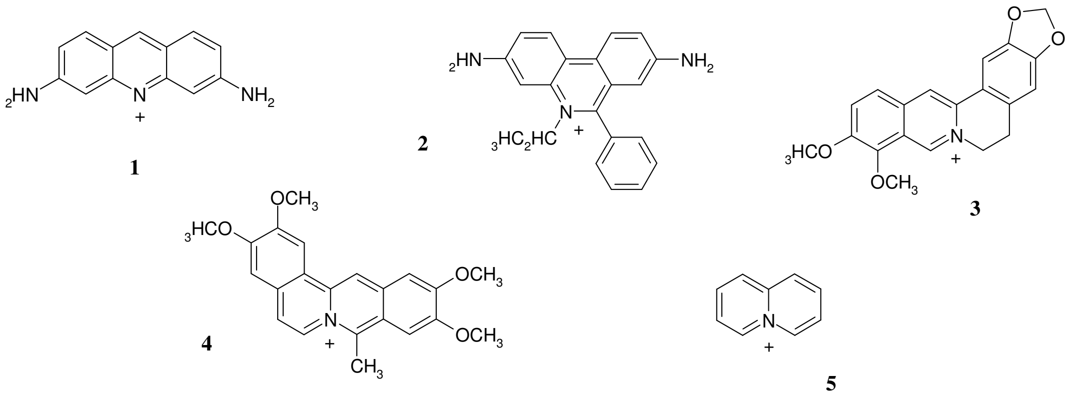

Figure 1.4 Examples of intercalators: 1 = proflavine; 2 = ethidium bromide; 3 = berberine; 4 = coralyne; 5 = quinolizinium ion.

Although there is a relationship between the binding energy of a DNA intercalator and its biological activity, as discussed earlier, cytotoxicity is not only dependent on the ability to interact with DNA, since there are many DNA intercalators that are incapable of working as cytotoxic agents [48]. To be effective, a drug must first overcome many barriers, including metabolic pathway, and cytoplasmatic and nuclear membranes. Once the drug is situated in the nucleus, it must be capable of interacting with DNA by intercalations, forming a stable complex with a relatively long half-life. Achieving entry into the nucleus and forming a DNA complex are only the first stage of a series of events that underlie the cytotoxic activity of the compound (Fig. 1.5).

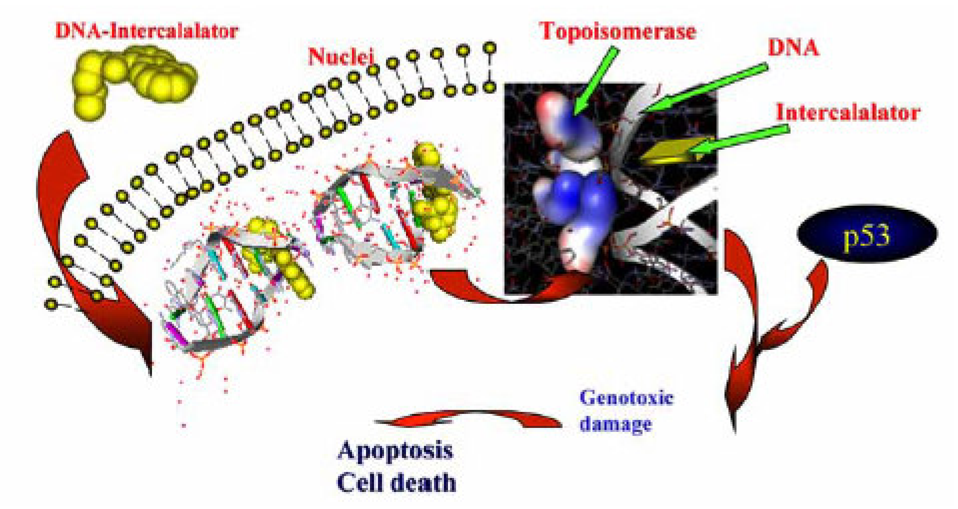
DNA-Intercalalator
Nuclei
Topoisomerase
DNA
Intercalalator
p53
Genotoxic damage
Apoptosis
Cell death

Figure 1.5 Schematic representation of the mechanism of cytotoxicity of DNA-intercalator.

Thus cytotoxicity is more than just an interaction with DNA. It could be a consequence of the binding with some essential proteins, associated with the double helix, as topoisomerase I and II, enzymes that are directly involved in DNA recognition, in the fundamental steps of cellular growth (i.e., S-phase or M-phase of cell cycle), in which the topology of DNA plays a significant role. A damage at DNA usually triggered a series of events that could involve p53 protein, which induces cell apoptosis (programmed cell death) [49-51]. As it can be seen that intercalators have a broad range of properties. The variety of compounds in this field is very extensive and some of them are found in clinical use or trails. Anyway, many efforts are still made to discover new compounds, in order to improve the selectivity and to overcome drug resistance.

1.3 DNA

The double helical structure of DNA discovered by Watson and Crick [52] has undergone rapid enrichment in subsequent years with the awareness that it has considerable flexibility. DNA is a structurally polymorphic molecule that can adopt a variety of conformations, which show significant deviation from canonical right-handed DNA (B-DNA) depending on the nucleotide sequence and environmental conditions.[53-60]. The main family of DNA forms identified based on crystallographic analysis of deoxyoligonucleotides are the right-handed B- and A-forms and the left-handed Z-form (Fig. 1.5). Furthermore, several other DNA structures like loops, bulges, hairpins, cruciforms, and higher order structures like triplexes [61], quadruplexes [62], etc. are known to exist.

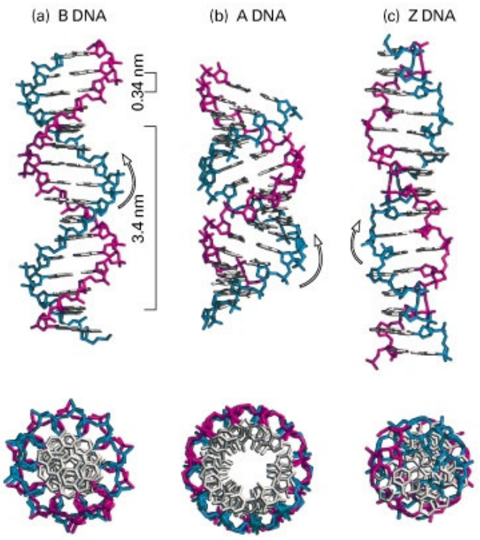
(a) B DNA
(b) A DNA
(c) Z DNA
0.34 nm
3.4 nm

Figure 1.5 Schematic representation of B-, A- and Z-form structures of DNA.

1.3.1 B-form of DNA

In the '50s Brown and Todd [63] revealed the chemical structure of nucleic acids, announcing that they are linear polymers of nucleotides whose sugar are bonded through phosphodiester groups-bridges at 3' and 5' positions (Fig. 1.6). At physiologic pH, the phosphodiester are acidic, so these polynucleotides have a negative charge (polyanions). A few years before, Chargraff has found that within DNA there are the same percentage of nucleotide *adenine* (A) respect to *thymine* (T) and of *guanine* (G) respect *cytosine* (C) [64].

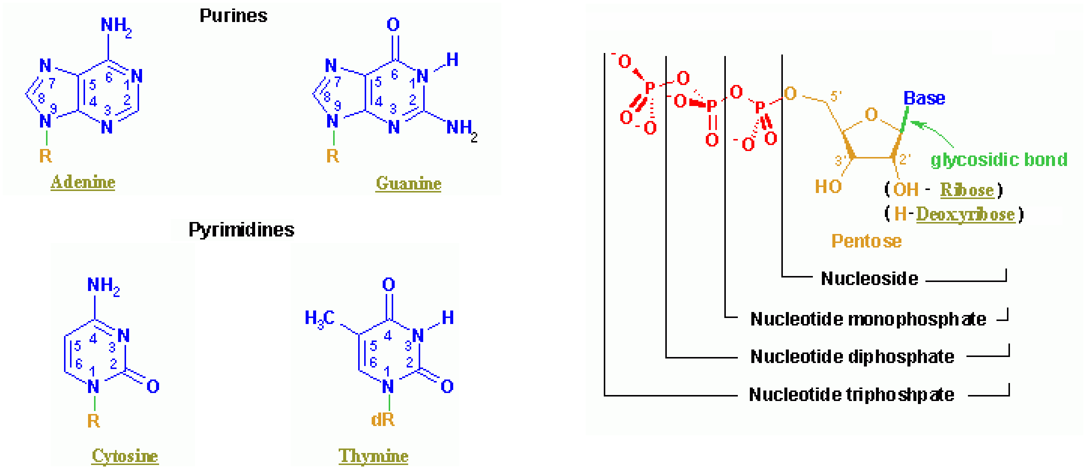
Purines
Adenine
Guanine
Pyrimidines
Cytosine
Thymine
Base
glycosidic bond
(OH - Ribose)
(H-Deoxyribose)
Pentose
Nucleoside
Nucleotide monophosphate
Nucleotide diphosphate
Nucleotide triphoshpate

Figure 1.6 Schematic representation of nucleotides and sugar bonded to phosphodiester groups.

Watson and Crick collected all this information and they proposed the molecular structure of B-form of DNA [52], that it is believed to be the native conformation of DNA in solution under physiological condition. It consists of two polynucleotide chains, which run in opposite directions (antiparallel) and wrap around each other, so that they cannot be separated without unwinding the helix. The aromatic bases are stacked within its chain and they occupy the core of the helix, while the phosphate backbone (groups) are externally exposed in a way that the interactions with solvent reduce repulsions between their negative charges. The sugars are 2'-deoxyribose (while in RNA are ribose). They are bonded with bases in 1' position and with phosphates in 5' and 3' positions. The plane of the bases are perpendicular respect to the double helix axis and the aromatic groups are partially stacked on each other. The ideal B-DNA has a pitch (rise per turn) of 34 Å, because it involves 10 base pairs (bp) per turn, and the aromatic rings have a thickness of 3.4 Å. Every base pair axis turns of 36° respect to the axis of the adjacent pairs and they are nearly perpendicular to helix axis.

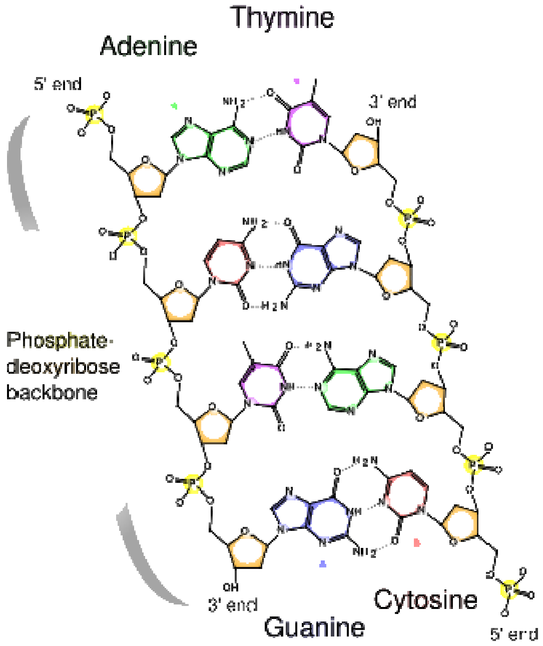

Figure 1.7 Geometry of the interactions of A-T and G-C.

Bases of opposite strands are coupled through hydrogen bond interactions ("complementary base pairing"), at every adenine of one strand corresponds a thymine in the opposite one (and vice versa). At the same way, any guanine interacts with a cytosine in the other strand (Fig. 1.7).

The bases pairs are interchangeable without having changes of sugar positions and conformation, and even the inversion of the basis within a pair (i.e., if A-T becomes T-A) doesn't have any effects on the global structure of DNA.

B-DNA present two exterior grooves generated by the helicoidal structure of the two strands. Considering a spatial central point of the base pair, the groove corresponding to the region where the angle CH_2-central point-CH_2 is $< 180°$ is called *minor groove*, while the opposite one is the *major groove* (Fig. 1.8).

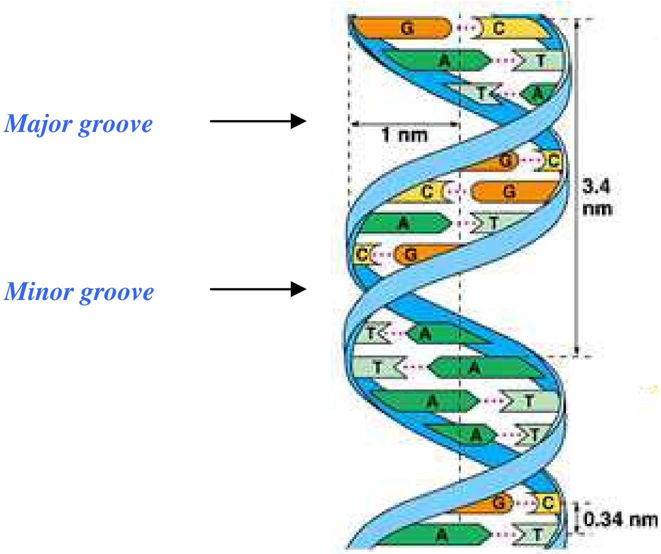

Figure 1.8 B-DNA double helix with the minor and major grooves highlighted.

The major groove is wide and easily accessible to proteins, while minor groove is narrow; this conformation is favoured at high water concentrations. Even if the conformation of a nucleotide unit is specified by seven torsion angles, in reality there is no an high flexibility because of a variety of constrains that restrict the conformational freedom. The base is not free to rotate about its glycosidic bond; purine residues may assume two sterically possible conformations, *syn* and *anti*, while for pyrimidines only the anti is acceptable (in the syn conformation the C5' atom of sugar would be too close to C2 substituent of base). Generally, all bases are in anti conformation, with the exception of Z-DNA isoform. The conversion from B- to Z-form, it means from anti to syn, is due to a the rotation of purinic base around its glycosidic bond; this explains why Z-form can be easily assumed by purine-pyrimidine alternated sequence. To reduce this tensioned situation the ring puckers; in fact four atom remain almost co-planar and the fifth one stays slightly out of plane (a few tenths of Å), reorienting the substituents in gauche or anti conformations. This ring conformation takes place in two way: if the out-of-plane atom is on the same side of C5’ substituent, it is called *endo*, while if it is on the opposite side of C5’, it is called *exo*. Generally the out-of-plane are either C2’ or C3’, with one atom endo and the other exo (and vice versa). The sugar conformation is important also because it regulated the relative positions of the two phosphate substituents. Finally, the conformational constrains of sugar rings and the substituents, the not covalent interactions of attraction (i.e., H-bond) or repulsion (i.e., between spatially close phosphate groups) and the steric interferences between residues make the sugar-phosphate backbone not a rigid but a conformationally constrained structure. Indeed, the angles and the torsions within double helices are relatively strain free and the double helices are conformationally relaxed; on the other hand, upon strand separation, the sugar-phosphate backbone assumes a random coil conformation.

1.3.2 A-form of DNA

The A-isoform is a reversible conformation of B-DNA (Fig. 1.5). The A-DNA helix is right-handed with 11 bp per turn; it is wider and flatter than B-form. The base pairs are pushed toward the minor groove, so that the base pairs tilt to 19 degrees with respect to helix axis which doesn’t pass through the centre of each base pair. The result is a shallow minor groove and a very deep major groove. Essentially all helical RNA is in A form under certain conditions particularly in RNA-DNA hybrids. In addition, the sugar ring changes from the C2’-endo conformation found in B-DNA to a C3’-endo one [65].

1.3.3 Z-form of DNA

The formation of Z-DNA in solution was first observed by Pohl and Jovin [56] in 1972 from the striking salt-induced cooperative conformational change of poly(dG dC).poly(dG-dC) from the near inversion of the B-form circular dichroic spectrum. Subsequently, Rich’s group(67) solved the first structure of left-handed Z-DNA in the oligonucleotide d(CGCGCG) from single crystal X-ray diffraction analysis. Both right handed B-DNA and left-handed Z-DNA are double helical conformations with antiparallel chains that are held together by Watson–Crick hydrogen bonding between the bases. However, there are remarkable differences between the Z- and B-forms in terms of shape, size, and helical parameters. The Z-DNA is longer and thinner than B-DNA and the bases are relatively farther from the helix axis, creating a deep narrow minor groove, while the major one is not properly a groove (Fig. 1.5). Another major difference between the B-form and the Z-form is the different orientation of the base pairs relative to the sugar phosphate chains. In effect, the base pairs in Z-DNA are flipped so that they are 180° away from the position they have in B-DNA. Conversion of a section of B-DNA to Z-DNA may be associated with an initial separation of the base pairs, a rotation, followed by a rejoining of base pairs. Rotation of the guanine residues occurs about their glycosyl bonds to give syn conformation from anti conformation. In case of cytidine, both the base as well as sugar rotates about the glycosidic bond. Thus, the conformation of the glycosidic bond alters between syn and anti conformation to produce the characteristic zig-zag sugar phosphate backbone in Z-DNA. Subsequently, it was established that Z-DNA can be generated in solutions in the presence of divalent cations-like Mg^{2+}, Ca^{2+}, and Ni^{2+} or millimolar concentration of polyamines. Anyway, also if Z-form can be formed in vivo given proper sequence and superhelical tension, its function remains obscure [66-68].

Table 1 Parameters of A-, B- and Z-DNA double helices.

Property	**A-Form**	**B-Form**	**Z-Form**
Direction of helical rotation	Right-handed	Right-handed	Left-handed
Diameter	~26 Å	~20 Å	~18 Å
Helical twist per base pair (in degrees)	34	36	60
Base pairs per turn of helix	11	10	12
Rise per base pairs along helix axis	2.3 Å	3.4 Å	3.8 Å
Orientation of N-glycolsidic bond	Anti	Anti	Anti for pyrimidines; syn for purines
Major groove	Narrow and deep	Wide and deep	Flat
Minor groove	Wide and shallow	Narrow and deep	Narrow and deep

1.4 ULTRAVIOLET RADIATION

Ultraviolet (UV) radiation is that portion of the electromagnetic spectrum that extends from the lower wavelength limit of human vision (usually defined as 380 to 400 nm) to wavelength as short as about 10 nm, where it overlaps the X-ray region (Fig. 1.9).

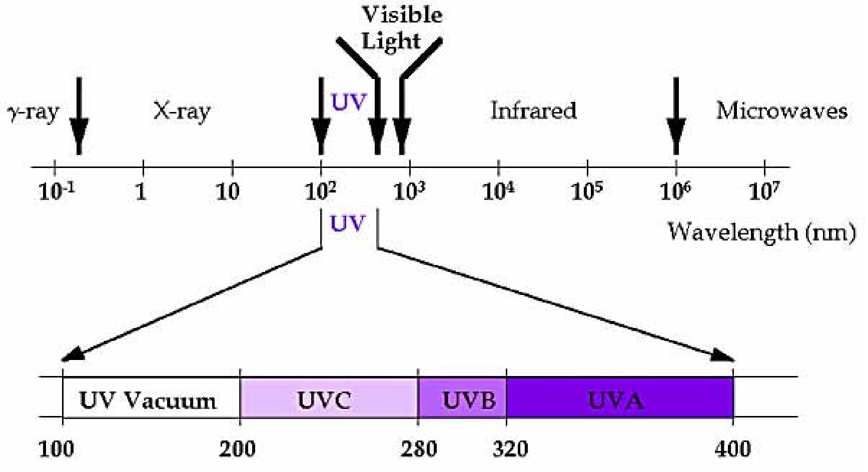

Figure 1.9 The ultraviolet (UV) components of the electromagnetic spectrum.

In the natural environment, the shortest wavelength of sunlight that can be routinely measured at the earth's surface is about 290 nm, largely due to the absorption properties of ozone and other atmospheric gases. So, the only environmentally relevant UV region is from 290 to 380 nm. However, artificial UV sources such as certain fluorescent lamps, mercury and xenon arcs, laser are readily available and extend the possibility of exposure of biological specimens to UV down to wavelengths of 190 nm. Below 190 nm, air (oxygen) and water begin to absorb UV heavily, making it difficult to expose biological samples except under extreme conditions (i.e., in a vacuum). Hence, UV photobiology is concerned mainly with the effects on biological processes due to exposure to photons in the wavelength range 190 to 380 nm [69].

The ultraviolet region, used for photobiological studies, could be divided into [70]:

- **Vacuum UV:** (10 to 190 nm), photons in the "vacuum" UV (V-UV) are heavily absorbed by water and oxygen (in air), both of which become essentially transparent (more than 50% transmission) to UV at wavelength above 190 nm. Because of this limited penetration, V-UV damage to cells is usually confined to a narrow region (a few micrometers) near the cell surface. Often it causes different types of cellular and molecular damage and its effects can be qualitatively different from those of other UV regions.

- **UV-C:** (190 to 290 nm), the shorter-wavelength end of UV-C (190 nm) is the wavelength region where air and water become transparent. The longer-wavelength limit (290 nm) is the shortest solar UV wavelength easily measured at the earth's surface. Thus, all of the UV-C is environmentally irrelevant. However, research in this range was central in elucidating many important features of cell functioning. DNA, the genetic material, has a peak of absorption near 260 nm that falls by a factor of six by 290 nm. This fact, combined with the readily available 254-nm "germicidal" UV fluorescent source, allowed for simple experimental molecular manipulation of DNA, and UV-C photobiology was central in establishing the then-new field of molecular biology.

- **UV-B:** (290 to 320 nm), the shorter-wavelength limit (290 nm) of UV-B region can be defined as the shortest UV wavelength routinely measurable at the earth's surface where it is about 1 million-fold less prevalent than 320-nm radiation. The longer-wavelength limit (320 nm) is where ozone and other atmospheric components begin to (more than 50%) attenuate sunlight appreciably. This absorption prevents much of the significant DNA damage that would result if no ozone layer existed. DNA absorption rapidly decreases toward the longer-wavelength end of this region [71]. Nevertheless, absorption of UV-B photons by DNA contributes to a wide variety of bioeffects. The UV-B is responsible for most of the damage inflicted on organisms by sunlight.

- **UV-A:** (320 to 380 nm), the shorter-wavelength limit of UV-A (320 nm) can be defined as that wavelength at which ozone becomes transparent. The longer-wavelength limit (380 nm) is where vision begins and UV ends. The UV-A region is also biologically effective and causes cellular death, mutation and DNA damage, although the primary chromophores for these effects may be non-DNA sensitizers that are chemically matched to the photon energy and act as intermediates in relaying the absorbed energy to DNA [72]. UV-A exposures from sunlight are considerable, constituting about 8% of the total sunlight spectrum (compared with less that 0.3% for UV-B).

1.4.1 Photosensitized reactions

Radiation is toxic (kills living cells), mutagenic (changes the genotype of cells, as assayed in the laboratory) and carcinogenic (removes the normal capacity to inhibit growth that most cells in multicellular organism possess, perhaps by induction of specific oncogenes). It is commonly accepted that cellular mutagenesis caused by ionizing and non-ionizing radiations of different energies results from changes in cellular DNA and it is generally believed that DNA is also an important target for cell killing resulting from radiation exposure in that the changes induced in the DNA can be lethal if not repaired [73]. This is the case for both ionizing radiation and non-ionizing UV radiation in the wavelength region between 200 nm and blue light, in the lower 400-nm region. In the case of UV radiation, the earliest evidence for role of DNA in cell killing and mutagenesis came from action spectroscopy. It was observed frequently that action spectra for the biological responses of cells exposed to UV of wavelength between 220 and 320 nm superimpose upon the absorption spectrum of DNA [70]. Thus, the probability that a UV-C or UV-B photon will kill a cell or cause a mutation is a direct function of the probability that it will be absorbed by DNA. The DNA absorbs these photons directly and, as a result, becomes modified, i.e., forming pyrimidine photoproducts, in particular cyclobutane dimers and [6-4]-pyrimidine adducts. Thus DNA is both the chromophore and the target of this radiation. DNA can also be chemically modified as a result of the absorption of photon energy by a non-DNA chromophore. In this type of reaction, the compound itself may not be chemically changed by the absorption of photons, but photon energy is passed to another compound (such as DNA) which becomes changed in turn. This process is known as photosensitization and the chromophore is called photosensitizer. Photons with wavelength longer than about 320 nm, which have been shown to cause damage in cellular DNA [74, 75], act via photosensitization reactions. Frequently, molecular oxygen becomes activated in the photosensitization process to form several reactive oxygen species, and this interaction of light, photosensitizer and oxygen is also known as photodynamic action.

Any naturally occurring compound that absorbs UV-A photons in living cell exposed to UV-A radiation has the potential to be a photosensitizer that will absorb photon energy and pass it to DNA, resulting in DNA damage. Several compounds found in mammalian and bacterial cells have been identified clearly as a sensitizer. These include porphyrins and their derivatives, which absorb strongly in the region near the lower 400-nm range; reduced nicotinamide coenzymes, such as NADH and NADPH; flavins, such as riboflavin and a variety of rare RNA bases, such as those found in tRNA of bacteria. It has been shown that all these sensitizers enhance DNA damage *in vitro* if they are present during exposure to UV-A photons [76]. The photosensitizers that play a role in DNA damage caused by UV-A radiation have not all been identified as yet; for instance, quinines and other participants in the electron transport chain are also possible candidates. In addition, certain drugs may act as exogenous photosensitizers, such as psoralens that are been used for treatment of skin disease, particularly psoriasis, in combination with UV-A irradiation (PUVA therapy) [77].

1.4.2 Mechanism of photosensitized reactions

UV-A irradiated sensitizers may induce DNA damage through various mechanisms. Generally, the pathway of energy transfer in a photosensitized reaction is:

$$\mathrm{PS} \xrightarrow{h\nu} \mathrm{PS^*} \xrightarrow{\mathrm{A}} \mathrm{A^*} + \mathrm{PS} \longrightarrow \text{products}$$

where PS is the photosensitizers, PS* is the excited-state photosensitizer, A and A* are the substrate and an excited substrate, respectively, and hν is the photon energy [78]. In the particular case of photosensitized reactions of DNA, the products formed are DNA lesions or photoproducts. Although the substrate (A) that receives the photon energy from the excited sensitizer, as shown before, may be DNA itself, by far the most common substrate in the photosensitized reactions of DNA is molecular oxygen, normally abundant in most living cells.

The excited sensitizers may react with DNA directly by one electron transfer (Type I mechanism) and/or *via* the generation of singlet oxygen ($^1O_2$) by energy transfer to oxygen (major Type II mechanism). Although less efficiently, the excited sensitizer may transfer an electron to oxygen, resulting in the formation of superoxide anion radical (O_2-•) (minor Type II mechanism) (Fig. 1.10).

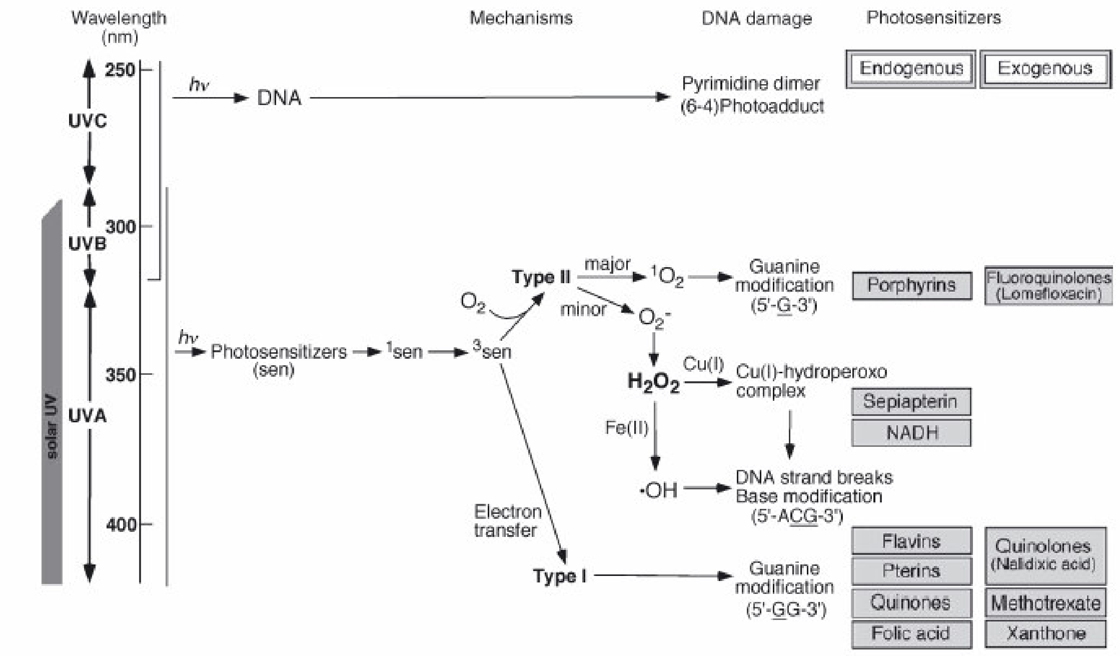
Wavelength (nm)
Mechanisms
DNA damage
Photosensitizers
250
300
350
400
UVC
UVB
UVA
solar UV
hν
DNA
Pyrimidine dimer
(6-4)Photoadduct
Endogenous
Exogenous
Type II
major
minor
$^1O_2$
O_2^-
O_2
Guanine modification (5'-G-3')
Porphyrins
Fluoroquinolones (Lomefloxacin)
hν
Photosensitizers (sen)
^{1}sen
^{3}sen
Cu(I)
H_2O_2
Cu(I)-hydroperoxo complex
Sepiapterin
NADH
Fe(II)
•OH
DNA strand breaks
Base modification (5'-ACG-3')
Electron transfer
Type I
Guanine modification (5'-GG-3')
Flavins
Pterins
Quinones
Folic acid
Quinolones (Nalidixic acid)
Methotrexate
Xanthone

Figure 1.10 Mechanism of UV-induced DNA damage in the presence of photosensitizers. ^{1}sen = excited singlet state of photosensitizer; ^{3}sen = excited triplet state of photosensitizer.

The mechanism of cellular DNA damage by UV-A would be dependent on various factors such as the content and the chemical properties of photosensitizers, their location within the cells and the concentration of oxygen. Pouget *et al.* have reported that $^1O_2$ is the main reactive species in the formation of UV-A-induced DNA damage within the cells, but hydroxyl radicals and Type I photosensitization may be involved [79].

- **Type I mechanism:** it involves the production of radical intermediates by direct interaction of an excited photosensitizers with DNA base *via* electron transfer. The initial step of this reaction does not require oxygen (O_2); however, either O_2 or O_2-• may participate in the subsequent radical reactions [80]. This mechanism is dependent on the oxidation potential of DNA bases and the reduction potential of the excited photosensitizer. Guanine has the lowest oxidation potential among the four DNA bases, that is, guanine is the most likely to be oxidized. It was demonstrated that UV-A radiation in the presence of photosensitizers, such as riboflavin, induce DNA damage at the 5'-G in 5'-GG-3' sequence in ^{32}P-labeled double stranded DNA fragments [81].

- **Major Type II mechanism:** it is based on energy transfer from an excited photosensitizer to molecular oxygen to produce $^1O_2$, which is a very powerful oxidant with a relatively long lifetime and reacts with many cellular macromolecules including DNA. A variety of endogenous and exogenous compounds have been shown to generate $^1O_2$ in response to UV-A irradiation and cause DNA damage to every guanine residue, without specificity for consecutive guanines. In addition, Ravanat *et al.* have demonstrated that $^1O_2$ is able to react directly with cellular DNA to generate 8-oxodG [82]. DNA damage and 8-oxodG formation induced by UV-A irradiated sensitizer were enhanced in D_2O because the lifetime of $^1O_2$ is markedly elongated (14 -fold).

- **Minor Type II mechanism:** the photosensitized reactions induces the formation of O_2^- by direct electron transfer from an excited photosensitizer to molecular oxygen, followed by dismutation to H_2O_2. Although O_2-• and H_2O_2 are not capable of causing DNA damage by themselves, but H_2O_2 can cause DNA damage in the presence of metal ions. Free hydroxyl radical (•OH) is generated by the reaction of H_2O_2 with Fe(II), and it is known that it causes DNA damage at every nucleotide with little or no site selectivity [83]. In contrast, H_2O_2 induces site-specific DNA damage particularly at thymine and guanine residues in the presence of Cu(II), and the primary reactive species causing the damage appears to be copper-oxygen complexes [84].

1.4.3 Clinical applications of phototherapy

Phototherapy consists basically in the use of light at different wavelength, depending on the therapeutic effect sought, in the treatment or therapy of some very specific groups of pathologies, but that in turn they are very common in their occurrence.

UV radiation, has been seen per decades with variations of frequency attaining great success in the treatment mainly of skin diseases and becoming important part of the therapy in modern dermatology. In classic phototherapy, the devices used are in wavelength ranges of 290-315 nm (UV-B) and 315-400 nm (UV-A), in contrast to some decades ago when less selective bands that corresponded almost to the entirety of the UV spectrum were used [85, 86].

Potentially, phototherapeutics have a considerable advantage over conventional drugs because side-effects are negligible. On one hand, a phototherapeutic without light does not have biological activity. On the other hand the radiation used, visible light or UV-A, is harmless without the phototherapeutic drug being present. Only as a result of simultaneous exposure to the phototherapeutic and light, can a biological effect occurs. The consequence of the latter is that the treatment can be very specific. In addition to pharmacokinetic parameters, as with conventional drugs, the properties of light contribute to an high extent to the specificity of a phototherapeutic (light can be directed very precisely to the treated tissue or cells and its wavelength region, intensity and exposure time can be controlled) [87].

The two major applications of phototherapy, in clinical use, are:

- **PUVA therapy:** the administration of psoralen (P) and long-wave ultraviolet radiation (UV-A) is the most widely used form of a drug-plus-light therapy and is commonly referred as “PUVA” [88, 89]. Psoralens are tricyclic aromatic compounds in which the furan ring is fused with a coumarin moiety, hence the name furocoumarin [90]. A number of linear and angular furocoumarin are in use for PUVA; some are commercialized, i.e., 8-methoxypsoralen (8-MOP) and 4,8,5’-trimethylpsoralen (TMP), while other are applied in clinical trials, i.e., 5-methoxypsoralen (5-MOP) and 6-methylangelicins (TMA). Originally, PUVA was used to treat psoriasis, a hyperproliferative skin disease and vitiligo, an acquired pigmentary alteration in the skin (77). Now, it is used for a wide variety of skin diseases. There is no controversy that PUVA with 8-MOP can promote human non-melanoma cancers [91, 92]. Among known side-effects which result from this combination, erythema and hyperpigmentation, a temporary failure to elicit an immune response to new antigens, is important to mention [93].

  A recent development of PUVA is an extracorporeal form of photochemotherapy called photopheresis or extracorporeal photochemotherapy [94]. After oral administration of 8-MOP, a little amount of the patients blood is collected and separated into three fractions: erythrocytes, leukocyte-enriched blood and plasma.

The erythrocyte fraction is immediately returned to the patient. The leukocyte/plasma fraction is exposed to UV-A within an irradiation chamber and thereafter returned to the patient [95-97]. The eventual result of the treatment is a specific suppressive response against the pathogenic clone of T cells. Furthermore, one has to take into account that only a small percentage of all leukocytes treated are malignant. The only side-effect noted is nausea [98].

- **Photodynamic therapy:** during the past 20 years there has been increasing interest in the use of porphyrins and other tetrapyrroles in combination with visible light for the treatment of tumours and other abnormal proliferating tissues. This therapeutic modality requires the presence of oxygen and is therefore called photodynamic therapy (PDT) [99-101]. In the predominant mechanism, a porphyrin excited by visible light transfer its excess of energy oxygen resulting in the formation of singlet oxygen which is very damaging to biological system. Simultaneously, the porphyrin falls back to its ground state, ready to repeat this energy transfer numerous times. The treatment is selective because only the combination of visible light and porphyrins is tissue-damaging and the compound is preferentially taken up in significant amounts by hyperproliferating cells and is retained there much longer than normal tissues. The short lifetime of singlet oxygen results in a very small range of action (0.1 µm) and limits the destruction of cells and tissues to its site of formation. The only documented side-effect of PDT is skin photosensitivity, which may persist for some weeks.

1.5 APOPTOSIS

Since the mid-nineteenth century, many observations have indicated that cell death plays a considerable role during physiological processes of multicellular organisms, particularly during embryogenesis and metamorphosis. The term *programmed cell death* was introduced in 1964, proposing that cell death during development is not of accidental nature but follows a sequence of controlled steps leading to locally and temporally defined self-destruction [102].

The term *apoptosis* had been coined in order to describe the morphological processes leading to controlled cellular self-destruction, and the death is an integral and necessary part of the life cycle of organisms. [103]. The apoptotic mode of cell death is an active and defined process which plays an important role in the development of multicellular organisms and in the regulation and maintenance of the cell populations in tissues upon physiological and pathological conditions. It should be stressed that apoptosis is a well-defined and possibly the most frequent form of programmed cell death, but that other, non-apoptotic types of cell death also might be of biological significance [104]. During development many cells are produced in excess which eventually undergo programmed cell death and thereby contribute to sculpturing many organs and tissues [105]. Also cells of an adult organism constantly undergo physiological cell death which must be balanced with proliferation in order to maintain homeostasis in terms of constant cell numbers. So, apoptotic processes are of widespread biological significance, being involved in development, differentiation, proliferation/homoeostasis, regulation and function of the immune system and in the removal of defect and therefore harmful cells. Thus, dysfunction or dysregulation of the apoptotic program is implicated in a variety of pathological conditions. Defects in apoptosis can result in cancer, autoimmune diseases and spreading of viral infections, while neurodegenerative disorders, AIDS and ischemic diseases are caused or enhanced by excessive apoptosis [106].

1.5.1 Morphological features of apoptosis

Apoptotic cells can be recognized by stereotypical morphological changes: the cell shrinks, shows deformation and looses contact to its neighbouring cells. Its chromatin condenses and marginates at the nuclear membrane, the plasma membrane is blebbing or budding, and finally the cell is fragmented into compact membrane-enclosed structures, called 'apoptotic bodies' which contain cytosol, the condensed chromatin, and organelles (Fig 1.11). The apoptotic bodies are engulfed by macrophages and thus are removed from the tissue without causing an inflammatory response. Those morphological changes are a consequence of characteristic molecular and biochemical events occurring in an apoptotic cell. Most notably the activation of proteolytic enzymes, which eventually mediate the cleavage of DNA into oligonucleosomal fragments, as well as the cleavage of a multitude of specific protein substrates which usually determine the integrity and shape of the cytoplasm or organelles [107]. Apoptosis is in contrast to the necrotic mode of cell-death, in which case the cells suffer a major insult, resulting in a loss of membrane integrity, swelling and dysrupture of the cells. During necrosis, the cellular contents are released uncontrolled into the cell's environment which results in damage of surrounding cells and a strong inflammatory response in the corresponding tissue [104].

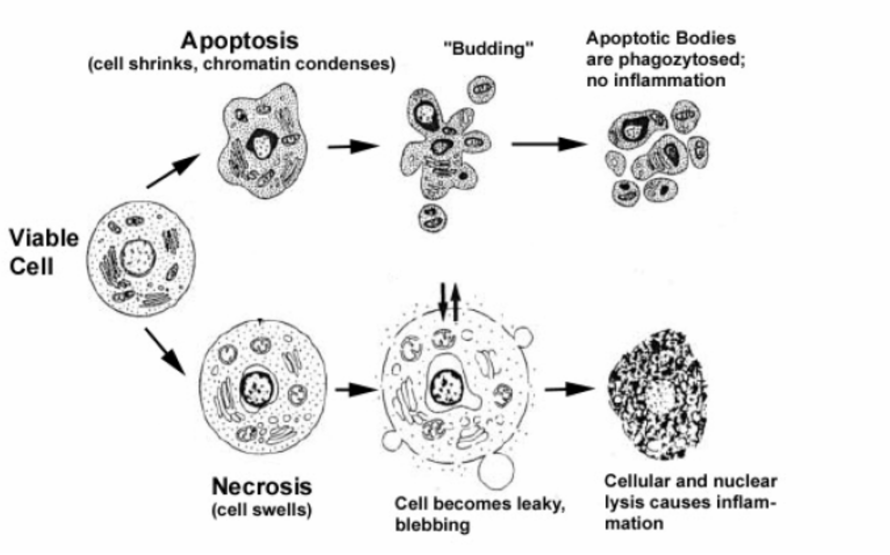
Apoptosis
(cell shrinks, chromatin condenses)
"Budding"
Apoptotic Bodies are phagozytosed; no inflammation
Viable Cell
Necrosis
(cell swells)
Cell becomes leaky, blebbing
Cellular and nuclear lysis causes inflammation

Figure 1.11 Hallmarks of the apoptotic and necrotic cell death process.

Apoptosis is a tightly regulated and at the same time highly efficient cell death program which requires the interplay of a multitude of factors. The components of the apoptotic signalling network are genetically encoded and are considered to be usually in place in a nucleated cell ready to be activated by a death-inducing stimulus [108, 109]. Apoptosis can be triggered by various stimuli from outside or inside the cell, for example by ligation of cell surface receptors, by DNA damage as a cause of defects in DNA repair mechanisms, treatment with cytotoxic drugs or irradiation, by a lack of survival signals, contradictory cell cycle signalling or by developmental death signals. Death signals of such diverse origin nevertheless appear to eventually activate a common cell death machinery leading to the characteristic features of apoptotic cell death.

1.5.2 Caspases are central initiators and executioners of apoptosis

The caspases are of central importance in the apoptotic signalling network which are activated in most cases of apoptotic cell death [110]. The term caspases is derived from **c**ysteine-dependent **asp**artate-specific prote**ases**. Their catalytical activity depends on a critical cysteine-residue within a highly conserved active-site pentapeptide QACRG, and the caspases specifically cleave their substrates after Asp residues. So far, 7 different proteases have been identified in *Drosophila*, and 14 different members of the caspase-family have been described in mammals, with caspase-11 and caspase–12 only identified in the mouse. Caspase-1 as well as caspases-4, -5, -11, and –12 appear to be mainly involved in the proteolytic maturation of pro-inflammatory cytokines such as pro-IL-1β and pro-IL-18 and their contribution to the execution of apoptosis remains questionable [111], while caspase-3, caspase-9, caspase-8, and additionally caspases-2, -6, -7, and –10 have been recognized to play an important role in the apoptotic signalling machinery [112]. In the cell, caspases are synthesized as inactive zymogens, the so-called procaspases, which at their N-terminus carry a prodomain followed by a large and a small subunit which sometimes are separated by a linker peptide. Upon maturation, the procaspases are proteolytically processed between the large and small subunit, resulting in a small and a large subunit. The prodomain is also frequently but not necessarily removed during the activation process. A heterotetramer consisting of each two small and two large subunits then forms an active caspase. The proapoptotic proteases can be divided into the group of initiator caspases, including procaspases-2, -8, -9 and –10, and into the group of executioner caspases, including procaspases-3, -6, and –7. Whereas the executioner enzymes possess only short prodomains, the initiator caspases possess long prodomains, containing death effector domains (DED) in the case of procaspases-8 and –10 or caspase recruitment domains (CARD) as in the case of procaspase-9 and procaspase-2.

Via their prodomains, the initiator caspases are recruited to and activated at death inducing signalling complexes either in response to the ligation of cell surface death receptors (*extrinsic apoptosis pathways*) or in response to signals originating from inside the cell (*intrinsic apoptosis pathways*) (Fig. 1.12).

- **Extrinsic pathways:** is mediated by the activation of so-called “death receptors”, which are cell surface receptors that transmit apoptotic signals after interaction with specific ligands. Death receptors belong to the tumour necrosis factor receptor (TNFR) gene superfamily. All members consist of cysteine rich extracellular subdomains which allow them to recognize their ligands with specificity, resulting in the trimerization and activation of the respective death receptor [113]. Subsequent signalling is mediated by the cytoplasmic part of the death receptor which contains a conserved sequence termed the death domain (DD). Adapter molecules like FADD or TRADD themselves possess their own DDs by which they are recruited to the DDs of the activated death receptor, thereby forming the so-called death inducing signalling complex (DISC). When bound to the DISC, several procaspase-8 molecules are in close proximity to each other and therefore are assumed to activate each other by autoproteolysis [111]. Active caspase-8 then processes downstream effector caspases which subsequently cleave specific substrates resulting in cell death. Cells harboring the capacity to induce such direct and mainly caspase-dependent apoptosis pathways were classified to belong to the so-called type I cells [114]. In type II cells, the signal coming from the activated receptor does not generate a caspase signalling cascade strong enough for execution of cell death on its own. In this case, the signal needs to be amplified via mitochondria-dependent apoptotic pathways. The link between the caspase signalling cascade and the mitochondria is provided by the Bcl-2 family member Bid. Bid is cleaved by caspase-8 and in its truncated form (tBID) translocates to the mitochondria where it acts in concert with the proapoptotic Bcl-2 family members Bax and Bak to induce the release of cytochrome c and other mitochondrial proapoptotic factors into the cytosol [115]. Cytosolic cytochrome c is binding to monomeric Apaf-1 which then, in a dATP-dependent conformational change, oligomerizes to assemble the apoptosome, a complex of wheel-like structure with 7-fold symmetry, that triggers the activation of the initiator procaspase-9. Activated caspase-9 subsequently initiates a caspase cascade involving downstream effector caspases such as caspase-3, caspase-7, and caspase-6, ultimately resulting in cell death [116].

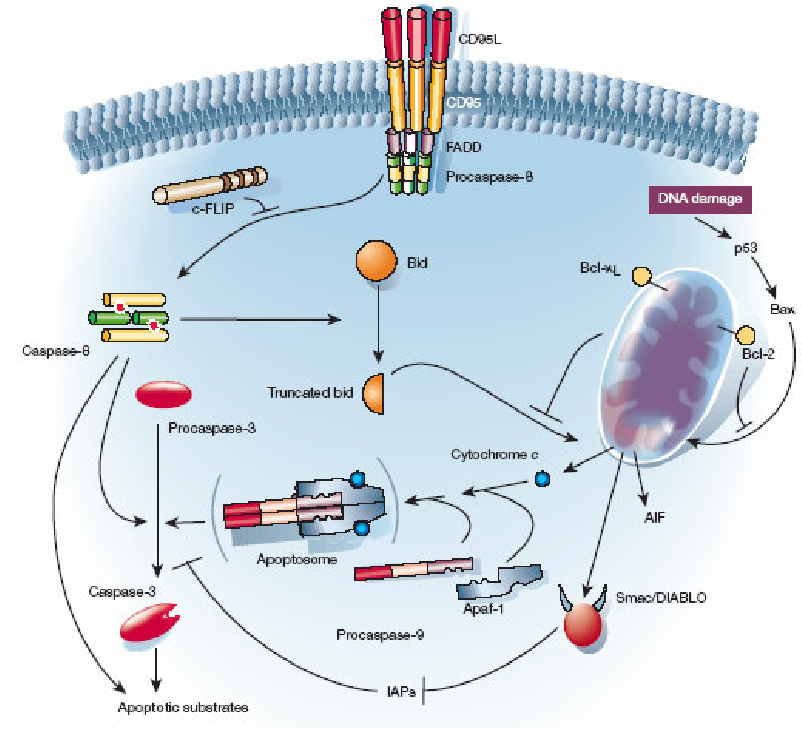
CD95L
CD95
FADD
Procaspase-8
c-FLIP
DNA damage
p53
Bid
Bcl-xL
Bax
Bcl-2
Caspase-8
Truncated bid
Procaspase-3
Cytochrome c
AIF
Apoptosome
Caspase-3
Apaf-1
Smac/DIABLO
Procaspase-9
IAPs
Apoptotic substrates

Figure 1.12 Schematic extrinsic and intrinsic caspase pathways.

- **Intrinsic pathways:** it involves procaspase-9 which is activated downstream of mitochondrial proapoptotic events at the so-called apoptosome, a cytosolic death signalling protein complex that is formed upon release of cytochrome c from the mitochondria [117]. In this case, it is the dimerization of procaspase-9 molecules at the Apaf-1 scaffold that is responsible for caspase-9 activation [111]. Once the initiator caspases have been activated, they can proteolytically activate the effector procaspases-3, -6, and -7 which subsequently cleave a specific set of protein substrates, including procaspases themselves, resulting in the mediation and amplification of the death signal and eventually in the execution of cell death with all the morphological and biochemical features usually observed [112]. The death-receptor and mitochondrial pathways converge at the level of caspase-3 activation. Caspase-3 activation and activity is antagonized by the IAP proteins, which themselves are antagonized by the Smac/DIABLO protein released from mitochondria. Downstream of caspase-3, the apoptotic programme branches into a multitude of subprogrammes, the sum of which results in the ordered dismantling and removal of the cell [118].

1.5.3 Mitochondria as central regulators of intrinsic apoptosis pathways

Besides amplifying and mediating extrinsic apoptotic pathways, mitochondria also play a central role in the integration and propagation of death signals originating from inside the cell such as DNA damage, oxidative stress, starvation, as well as those induced by chemotherapeutic drugs [119] (Fig. 1.13).

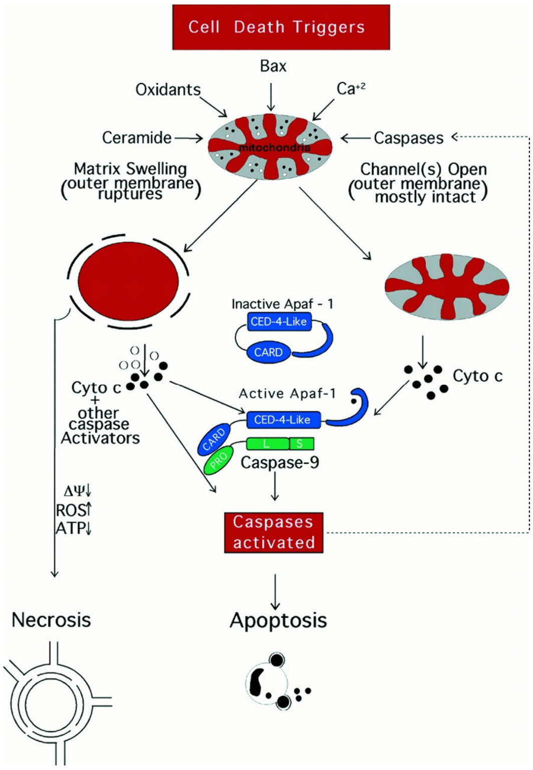
Cell Death Triggers
Bax
Oxidants
Ca^{+2}
Ceramide
mitochondria
Caspases
Matrix Swelling (outer membrane ruptures)
Channel(s) Open (outer membrane mostly intact)
Inactive Apaf - 1
CED-4-Like
CARD
Cyto c
Cyto c + other caspase Activators
Active Apaf-1
CED-4-Like
CARD
PRO
L
S
Caspase-9
$\Delta\Psi\downarrow$
$ROS\uparrow$
$ATP\downarrow$
Caspases activated
Necrosis
Apoptosis

Figure 1.13 Involvement of mitochondria in apoptotic pathways.

Most apoptosis-inducing conditions involve the disruption of the mitochondrial inner transmembrane potential ($\Delta\psi$) as well as the so-called permeability transition (PT), a sudden increase of the inner mitochondrial membrane permeability to solutes with a molecular mass below approximately 1.5 kDa. Concomitantly, osmotic mitochondrial swelling has been observed by influx of water into the matrix with eventual rupture of the outer mitochondrial membrane, resulting in the release of proapoptotic proteins from the mitochondrial intermembrane space into the cytoplasm [120]. Released proteins include cytochrome c, which activates the apoptosome and therefore the caspase cascade, but also other factors such as the apoptosis-inducing factor AIF, the endonuclease endoG and Smac/Diablo. Interestingly, PT is always followed by $\Delta\psi$, but

$\Delta\psi$ is not always caused by PT, and cytochrome c release has been observed even in absence of $\Delta\psi$. In addition to the release of mitochondrial factors, the dissipation of $\Delta\psi$ and PT also cause a loss of the biochemical homeostasis of the cell: ATP synthesis is stopped, redox molecules such as NADH, NADPH, and glutathione are oxidized, and reactive oxygen species (ROS) are increasingly generated [121]. Increased levels of ROS directly cause the oxidation of lipids, proteins, and nucleic acids, thereby enhancing the disruption of $\Delta\psi$ as part of a positive feedback. Several possible mechanisms for PT have been proposed, but there appears to exist consent that a so-called permeability transition pore (PTP) is formed consisting of the adenine nucleotide translocator (ANT) and the voltage-dependent anion channel (VDAC) as its core components. ANT is the most abundant protein of the inner mitochondrial membrane and as a transmembrane channel is responsible for the export of ATP in exchange with ADP (antiport). VDAC, also called porin, is the most abundant protein of the outer mitochondrial membrane and forms a non-selective pore through the outer membrane. Indicated by direct protein-protein interactions, VDAC-ANT complexes presumably connect inner and outer mitochondrial membrane to so-called ‘contact sites’, corresponding to a close association of the two membranes and thereby possibly constituting the PT pore [122]. Since PT, loss of $\Delta\psi$, and release of mitochondrial proteins are of central importance in mediating and enhancing apoptotic pathways, those mitochondrial events must be kept under strict control of regulatory mechanisms which are in many ways dependent on members of the Bcl-2 family.

1.5.4 Disease as a consequence of dysregulated apoptosis

In the adult human body several hundred thousand cells are produced every second by mitosis, and a similar number die by apoptosis for the maintenance of homeostasis and for specific tasks such as the regulation of immune cell selection and activity. Dysregulation of apoptotic signalling can play a primary or secondary role in various diseases with insufficient apoptosis leading for example to cancer (i.e., cell accumulation, resistance to therapy, defective tumour surveillance by the immune system), autoimmunity (failure to eliminate autoreactive lymphocytes), persistent infections (failure to eradicate infected cells), whereas excessive apoptosis contributes to neurodegeneration (i.e., Alzheimer’s disease, Parkinson’s disease, Huntington’s disease, amyotrophic lateral sclerosis), autoimmunity (uncontrolled apoptosis induction in specific organs), AIDS (depletion of T lymphocytes), and ischemia (stroke, myocardial infarction) [123]. Malfunction of the death machinery results from the mutation of genes that code for factors directly or indirectly involved in the initiation, mediation, or execution of apoptosis, and several mutations in apoptosis genes have been identified as a causing or contributing factor in human diseases. Of special interest is the involvement of defective apoptosis pathways in tumour formation, progression, and metastasis as well as the occurrence of multidrug resistance during cancer therapy. During the last years it became more and more evident that tumorigenesis is not merely the result of excessive proliferation due to the activation of oncogenes but to the same extent depends on the – frequently concurrent - impairment of apoptosis checkpoints [124]. Intriguingly, many of the alterations that induce malignant transformation, such as oncogene-driven deregulated proliferation and invasion, actually sensitize a cell to apoptosis, and therefore only those oncogenic transformed cells will survive and become malignant which additionally acquire defects in apoptosis pathways and therefore are protected against cell death induction. A transformed cell can achieve protection against apoptosis by inappropriate activation or expression of antiapoptotic proteins (which usually act as oncogenes), or by the inactivation of proapoptotic factors (which usually are tumour-suppressors).

1.6 CELL CYCLE

Usually the cells have a specific life-time because they are involved in the “division process” through the generation of the “daughter cells” with the same morphologic, physiologic and genetic features. This course of events, that characterized all the modifications implied in the life of a cell, is called cell cycle. The process is based upon the rotation of two principal periods: the interphase (or inter-mitotic phase) and the mitosis. Interphase generally lasts at least 12 to 24 hours. During this periods, the cell is constantly synthesizing RNA, producing protein and growing in size. By studying molecular events in the cells, it is possible to determine that interphase can be divided into four steps: G0 (Gap or growth 0), G1 (Gap or growth 1), S (synthesis) and G2/M (Gap or growth 2 and Mitosis) (Fig. 1.14) [125].

- **G0 phase:** there are times when a cell will leave our cycle and quit dividing. This may be a temporary resting period or more permanent. An example of the latter case is a cell that has reached an end stage of development and will no longer divide (i.e., neuron). This is very common for cells that are fully differentiated. Cellular senescence is a state that occurs in response to DNA damage or degradation that would make a cell's progeny non-viable; it is often a biochemical alternative to the self-destruction of such a damaged cell by apoptosis.

- **G1 phase:** during this phase the biosynthetic activities of the cell, which had been considerably slowed down during M phase, resume at a high rate. The cells increase in size, produce RNA and synthesize proteins, mainly those needed for DNA replication. An important cell cycle control mechanism activated during this period (G1 checkpoint) ensure that everything is ready for DNA synthesis.

- **S phase:** the S phase starts when DNA synthesis commences; when it is complete, all of the chromosomes have been replicated, i.e., each chromosome has two (sister) chromatids. Thus, during this phase, the amount of DNA in the cell has effectively doubled, though the ploidy of the cell remains the same. Rates of RNA transcription and protein synthesis are very low during this phase.

- **G2 phase:** during the gap between DNA synthesis and mitosis, the cell will continue to grow and produce new proteins, many of these are involved in the production of microtubules, which are required during the process of mitosis. Inhibition of protein synthesis during G_2 phase prevents the cell from undergoing mitosis. At the end of the this stage there is another checkpoint (G2 checkpoint) to determine if the cell can now proceed to enter M-phase and divide.

- **Mitosis or M-phase:** cell growth and proteins production stop at this stage in the cell cycle. All of the cell’s energy is focused on the complex and orderly division into two similar daughter cells. Mitosis is the process by which a cell duplicates the chromosomes in its cell nucleus, in order to generate two, identical, daughter nuclei. It is generally followed immediately by cytokinesis, which divides the nuclei, cytoplasm, organelles and cell membrane into two daughter cells containing roughly equal shares of these cellular components. So, the process is characterized by alterations of the architecture of the cell, because it requires breakage of nuclear membrane, chromatin condensation and reorganization of cytoskeleton [126]. The M-phase can be divided into six stages: prophase, prometaphase, metaphase, anaphase, telophase and cytokinesis. Mitosis is much shorter than interphase, lasting perhaps only one or two hours. As both G1 and G2, there is a checkpoint in the middle of the this stage (Metaphase checkpoint) that ensures the cell is ready to complete cell division.

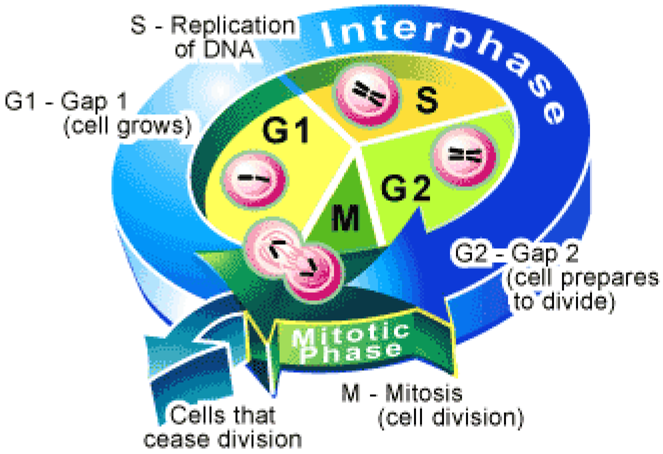
S - Replication of DNA
Interphase
G1 - Gap 1 (cell grows)
G1
S
G2
M
G2 - Gap 2 (cell prepares to divide)
Mitotic Phase
M - Mitosis (cell division)
Cells that cease division

Figure 1.14 Schematic representation of cell cycle.

Cell cycle checkpoints are used by the cell to monitor and regulate the progress of the cell cycle [127]. Checkpoints prevent cell cycle progression at specific points, allowing verification of necessary phase processes and repair of DNA damage. The cell cannot proceed to the next phase until checkpoint requirements have been met. Several checkpoints are designed to ensure that damaged or incomplete DNA is not passed on to daughter cells. Two main checkpoints exist: the G1/S checkpoint and the G2/M checkpoint. G1/S transition is a rate-limiting step in the cell cycle and is also known as restriction point. An alternative model of the cell cycle response to DNA damage has also been proposed, known as the post-replication checkpoint. p53 plays an important role in triggering the control mechanisms at both G1/S and G2/M checkpoints.

A dysregulation of the cell cycle components may lead to tumor formation. Some genes like the cell cycle inhibitors, RB (retinoblastoma), p53 etc., when they mutate, may cause the cell to multiply uncontrollably, forming a tumor. Although the duration of cell cycle in tumor cells is equal to or longer than that of normal cell cycle, the proportion of cells that are in active cell division (versus quiescent cells in G0 phase) in tumor cells are much more compared to that in normal cells. Thus there is a net increase in cell number as the number of cells that die by apoptosis or senescence remains the same. The cells which are actively undergoing cell cycle are targeted in cancer therapy as the DNA is relatively exposed during cell division and hence susceptible to damage by drugs or radiation. This fact is made use of in cancer treatment; by a process known as debulking, a significant mass of the tumor is removed which pushes a significant number of the remaining tumor cells from G0 to G1 phase (due to increased availability of nutrients, oxygen, growth factors etc.). Radiation or chemotherapy following the debulking procedure kills these cells which have newly entered the cell cycle [128].

1.7 TOPOISOMERASE I AND II

DNA topoisomerases are essential enzymes for cell survival, present in all organisms. They modify the topology of DNA in connection with a number of nuclear process, such as replication, transcription, chromatin remodelling, chromatin condensation/decondensation, recombination and repair. These enzyme alter the topological state (such as over- and underwinding, knotting or tangling) of nucleic acids by generating transient breaks in the sugar-phosphate backbone of DNA. In order to maintain the integrity of the genetic material during this process, topoisomerases form a covalent bonds with the DNA termini created by their actions. This covalent linkage is a hallmark of all topoisomerases. As a consequence of their reaction mechanisms, these enzyme alter only the spatial orientation of the double helix, so, the chemical structure of DNA product generated by them are identical to those of their initial substrate molecules [129-131]. There are proteins able to introduce either negative or positive supercoils into the DNA (bacterial DNA Gyrase and reverse Gyrase, respectively), others that relax only negative supercoils, or that relax supercoils of both signs. The enzymes are the primary target for a number of clinically important cytotoxic drugs. Topoisomerase-targeted drugs kill bacterial and cancer cells in a unique and insidious fashion. Rather than robbing the cell of essential enzyme functions, they increase the concentration of covalent topo-cleaved DNA complex that are requisite, but fleeting intermediates in the catalytic cycle of these enzymes. As a result of this action, drugs “poison” topoisomerases and convert them to potent cellular toxins that generate breaks in the genetic materials of treated cells. Enzyme cleaving only one strand of the DNA are defined as type I topoisomerases and are additionally classified as type IA and type IB subfamily. The proteins that cleave both strands of the helix are called type II topoisomerases and are divided into α and β isoforms [132-136].

1.7.1 Topoisomerase I

The reaction of topoisomerase I with DNA is schematically illustrated in Fig. 1.15. The topoisomerization cycle begins with the binding of the enzyme to the double-stranded superhelical DNA. At this point the interaction is controlled to a large extent by the surface and charge complementarity of the two reacting species. The conformational adaptation of the two partners results in the formation of a tight "kissing" complex whereby the active site tyrosine of human topoisomerase I (Y723) is brought into a favourable position for attack of the facing DNA strand and subsequent formation of a covalent adduct. The "bite" of topoisomerase I induces the release of the superhelical tension in DNA which is relaxed by a mechanism called controlled rotation [137-139]. Once the DNA is partially relaxed, the covalent intermediate is religated, leaving intact the Y723 residue ready for a subsequent "kiss and bite" catalytic cycle. Depending on the point of the reaction cycle at which the drugs will act, i.e., before or after the “bite”, topoisomerase I inhibitors will reduce or increase the extent of DNA cleavage. By mechanistically point of view, topoisomerase I-mediated DNA strand scission is accomplished by nucleophilic attack of the tyrosine active site OH group on an internucleotide phosphate ester linkage. The transient covalent binary complex involves the attachment of the enzyme via an oligonucleotide 3’-phosphate, with the release of a free DNA strand containing a 5’-OH group [140, 141].

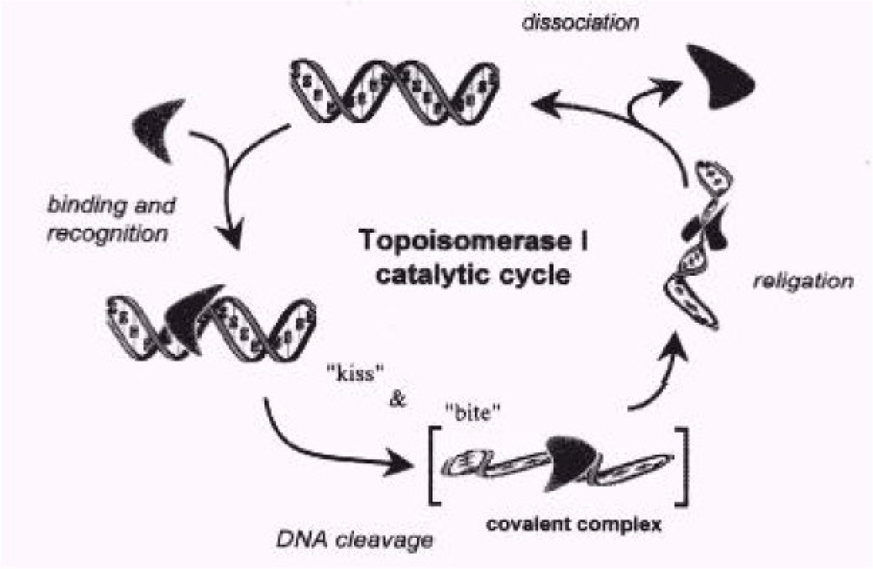

Figure 1.15 The topoisomerization reaction. Schematically, the cyclic "kiss and bite" process involves binding of topoisomerase I to DNA, followed by DNA cutting and then religation.

CPT (camptothecin) is arguably one of the most potent topoisomerase I inhibitors. However, in addition to CPT and its derivatives, a relatively important number of topoisomerase I inhibitors with diverse structures and origins have been identified, as benzophenanthridines derivatives (i.e., coralyne), benzimidazoles derivatives (i.e., Hoechst 33258 and Hoechst 33342) and indolocarbazoles derived from rebeccamycin [130]. The drugs, which include a variety of natural products, can be divided into two classes. Topoisomerase I suppressors correspond to compounds which inhibit the enzyme but do not stabilize the intermediate DNA-topoisomerase I covalent complex. Their interaction with the free enzyme inhibits binding of the protein to the DNA cleavage site, thus preventing all subsequent steps in the catalytic cycle. In contrast, the topoisomerase I poisons, like CPT, act after the cleavage of DNA by the enzyme and inhibit the religation. In this case, the drug may freeze the enzyme-DNA complex via three possible routes: (i) the enzyme binds to the preformed drug-DNA complex, (ii) the drug specifically recognizes the enzyme-DNA binary complex, and (iii) the drug-enzyme association interacts with DNA [130].

1.7.2 Topoisomerase II

One round of catalysis by topoisomerase II is shown in Fig. 1.16. Briefly, the enzyme binds two segments of DNA to initiate a round of catalysis and, in the presence of a divalent cation, the two subunits of the enzyme each cleave one strand of the double helix of DNA. The two scissile bonds are located four base pairs apart directly across the major groove from one another. Thus, cleavage generates DNA molecules with 4-base single-stranded cohesive ends on their 5’-termini. It is notable that this reaction is reversible and that the enzyme establishes a DNA cleavage-religation equilibrium.

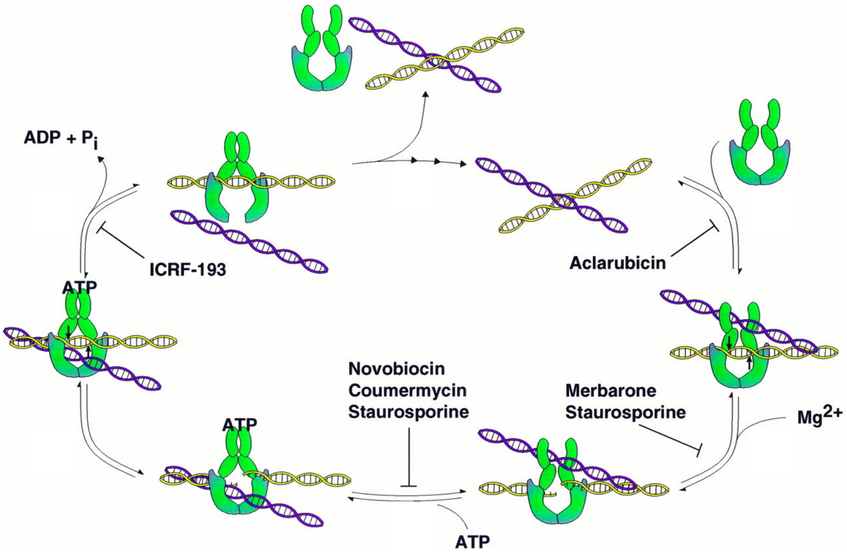

Figure 1.16 Schematic catalytic cycle of topoisomerase II.

The protein binds two ATP molecules and undergoes a conformational change that causes the passage of the intact DNA segment through the cleaved double helix. DNA strand passage appears to be faster if one of the two ATP molecules is hydrolyzed. The transported DNA is passed into a central cavity in topoisomerase II through an N-terminal gate. This one is closed and the enzyme forms a protein clamp on the DNA. Following DNA translocation, the protein reseals the original nucleic acid break, and the enzyme once again establishes a DNA cleavage-religation equilibrium. Then, topoisomerase II hydrolyzes the second ATP molecule, which opens a C-terminal gate on the protein and allows the transported DNA segment to be resealed. Finally, the enzyme returns to its original conformation and regains the ability to begin a new round of catalysis [142-146].

As a result of its catalytic mechanism, topoisomerase II can relax under- or overwound (i.e., negatively or positively supercoiled) DNA molecules and can remove knots and tangles from the genome. It is these latter functions that make the enzyme essential for cell survival. In the absence of the protein, cells cannot segregate daughter chromosomes and die as a result of mitotic failure [144].

A first class of drugs, that affect the activity of the enzyme by inducing the permanent formation of the cleavable complex, is called “poison”. Belonging to this first class some drugs as etoposide, mitoxantrone, amsacrina and epipodophyllotoxins. Topoisomerase II poisons can be categorized into three broad classes: the first increases levels of enzyme–DNA cleavage complexes by interacting with topoisomerase II at the protein–DNA interface in a non-covalent manner; the second acts by covalently modifying the enzyme; and the third acts by covalently modifying the structure of DNA. In contrast to poison, a second class of agents act by inhibiting the catalytic activity of the enzyme and display no ability to stimulate DNA cleavage. Originally, topoisomerase II “catalytic inhibitor” were defined by antibacterial compounds such as novobiocin and coumermycin. Recently many agents that display high activity toward eukaryotic type II topoisomerase have been describe, as for example merbarone, aclarubicin and staurosporin. Interesting is also a third class of compounds called “dual or mixed poison” because they act toward both type of topoisomerase. Some examples are represented by TAS 103 and DACA [130, 142, 145].

2. AIM OF THE PROJECT

2. AIM OF THE PROJECT

The investigation of the interactions of nucleic acids with small-molecule ligands is an active research area. Along these lines, especially important are the ligands capable of structure- or sequence-selective binding to nucleic acids, since such compounds may purposefully influence the biological functionality of genetic material in vivo (Fig. 2.1).

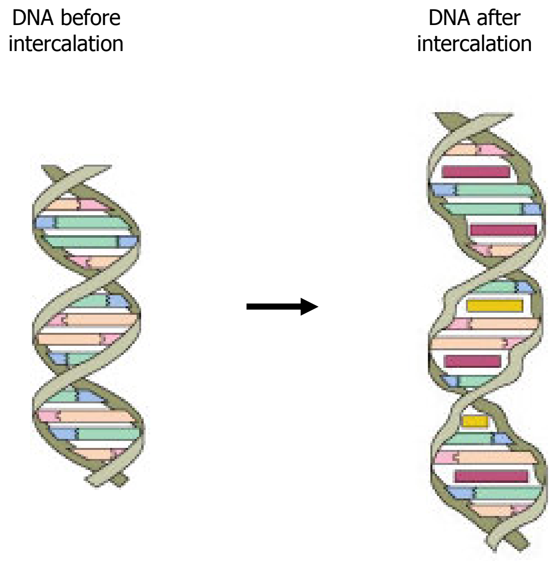

Figure 2.1 Effect of intercalator agent on DNA structure.

The condensed poly(hetero)aromatic compounds are usually regarded as representative DNA intercalators, especially if they possess electron-deficient or charged aromatic cores. However, only a few ligands are known that bind to the DNA by the intercalative mode exclusively, i.e., by insertion between the neighbouring base pairs of DNA. A vast number of ligands, which have an intercalating part endowed with a variety of substituents, bind to the DNA by a mixed mode, since the substituents occupy the DNA grooves upon binding and thus determine the selectivity and binding of the ligand. Thus, in the case of the “classical” intercalator ethidium bromide, the phenyl ring occupies the minor groove, resulting in an overall heterogeneous DNA binding. At the same time, even relatively small changes in the structure of the ligands may lead to the inversion of the binding mode or complete suppression of DNA binding, which has been shown for the ethidium derivatives and substituted 9-methylacridinium salts.

The effect of the side chains containing amino and hydroxyl substituents on the DNA affinity and binding mode of mono- and disubstituted anthracenes has been systematically investigated. In view of the complexity of the ligand-DNA recognition process, a study with model compounds, which possess only one DNA-binding mode, is desired. Such an investigation might reveal the base or sequence preference of the intercalating chromophore, unmodified by the side-chain substituents. However, the investigation of the DNA binding properties of unsubstituted arenes and heteroarenes, such as anthracene, pyrene, and acridine, is hampered by their low solubility in water, and the attachment of the water-soluble side groups, which at the same time may influence the DNA binding properties, is necessary.

It was amply demonstrated that the quinolizinium cation represents a promising platform for the DNA-binding ligands, since the annelated derivatives of this ion are very water-soluble due to the presence of an intrinsic positive charge. Thus, benzo-[*b*]quinolizinium (acridizinium) cation and naphthoquinolizinium derivatives are unsubstituted heteroaromatic compounds, capable of binding to double stranded DNA (dsDNA). Recently, the studies were extended to unsubstituted cationic heterocycles to other four-ring polyacenes, namely, linear and angular dibenzoquinolizinium derivatives, which may be considered as water-soluble analogues of tetracene and chrysene, respectively. Both derivatives exhibit an intercalative mode of binding to dsDNA with moderate binding constants ($K = 1\text{-}3 \times 10^5\ \mathrm{M}^{-1}$) and a slight preference for association with GC-rich DNA regions [37, 43-47].

While the association of cationic dyes to DNA is a reversible process, the DNA damage, which frequently occurs on irradiation of dye-DNA complexes, is often irreversible. The damage of DNA, mostly oxidative decay, by exogeneous molecules is an important event in cellular systems. Although enzymatic repair of damaged sites is possible, the destruction of the DNA may also lead cell death, mutagenesis, carcinogenesis, or aging in the absence of an efficient repair mechanism. Thus, these irreversible reactions may have an important influence on the physiological function of the DNA, namely the gene expression (Fig. 2.2). Among the classes of compounds that react with DNA, many cationic organic dyes are known to induce frank strand breaks or base modifications in DNA upon irradiation. If this process is highly selective, such photoinduced DNA damage offers a promising tool to destroy DNA on purpose, for example in unwanted cell tissue such as cancer cells or in contaminated donor-blood samples.

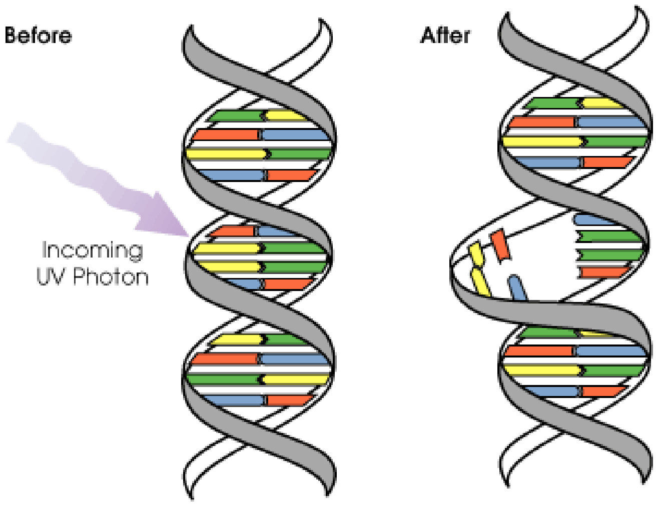

Figure 2.2 Mechanism of DNA photodamage.

In fact, this methodology is already well established in photodynamic chemotherapy. It was observed recently that the acridizinium derivatives thereof bind to DNA mainly by intercalation and that the irradiation of plasmid DNA (pBR322) in the presence of the tested compounds leads to DNA damage.

The compounds analyzed in this project are a penta- and hexacyclic derivatives of quinolizinium ion, namely, diazoniapentaphene derivatives, diazoniaanthra[1,2-a]anthracenes, diazoniahexaphene and a partly saturated hydroxyl-substituted diazoniapentaphene. The investigations of these compounds allow to evaluate both the influence of the position of the positive charge and if the extension of π system may enhance the interaction between DNA base pair. Finally, biological studies are carried out, because they cytotoxic and photocytotoxic activity was never been consider before.

3. DNA-BINDING PROPERTIES

3.1 COMPOUNDS

Cationic organic dyes are usually regarded as classical intercalators. It is commonly recognized that a positive charge enhances the propensity of a molecule to bind to DNA due to attractive ionic interactions between the cation and the phosphate backbone. In most cationic dyes, this positive charge is established by an exocyclic ammonium functionality or by an endocyclic pyridinium moiety. These functionality are usually quaternized by alkylation or protonation. In the latter case, however, this lead to a significant influence of the pH on the DNA-binding properties. In contrast, cationic dyes with an exocyclic quaternary *bridgehead* nitrogen atom are rather rare and few systematic studies exist for this class of molecules.

The compounds used in this project (Fig. 3.1) are penta- and hexacyclic derivatives of quinolizinium ion, namely diazoniapentaphene derivatives, diazoniaanthra[1,2-a]anthracenes, diazoniahexaphene, and a partly saturated hydroxyl-substituted diazonia pentaphene. They were synthesized in the laboratory of Prof. Heiko Ihmels, Department of Organic Chemistry II, University of Siegen, Germany. The synthesis was based on the idea that an extension of π system as well as the introduction of a second positive charge, provided by another quaternary nitrogen atom, could increase the affinity of the molecules toward the double helix of DNA, inducing a more stable complex than one created by the other tri- and tetracyclic and indolo derivatives already studied [37, 43-47]. Furthermore, these annelated quinolizinium derivatives may serve as a useful platform for the design of intercalating dyes.

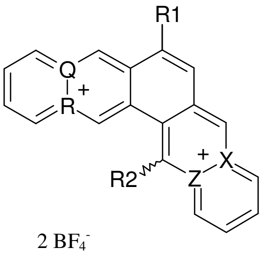

	Q	X	Y	Z	R1	R2
1a	N	N	C	C	H	H
1b	N	N	C	C	Me	Me
1c	C	N	N	C	H	Me
1d	C	N	N	C	H	H
1e	C	C	N	N	H	H

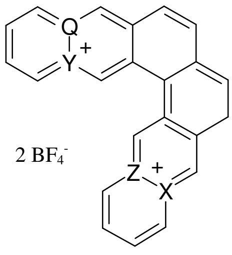

	Q	X	Y	Z
3a	C	C	N	N
3b	N	N	C	C
3c	C	N	N	C

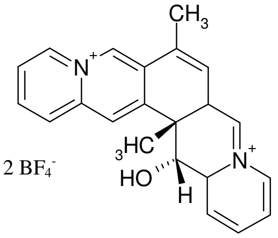

2

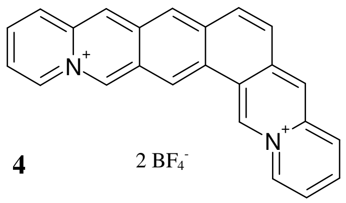

4

Figure 3.1 Chemical structures of penta- and hexacyclic derivatives of quinolizinium ion.

The association of these compounds with DNA induces modification on their spectroscopic properties. The absorption of circular or linearly polarized light can be used in circular dichroism (CD) and linear dichroism (LD) spectroscopy to gain some informations about the orientation of the dye molecule relative to the DNA and to deduce the binding mode. Moreover, there is also an influences on the absorption and emission properties, so that interaction of the compounds with DNA may be evaluated qualitatively and quantitatively by spectrophotometric and spectrofluorimetric titrations. These spectroscopic methods are especially advantageous because organic dyes absorb and emit at wavelengths that do not interfere with the absorption of DNA bases (λ_{max} ~ 260 nm).

3.2 CIRCULAR DICHROISM SPECTROSCOPY

Circular dichroism (CD) is defined to be the differential absorption of right- and left-handed circularly polarized light. Although circular dichroism is not observed for achiral molecules, when they form complexes with DNA, they are placed within a chiral environment and give an induced CD (ICD) signal. The ICD results from non-covalent interaction between the bound dye and the double helix of DNA, so it confirms the dye-DNA interaction and might provide further information about the position of the molecule in its complex with the double helix. Usually, an intercalator has a weak and negative ICD signal, while a groove binder give a relatively strong positive ICD. Otherwise, this is a general remark; there are many experimental data that prove the opposite theory. So it is necessary to give a proper interpretation of the spectra and to compare them to other type of investigation to gain the correct results [148, 149].

Thus aqueous solution of achiral acridizinium salts have no CD activity, while the macromolecule of B-DNA has a spectrum characterized by a negative band at $\lambda \sim 240$ nm, and a positive one at $\lambda \sim 270$ nm. The CD spectra of all compounds (Fig. 3.2) exhibit a perturbation of both positive and negative bands of DNA in the presence of increasing concentrations of dyes. Additionally, an ICD signals are observed in the regions of the absorption of the ligands (300-450 nm), which are mostly negative. However, in the case of the pentacyclic derivatives **1d** and, particularly, **1e**, a weak positive ICD were observed. The compound **2** does not leads to a significant changes in the CD spectrum of the double helix, also at high ligand-to DNA ratios, and a weak ICD signals were observed. The hexacycles **3a** and **3b**, at higher dye-to DNA ratios, present a bi-signate ICD signals with additional weak positive bands which are indicative of the exciton interaction between the bound ligands. These exciton bands presumably arise because of aggregation of the dye and association of these aggregates with the DNA backbone. The spectra of the hexacyclic derivative **4** reveal a bathochromic shift of the positive CD signal of the macromolecule and an isoelliptic point at 280 nm was observed and then it presents a strong well-resolved positive ICD in the region of absorption of the compound.

Finally, the spectra of the different ligands show both some changes of the CD signal of DNA and positive ICD signals, and these data confirm the interaction of the derivatives with the double helix of DNA, but it is difficult, at the moment, deduced the geometry of the binding. Detailed considerations can be done about the compounds **2** and **4** because while the pentacycle exhibits a weak affinity toward the macromolecule, the hexacycle presents a very strong-defined signal, typical of the groove binders.

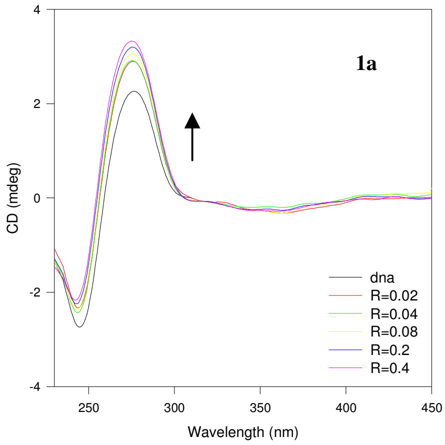
1a
CD (mdeg)
4
2
0
-2
-4
250
300
350
400
450
Wavelength (nm)
dna
R=0.02
R=0.04
R=0.08
R=0.2
R=0.4

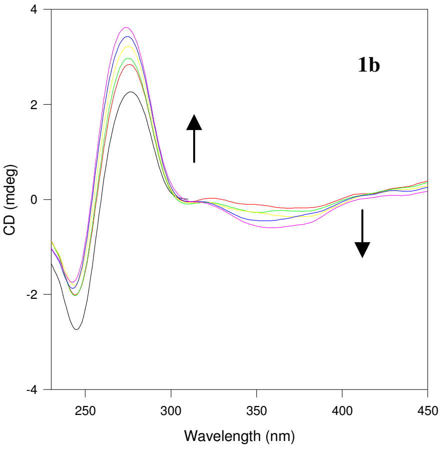
1b
CD (mdeg)
4
2
0
-2
-4
250
300
350
400
450
Wavelength (nm)

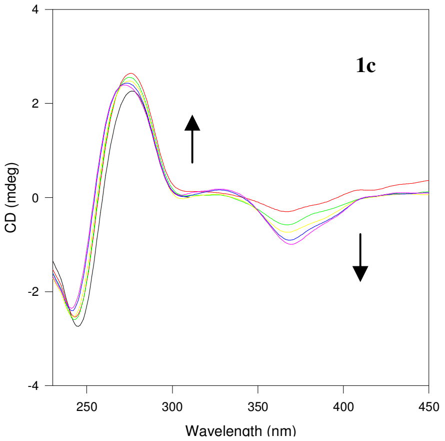
1c
CD (mdeg)
4
2
0
-2
-4
250
300
350
400
450
Wavelength (nm)

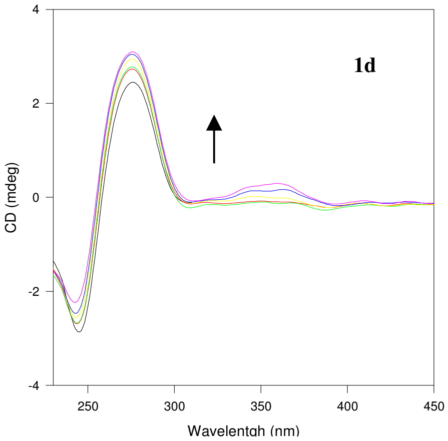
1d
CD (mdeg)
4
2
0
-2
-4
250
300
350
400
450
Wavelength (nm)

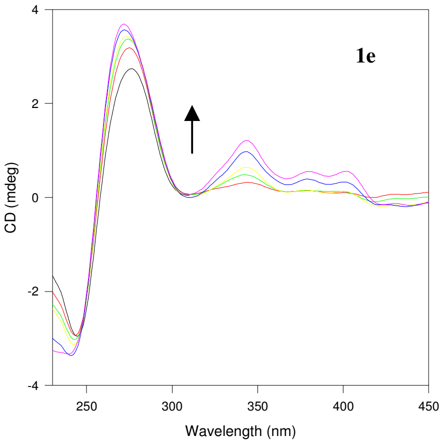
1e
CD (mdeg)
4
2
0
-2
-4
250
300
350
400
450
Wavelength (nm)

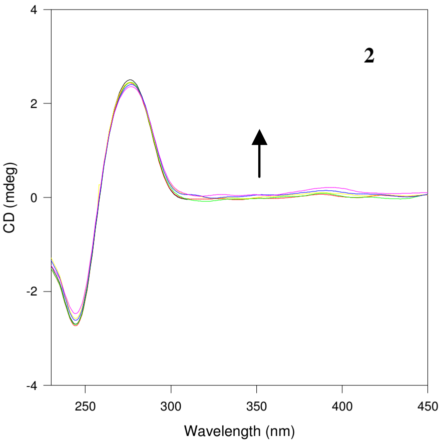
2
CD (mdeg)
4
2
0
-2
-4
250
300
350
400
450
Wavelength (nm)

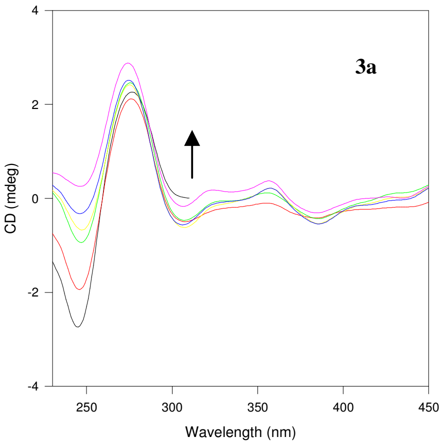
3a
CD (mdeg)
4
2
0
-2
-4
250
300
350
400
450
Wavelength (nm)

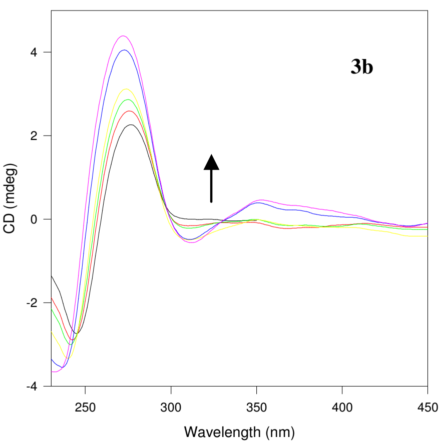
3b
CD (mdeg)
4
2
0
-2
-4
250
300
350
400
450
Wavelength (nm)

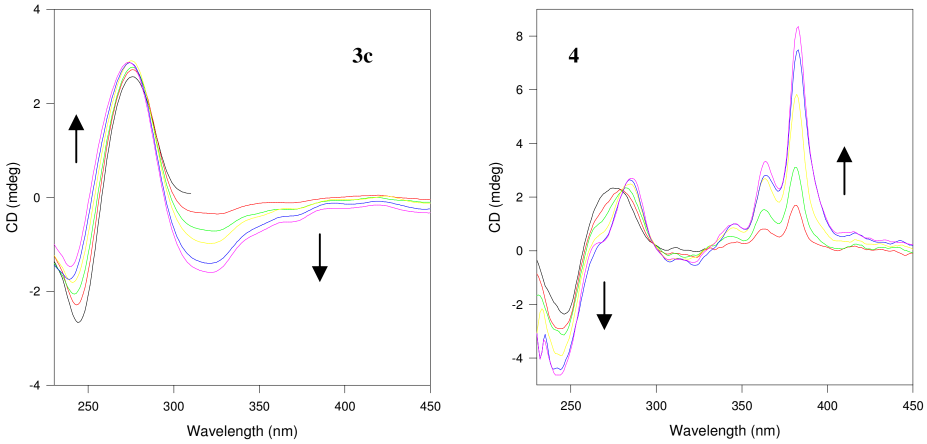

Figure 3.2 CD spectra of the compounds in the presence of stDNA (30 µM) at different ligand-to-DNA ratios (*r* = 0, 0.02, 0.04, 0.08, 0.2, 0.4).

3.3 LINEAR DICHROISM SPECTROSCOPY

Linear dichroism is defined as the differential absorption of linearly polarized light. For determination of the binding mode of a dye-DNA complex, flow-LD spectroscopy has been shown to be very useful. In a hydrodynamic field most of the DNA molecules are partially arranged along the flow lines (with the flow lines as reference axis, α ~ 90°), so that the DNA bases afford a clear negative LD signal (λ ~ 260 nm). Consequently an intercalator should also give a negative LD signal, because the coplanar arrangement. In contrast a groove binder should give a positive signal, which is relatively weak compared with that of an intercalator [148, 150].

The LD signals of the complexes of DNA with the dyes are negative at different ligand-to-DNA ratios, both in the UV region and a longer wavelengths, where only the molecules absorb (300-450 nm) (Fig. 3.3, top panels). The negative LD signals in the long-wavelength region indicate that the ligands are coplanar with the nucleic bases upon binding with DNA. The addition of the compounds also lead to a significant increase in the magnitude of the LD signal of the absorption band of DNA bases, which usually reveals stiffening of the DNA molecule and a better orientation of the double helix along the flow lines.

In the case of the compound **2**, only a weak LD signal in the region of the ligand absorption was observed in the presence of DNA. Interestingly, the signal is negative at low ligand-to DNA ratios but becomes bi-signate at higher ligand loading (*r* = 0.2). At the same time, the addition of this compound to DNA results in a moderate decrease in the magnitude of the LD signal of the DNA bases, which indicate a weak interaction between dsDNA and the molecule.

The hexacycle **4** reveals a negative LD signal in the region of the absorption of the chromophore, typical of intercalation. This result is in contrast with the data obtained from CD spectrum, but whereas circular dichroism is useful to check an interaction with DNA, linear dichroism gives proper information about the geometry of binding.

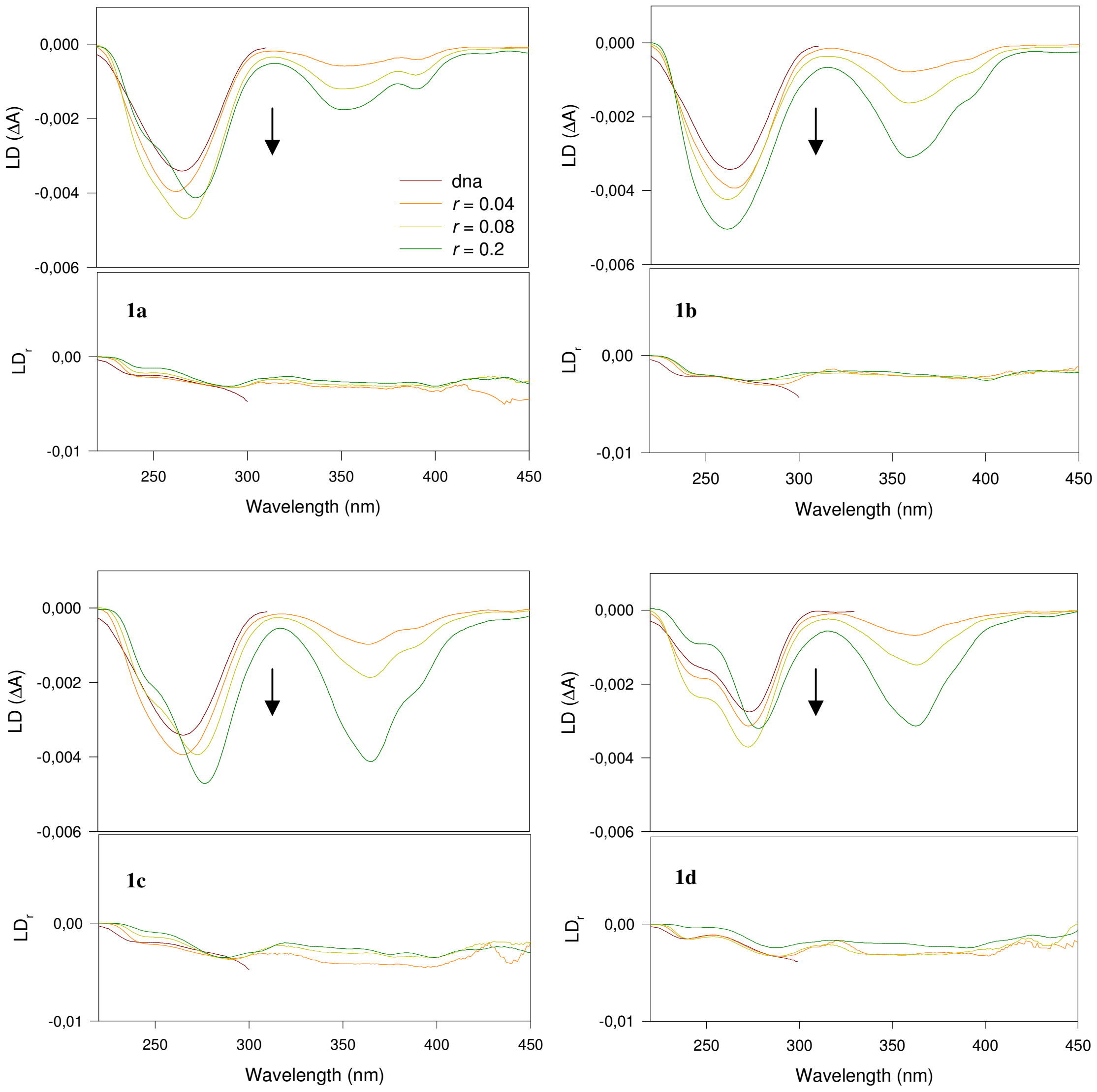

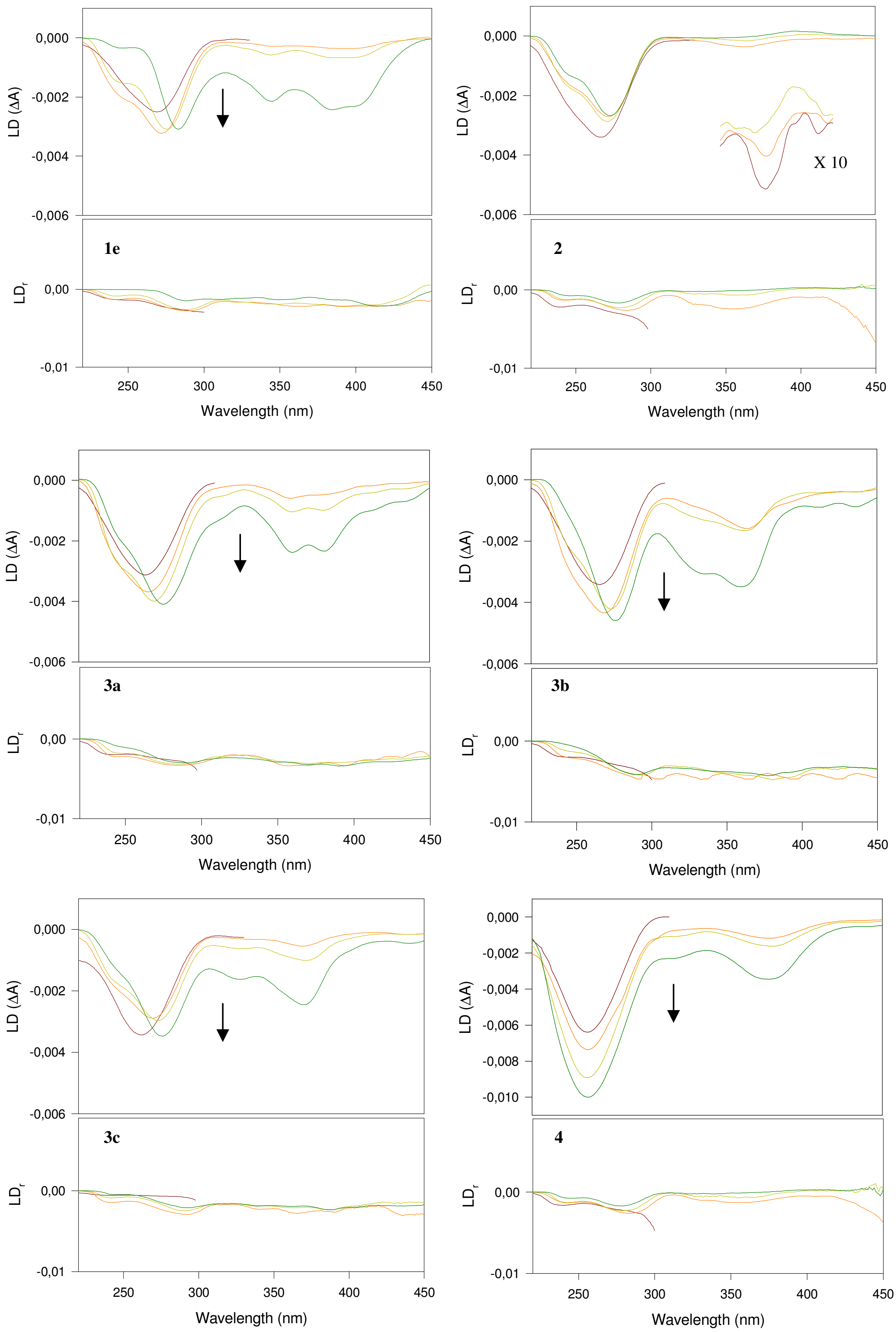

Figure 3.3 Linear dichroism (LD, top panels) and reduced LD (LD$_r$, bottom panels) spectra of the compounds in the presence of stDNA (2.72 mM) at different ligand-to DNA ratios (r = 0, 0.04, 0.08, 0.2). The more intense LD signals of DNA and compound **4** result from a new setup of the instrument, which allows a better orientation of the macromolecule in the flow cuvette.

The “reduced” linear dichroism (LDr), i.e., the wavelength-dependent LD, is obtained by dividing the LD value by the absorbance of the unoriented sample. The reduced LD spectra (Fig. 3.3, bottom panels) of DNA-ligand complexes provide further information about the average of orientation of the molecular plane of the aromatic dye relative to those of the DNA bases and allow to distinguish between homogeneous and heterogeneous binding. Practically constant LDr spectra were observed in the region of the absorption of the chromophore at all ligand-to-DNA ratios, which confirms that one binding mode is adopted almost exclusively under these conditions. In contrast to the other derivatives, the reduced LD spectrum of the pentacycle **2** indicates an inhomogeneous binding mode, i.e., at low ligand concentrations it binds by intercalation with low affinity, whereas at higher concentrations an additional binding mode takes place, presumably the outside stacking, with a different orientation of the dye.

3.4 SPECTROPHOTOMETRIC TITRATIONS

In a complex with DNA the guest molecule is positioned in an environment which is different from that of the uncomplexed compound in solution. The guest molecules usually have different absorption properties in the complexed and uncomplexed forms. Thus, on addition of DNA to a solution of an intercalator or groove binder, a shift of the absorption maximum to longer wavelengths (bathochromic shift or red shift) and a decrease of the absorbance (hypochromicity) occurs. In practice the association process is monitored by a spectrophotometric titration, during which aliquots of DNA solution are added to a solution of the guest molecule and the absorption spectra at each dye-to-DNA ratios are determined.

The spectrophotometric titrations of all compounds were monitored in an aqueous buffer with stDNA (Fig. 3.4). The absorption maximum of most derivatives exhibit a bathochromic shift of 5-10 nm upon formation of a complex with DNA, relative to the free ligands (Table 2). A significant decrease of the absorbance takes place (hypochromism) with a partial loss of the fine structure of the absorption bands; this is indicative of an associative interaction between the dyes and the macromolecule. Further information might be extracted from the titrations if isosbestic point are observed. They appear when each absorption spectrum of the titration has the same absorbance at a particular wavelength, i.e., a point of intersection in all absorption spectra (Table 2).

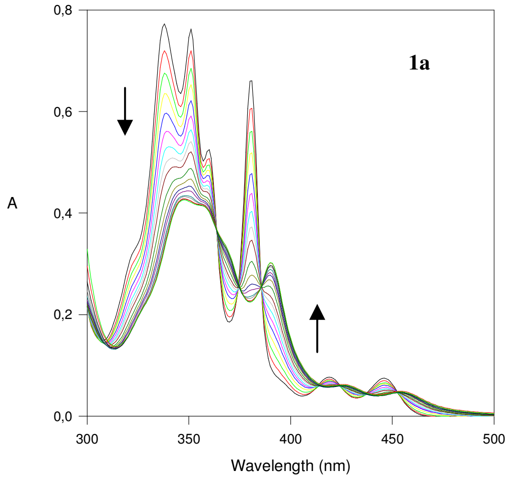

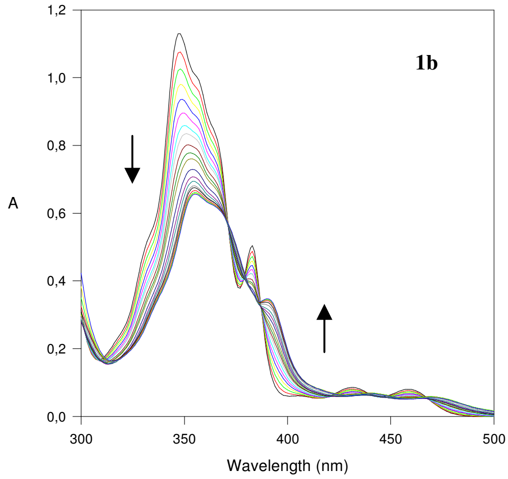

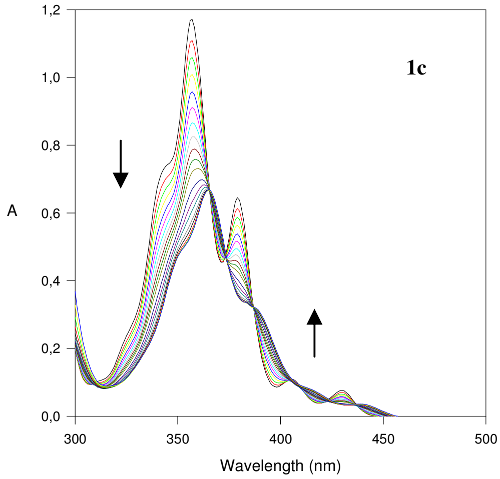

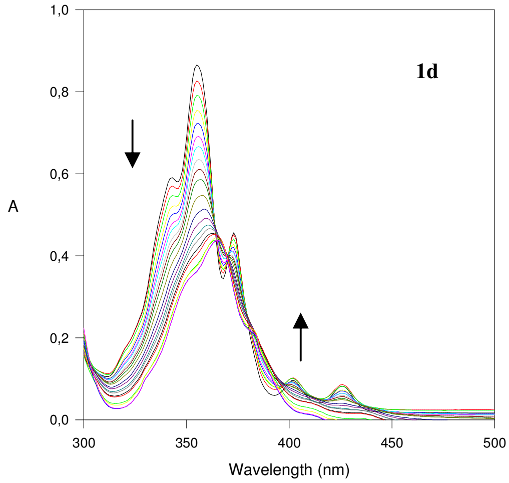

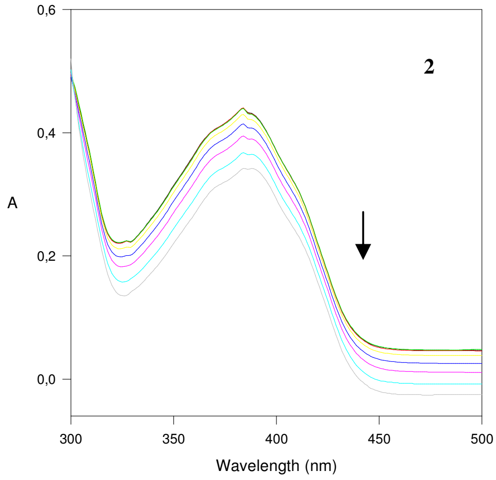

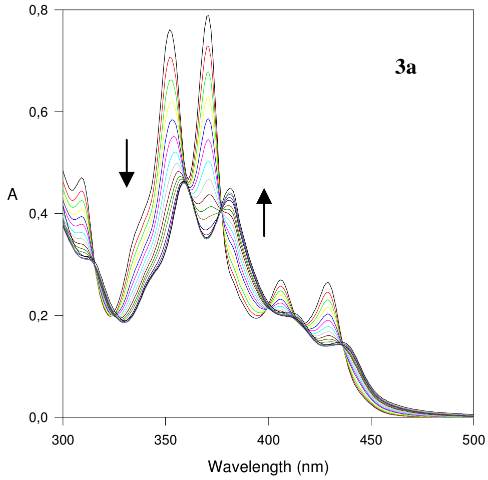

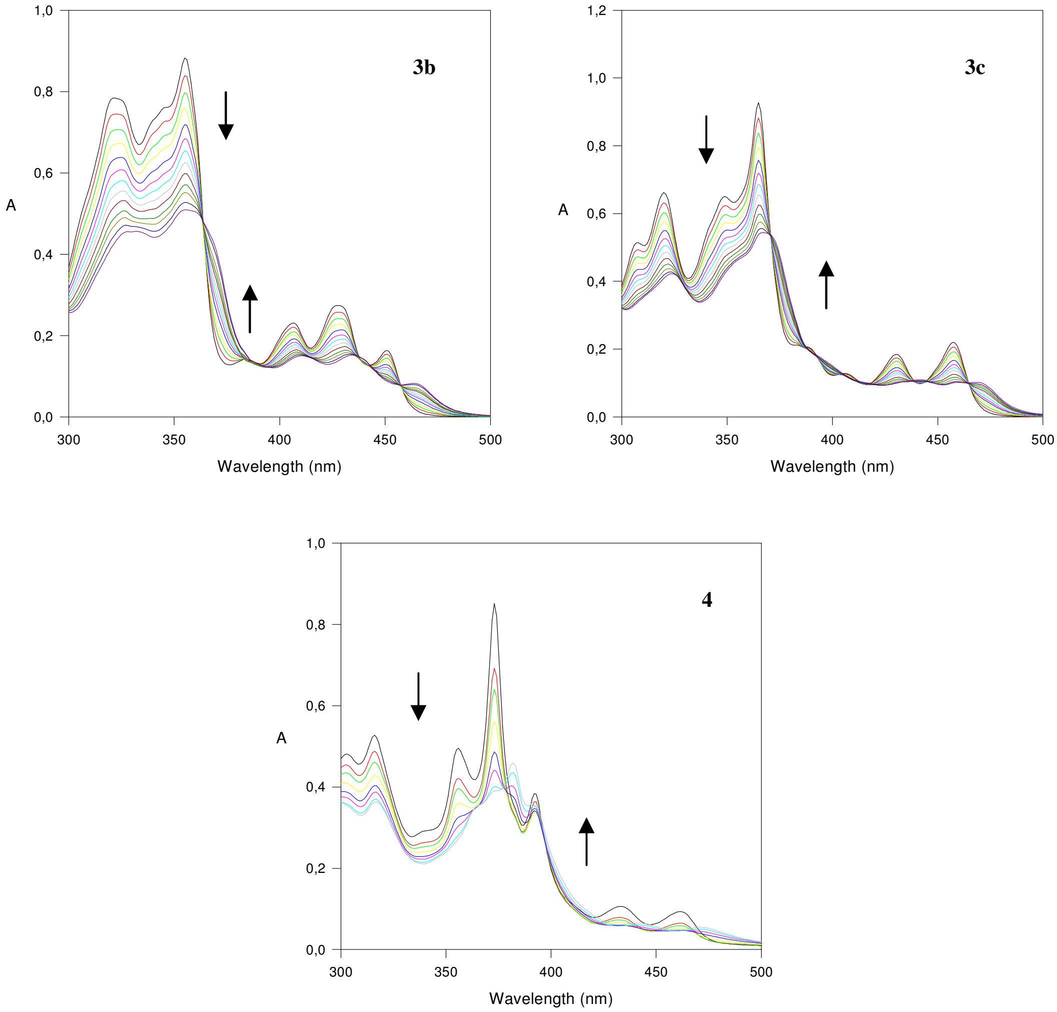

Figure 3.4 Spectrophotometric titrations of stDNA (0-0.1 mM) to all compounds at a ligand concentration of 20 µM, in ETN aqueous buffer at 25°C. Arrows indicate the changes of the intensity of the absorption bands upon addition of stDNA.

Such isosbectis points reveal that each absorption spectrum arises from almost exclusively two different species (i.e., complexed and uncomplexed dye). Because it is likely that each binding mode results different absorption properties, an isosbestic point indicates that mainly one particular binding mode between the DNA and the guest molecule occurs.

The pentacycle **2**, after the addition of DNA, shows only a minor hypochromic effect. No isosbestic point is detected. These data confirm the result obtained from circular and linear dichroism. In the case of the hexacycle **4**, was observed only hypochromism but no red shift. Upon addition of DNA, another species takes place, with a maximum at 381 nm. It can also be observed two different isosbestic points: the first one at low concentration of DNA, before the appearance of the second specie; the other at high concentration. These data suggest the idea that the derivative can interact with DNA with two different binding mode: at low dye-to-DNA ratios as an intercalator whereas at high ratios as a groove binder. This result is supported by the assumed contrasting data obtained from circular and linear dichroism.

Data from spctrophotometric titrations can also be utilized to determine the association constant (*K*) between the dye and DNA and absorbance data (A_{obs}) at fixed wavelength are used to calculate the concentration of bound dye (C_b), the concentration of uncomplexed dye (C_b) and the number of bound dye molecules per base pair (*r*) while the absorbance of the bound dye (A_b) is acquired from the absorption spectrum at full saturation (for detailed description see experimental procedures, section 6.2.3.3). All these data are exploited to obtained the Schatchard plot [151] (Fig. 3.5), that is a plot of *r/c* against *r*. Binding analysis of the experimental data is performed according to the model developed by McGhee and von Hippel [152] to determine the binding constant (*K*) and the binding site-size (*n*) (Table 2).

Table 2 DNA binding constants (*K*), binding-site size and isosbestic points of the penta- and hexacyclic derivatives.

COMPOSTI	**Δλ (nm) (bathochromic shift)**	**K (10^5 M^{-1})[a]**	***n* / bp[b]**	**Isosbestic points**
1a	10 nm	1.8±0.1	2.0±0.1	364[d], 374, 385 nm
1b	8 nm	1.8±0.1	2.5±0.2	371[d], 380, 386 nm
1c	10 nm	1.8±0.2	2.5±0.2	365[d], 374, 387 nm
1d	5 nm	1.2±0.1	2.5±0.2	363[d], 370, 378 nm
1e[c]	12 nm	5.7±0.2	2.8±0.2	311, 345, 398 nm
2	n.d.[e]	n.d.	n.d.	n.d.
3a	11 nm	6.4±0.3	2.0±0.1	315[d], 377 nm
3b	6 nm	4.6±0.2	2.0±0.1	363[d] nm
3c	6 nm	5.0±0.3	2.2±0.2	371[d] nm
4	n.d.	6.2±0.3	2.0±0.1	399[d] nm

[a] Apparent binding constants. [b] Binding-site size (in base pairs) calculated from fitting according to the McGhee and von Hippel model. [c] From ref. 45 and from spectrofluorimetric titrations with ctDNA. [d] λ_{exc} used for spectrofluorimetric titrations. [e] n.d.= not determined.

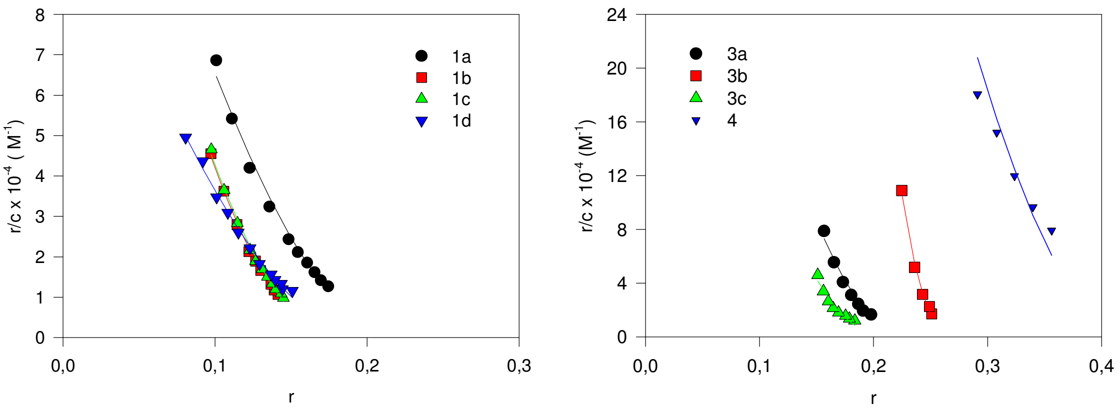

Figure 3.5 Schatchard plots of spectrophotometric titrations of stDNA. Symbols represent the experimental data, while solid lines are the best fit of the experimental data to the McGhee and von Hippel equation [155]. Left panel: pentacyclic derivatives; right panel: hexacyclic derivatives.

The binding constant depends on the structure of the compounds. All pentacycles have similar *K* (1-2 x 10^5 M^{-1}), whereas the hexacyclic derivatives have higher DNA affinity. For the compound **2** was impossible to calculate the binding constant because its low affinity for DNA, as previously demonstrated. In the case of **4** was used only the first part of titration to determine the value of *K*, and probably it is the combination of at least two binding constants, as the photometric DNA titration indicates more than one binding mode, and the two binding constants could not be resolved from the available data. The binding-site size (*n*) is a measure of the binding sites (i.e., base pairs) occupied by one guest molecule and give additional information about the binding mode. Thus, a significant difference between the binding-site size of intercalator and groove binders is observed. According to the neighbour-exclusion principle, an intercalator occupies two binding site, so that at full saturation, an alternating sequence of occupied and free binding sites is observed. Thus, perfect intercalators have a binding-site size of *n*=2. A groove binder, however, covers several base pairs on binding to DNA, so *n* is significantly larger than 2. For all derivatives , the number of base pairs were *n*=2.0-2.5 bp, so, according to the neighbour-exclusion principle, the compounds interact with the double helix by an intercalative mode of binding. These data confirm the results obtained from circular and linear dichroism. For the pentacycle AG 101 was impossible to calculate the binding-site size, as previously mentioned, while for the hexacycle AG 150 the value obtained is referred only at the first part of titration, at low ligand-to-DNA ratios.

The values of *K* and *n* for the compound **1e** were already been demonstrated [45].

3.5 SPECTROFLUORIMETRIC TITRATIONS

If a molecule has emission properties such as fluorescence or phosphorescence, addition of DNA can result in a bathochromic shift of the emission maximum, as in the spectrophotometric titrations. More significantly, the emission intensity can change on complex formation and might be observed either an increase or a decrease of intensity maximum. It must, nevertheless, be consider that the absorption at a particular wavelength also changes on the DNA addition, which also leads to a modification of the emission intensity on excitation at this wavelength. To avoid this secondary effect, which does not reflect the direct influence of the DNA on the dye emission properties, the fluorophore should be excited at the isosbestic point, which is obtained from spectrophotometric titrations.

On addition of stDNA, the fluorescence is significantly quenched (Fig. 3.6); however a shift of red maximum was not observed. It may be concluded that the emission of DNA-bound derivatives is totally quenched and the observed reduced fluorescence results solely from the non-associated dye molecule. It could be noticed that the affinity to DNA of hexacyclic derivatives are larger than that of the pentacycle (Fig. 3.7). Such an efficient quenching of the excited state usually requires a close proximity between the fluorophore and the quencher, which is realized in an intercalative binding mode. The compound **2** shows a decrease of emission maximum but it is due to of the λ_{exc} used and not of the quenching of stDNA. For the derivative **4** was utilized as λ_{exc} the value of the isosbestic point of the first part of the spectrophotometric titration.

These data confirmed the results obtained from previous experiments.

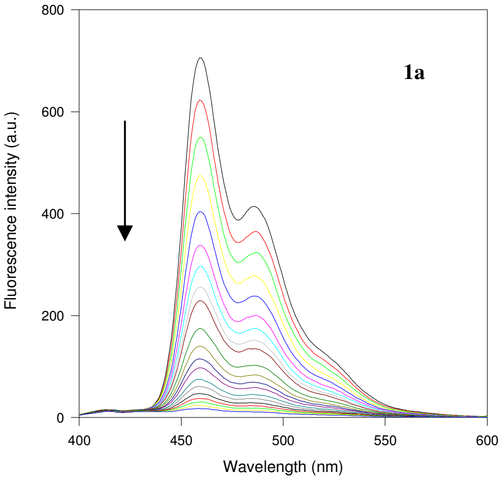
1a
Fluorescence intensity (a.u.)
0
200
400
600
800
Wavelength (nm)
400
450
500
550
600

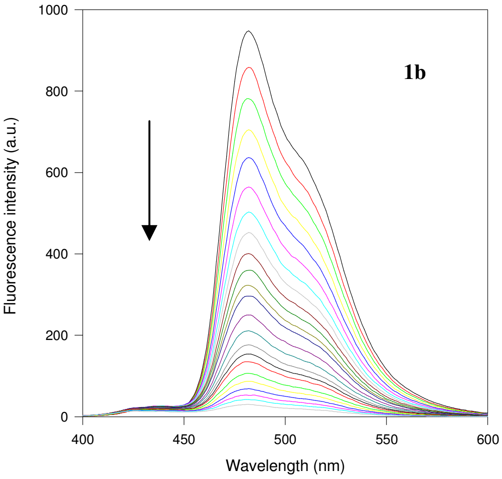
1b
Fluorescence intensity (a.u.)
0
200
400
600
800
1000
Wavelength (nm)
400
450
500
550
600

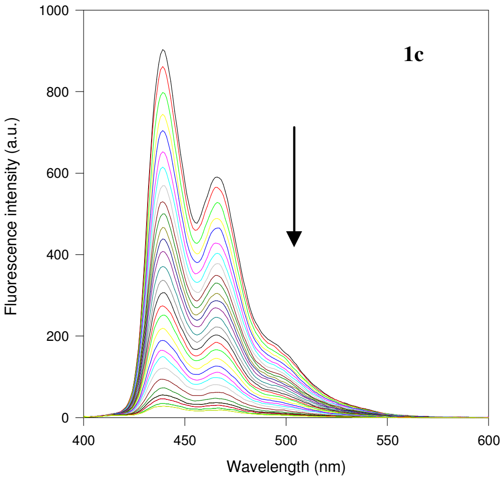
1c
Fluorescence intensity (a.u.)
0
200
400
600
800
1000
Wavelength (nm)
400
450
500
550
600

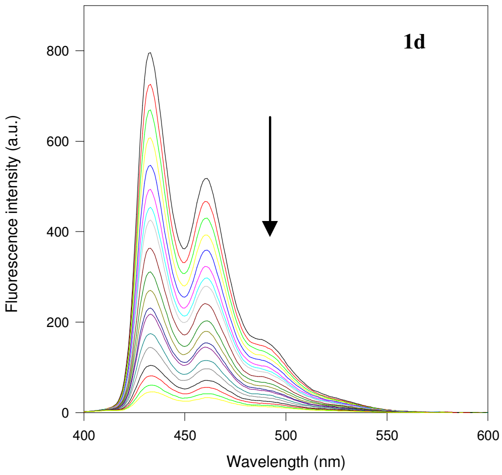
1d
Fluorescence intensity (a.u.)
0
200
400
600
800
Wavelength (nm)
400
450
500
550
600

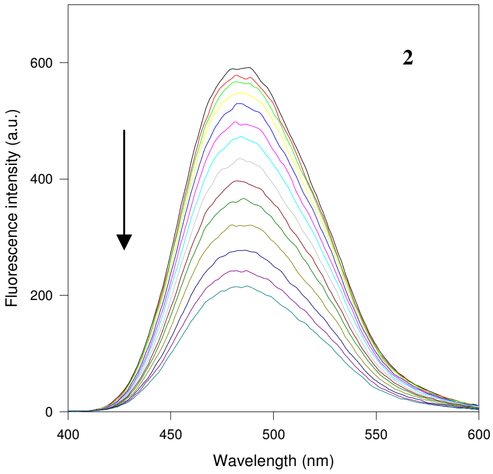
2
Fluorescence intensity (a.u.)
0
200
400
600
Wavelength (nm)
400
450
500
550
600

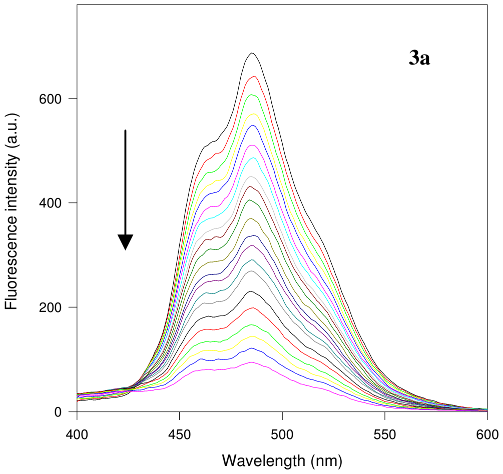
3a
Fluorescence intensity (a.u.)
0
200
400
600
Wavelength (nm)
400
450
500
550
600

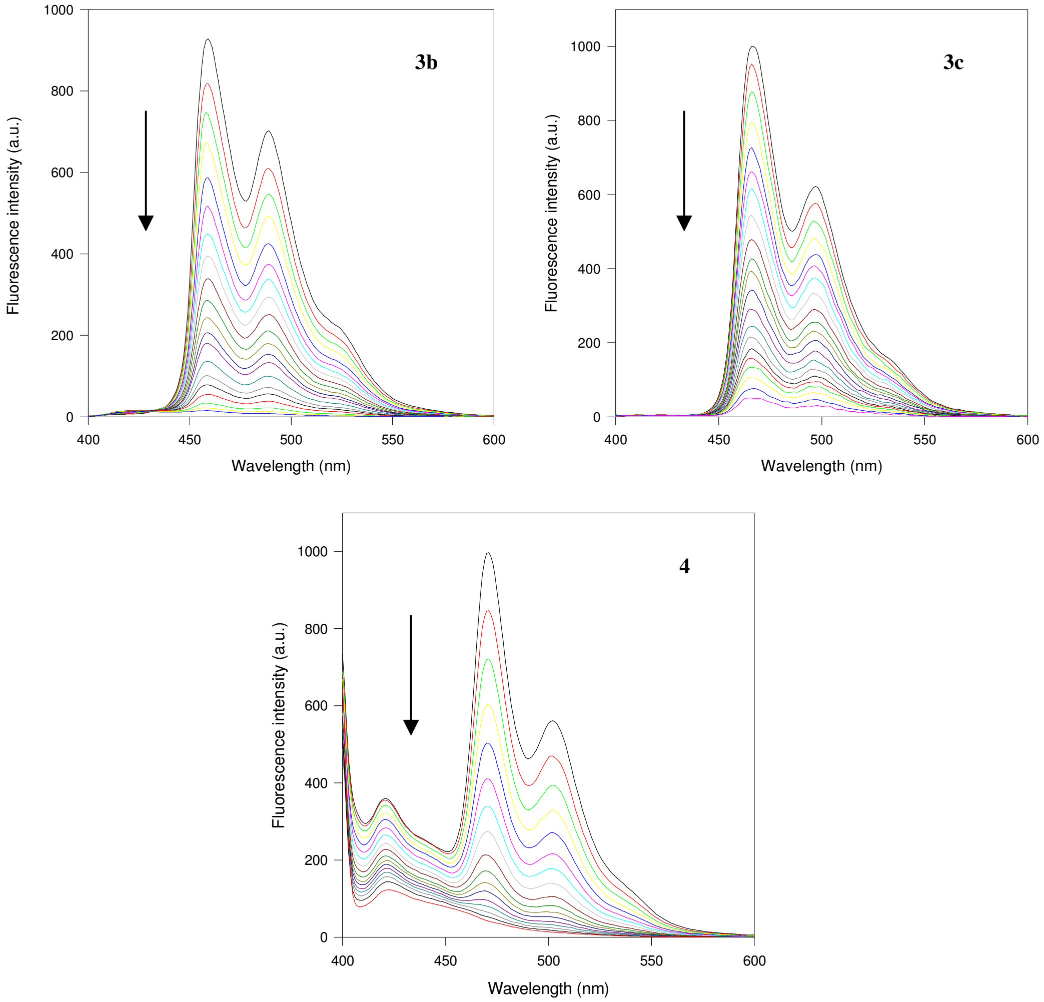

Figure 3.6 Spectrofluorimetric titrations of stDNA (0-0.1 mM) to all compounds, in ETN aqueous buffer at 25°C. [Pentacycle]=2 μM; [Hexacycle]=1 μM. The dyes were excited at the isosbestic point found in the spectrophotometric titrations (Table 1). Arrows indicate the changes of the intensity of the emission bands upon addition of stDNA.

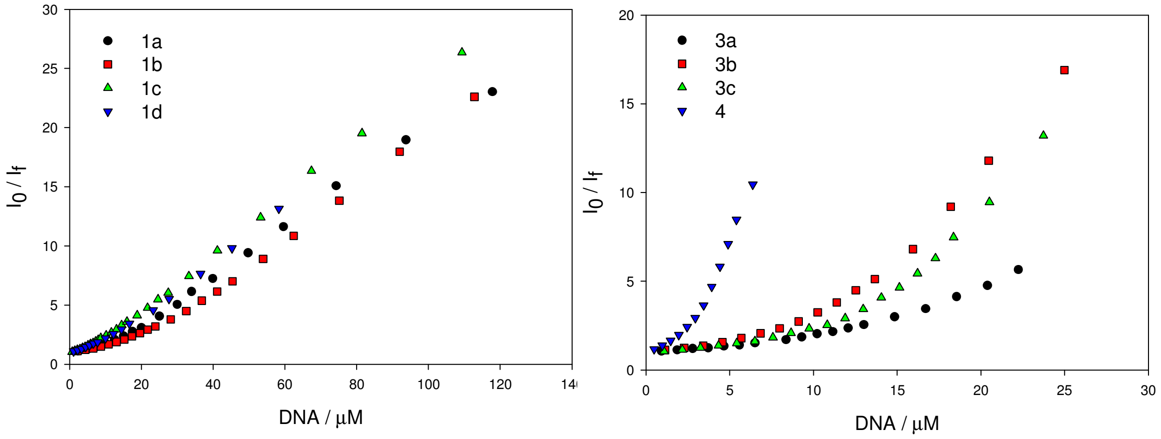

Figure 3.7 Fluorescence quenching of the compounds on addition of stDNA. Left panel=pentacyclic derivatives; right panel=hexacyclic derivative.

3.6 DNase I FOOTPRINTING

DNase I footprinting assay is a method of studying DNA-protein or DNA -drug interaction and identifying the DNA sequence to which a ligand binds. First, a target DNA fragment, about 100-300 bp in length, is either PCR generated or cut from a vector and then uniquely ^{32}P-5'or -3' labeled (at only one end) and incubated with guest molecule, followed by controlled digestion with a specific enzyme, usually the deoxyribonuclease DNase I, which cuts the probe randomly but only once. The digested DNA is recovered from the reaction and resolved on a polyacrylamide gel along with G+A chemical sequencing reaction which uses the same probe as template. The regions bound by ligand will be protected from DNase I digestion and will be shown as a blank area on the gel track, while the exact ligand-bound sequence can be read out by comparing the location of the blank with the sequencing reaction. By varying the concentration of the ligand, its binding affinity can be estimated.

Footprinting experiments were carried out using two DNA fragments having different arrangement of base pairs and different length. Both probes were used as substrates for the endonuclease DNase I, which is a sensitive enzyme for mapping DNA-binding sites of small molecules [153-155]. In both cases, the products of digestion, after the action of DNase I by the probes in the absence and in the presence of the selected compound, were resolved by polyacrylamide gel electrophoresis. The 5'-labeled fragment are called IM 18/20, with AT rich sequences, and pUC 18, a DNA restriction fragment obtained from the digestion of the plasmid pUC 18 with the restriction enzyme Hind III, with GC rich sequence (Fig. 3.8). These two probes were chosen in order to distinguish a potential site selectivity toward particular sequences along the double helix.

IM 18/20 (132-bp)

5′- ATGCTC CAGA AAGCCGGCAC TCAGTCTACA AACGCGTCAT CCTTGATCAT
3′- TACGAGGTCT TTCGGCCGTG AGTCAGATGT TTGCGCAGTA GGAACTAGTA

GCATGTTCAC AGAAATTTCT CTAGATCTAA GCTAAACTCT AGTACTAGTC
CGTACAAGTG TCTTTAAAGA GATCTAGATT CGATTTGAGA TCATGATCAG

TTCAAGCAAG TGGAGCTCTC CTAACCGACT TT -3′
AAGTTCGTTC ACCTCGAGAG GATTGGCTGA AA -5′

pUC 18 (236-bp)

5′- GTCGTTCGGC TGCGGCGAGC GGTATCAGCT CACTCAAAGG CGGTAATACG
3′- CAGCAAGCCG ACGCCGCTCG CCATAGTCGA GTGAGTTTCC GCCATTATGC

GTTATCCACA GAATCAGGGG ATAACGCAGG AAAGGAACATG TGAGCAAAAG
CAATAGGTGT CTTAGTCCCC TATTGCGACC TTTCCTTGTAG ACTCGTTTTC

GCCAGCAAAA GGCCAGGAAC CGTAAAAAGG CCGCGTTGCT GGCGTTTTTC
CGGTCGTTTT CCGGTCCTTG GCATTTTTCC GGCGCAACGA CCGCAAAAAG

CATAGGCTCC GCCCCCCTGA CGAGCATCAC AAAAATCGAC GCTCAAGTCA
GTATCCGAGG CGGGGGGACT GCTCGTAGTG TTTTTAGCTG CGAGTTCAGT

GAGGTGGCGA AACCCGACAG GACTATAAAG ATACCA -3′
CTCCACCGCT TTGGGCTGTC CTGATATTTC TATGGT -5′

Figure 3.8 Sequence of the two radiolabeled fragments used: IM 18/20 and pUC 18.

The compound tested is the hexacycle **3b** because the high affinity toward DNA demonstrated in the previous experiments.

DNase I footprinting was initially performed using IM 18/20. This 132-bp DNA fragment was incubated with increasing concentrations of the selected compound (0-10 μM) for 3h at 37°C to establish equilibrium, and then the samples were exposed to DNase I. The autoradiogram (Fig. 3.9) reveals the presence of only one binding site but with a weak interaction, so the hexacycle shows a low affinity toward sequence of DNA rich in adenine and thymine.

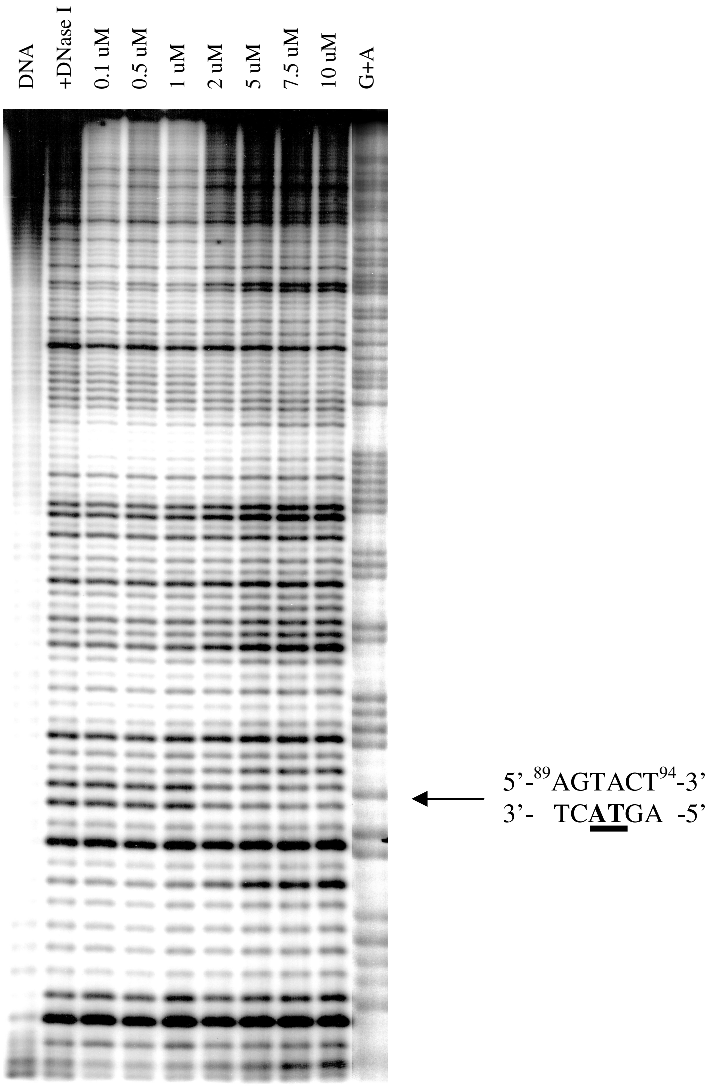

Figure 3.9 Dnase I footprinting of **3b** on the 132-bp fragment IM 18/20. [**3b**]= 0 μM, 0.1 μM, 0.5 μM, 1 μM, 2 μM, 5 μM, 7.5 μM and 10 μM. The products of nuclease digestion were resolved on a 10% polyacrylamide gel containing 8 M urea. DNA lane: fragment alone; +Dnase I lane: fragment of DNA digested with the enzyme without compound. G+A lane: marker specific for guanines and adenines obtained after treatment with piperidine (Maxam and Gilbert techniques) [156].

To further investigate the sequence selectivity of the hexacycle **3b**, additional footprinting experiments were carried out with the radiolabeled 236-bp Hind III restriction fragment from plasmid pUC 18, rich in guanine and cytosine. It can be seen from the autoradiogram (Fig. 3.10) that there are five binding sites (numbered 1-5). Sites 1 and 3 reveals a clearly affinity toward the double helix (< 2 μM), particularly for CG or CGXCG sequences (Fig. 3.11), while sites 2, ,4 and 5 show a weaker interaction toward the selected fragment (> 10-15 μM).

This study constitutes the first characterization of the DNA sequence recognition properties of the quinolizinium derivative **3b**, which demonstrate a clear affinity for CG rich sequence and a weak binding toward adenine and thymine. Otherwise, it will be useful to perform some experiment with 3’-labeled fragments to confirm these previous results.

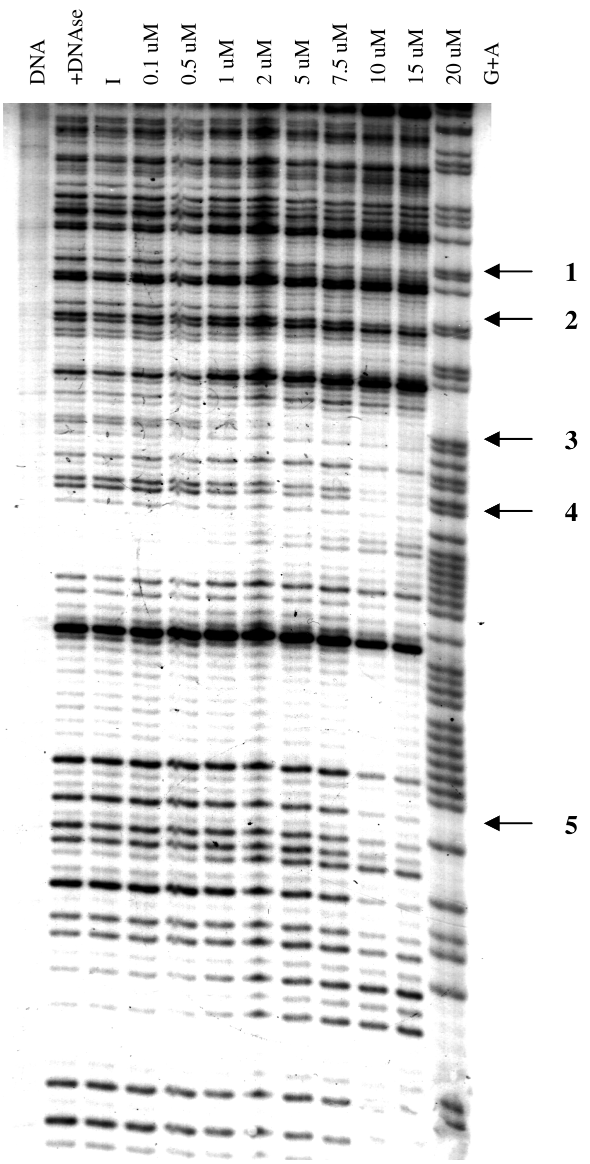

Site 1
5’-^{99}AGGCCA^{104}-3’
3’- TC**CG**GT -5’

Site 2
5’-^{108}AAAGGC^{113}-3’
3’- TT**TC**CG -5’

Site 3
5’-^{128}AGGCCGCG^{135}-3’
3’- TC**CG**G**CG**C -5’

Site 4
5’-^{137}TGCTGGCG^{144}-3’
3’- A**CG**AC**CG**C -5’

Site 5
5’-^{167}CTGACG^{172}-3’
3’- GA**CT**GC -5’

Figure 3.10 Left panel: Dnase I footprinting of **3b** on the 236-bp Hind III restriction fragment of plasmid pUC 18. [**3b**]= 0 μM, 0.1 μM, 0.5 μM, 1 μM, 2 μM, 5 μM, 7.5 μM, 10 μM, 15 μM and 20 μM. The products of nuclease digestion were resolved on a 10% polyacrylamide gel containing 8 M urea. DNA lane: fragment alone; +Dnase I lane: fragment of DNA digested with the enzyme without compound. G+A lane: marker specific for guanines and adenines obtained after treatment with piperidine (Maxam and Gilbert techniques) [156]. Right panel: sequence of binding sites from 1 to 5.

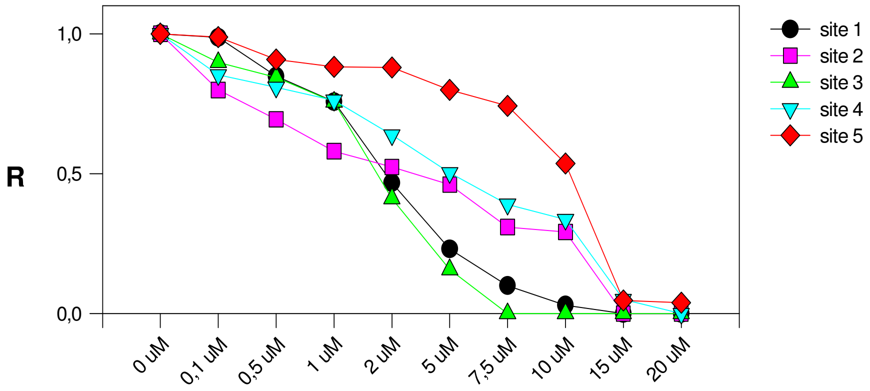

Figure 3.11 Footprinting plots for the binding of **3b** to sites 1-5. The relative band intensity R corresponds to the ratio I_c / I_o where I_c is the intensity of the band at the ligand concentration *c* and I_o is the intensity of the same band in the absence of the compound.

3.7 CONCLUSIONS ON DNA-BINDING PROPERTIES

In summary, the penta- and hexacyclic derivatives of quinolizinium ion are a useful class of compounds that bind strongly to the double stranded DNA. The DNA affinity is mainly determined by the shape of the polycyclic system and the two cationic charges, whereas both the position of the heteroatoms and the presence of additional substituents as methyl groups have a little influence on the DNA binding properties.

The results of all experiments are in agreement and reveal that the pentacyclic derivatives interact weakly with the macromolecule compared to hexacycle, but both by an intercalative mode of binding. Only the compound **4** results in a preferential groove binding mode at larger ligand-to DNA ratios, while at low ratios it interacts by intercalation. The binding constants (*K*) calculated for pentacycle are similar (1-2 x 10^5 M^{-1}), while hexacyclic derivatives have higher DNA affinity (~ 5 x 10^5 M^{-1}). CD spectroscopy investigations suggest the idea that only one part of the compounds is intercalated between the DNA base pairs, whereas the remaining part of the ligand points outside the intercalation pocket. The hexacycle **3b** seems to bind preferentially to GC rich sequence on double stranded DNA, and these consideration could be extended also to other derivatives, especially the other hexacycle. To further evaluate the correct binding-site, it will be useful to carried out some experiment with 3’-labeled DNA. Finally the extension of π system as well as the introduction of a second positive charge, provided by another quaternary nitrogen atom, strongly increase the affinity of the compounds toward the double helix of DNA, inducing a more stable complex than one created by the other tri- and tetracyclic and indolo derivatives already studied [37, 43-47].

4. DNA-PHOTOCLEAVAGING PROPERTIES

4.1 DNA-PHOTOCLEAVAGE

Nowadays there is a growing interest in new compounds which have photobiological effects as they can be applied as phototherapeutics agents. The photosensitization of cells and tissues using photoactive drugs has been exploited in variety of phototherapies for the treatment of multiple diseases. In fact in the last 20 years there was the development of dyes used for photodynamic therapy, in particular porphyrins and porphyrins-based compounds, or new psoralen derivatives to apply for the well-known PUVA (psoralen plus UV-A) therapy. Moreover, photosensitization approaches have also been investigated for antimicrobial use, disinfections of blood products as well as for wound closure in photochemical tissue bonding [77, 78, 88].

Planar polycyclic aromatic molecules are known to intercalate into double stranded DNA. Apart from the theoretical treatment of such host-guest interactions, the consequences of DNA intercalation by exogenous molecules have attracted considerable interest in medicinal chemistry because it may results in a hindered or suppressed function of the nucleic acid in physiological processes. The motivation for these studies increases if the DNA-targeted compounds are also photosensitizers against nucleic acids, because the light can be used then as a trigger for the nuclease activity. While the association of heterocycles compounds to DNA, and thus the DNA modification, is reversible process, the DNA damage, which frequently occurs on irradiation of drug-DNA complexes, is often irreversible, depending on the extent of DNA damage. The latter DNA damage often leads to cell death or mutations, and must be avoided in healthy system. However, it may be applied in photochemotherapy to remove unwanted cells [79, 80].

In order to investigate the DNA photocleavage activity of quinolizinium derivatives, the compounds were irradiated, in buffer aqueous solutions, in the presence of supercoiled DNA plasmid pBR322, at different dye-to-DNA ratios and at increasing UV-A doses. The photosensitized DNA-cleavage products were resolved by agarose-gel electrophoresis. In “dark conditions” the molecules do not promote any DNA strand breaks (Fig. 4.1). At low dye-to-DNA ratios (0.04-0.2), at which the dye is intercalated into DNA, no significant cleavage of the plasmid DNA was observed. As the ratios increase (0.8-2), i.e., the dye is externally bound to the macromolecule, a significant nicking of the supercoiled plasmid took place. Thus intercalation of the derivatives into double stranded DNA is not a prerequisite for DNA photocleavage.

The hexacyclic compounds are more active than pentacycle, with a more marked breaks also at dye-to-DNA ratio of 0.08, especially the derivatives **3c** and **4**. Only the pentacycle **1d** shows an activity similar to the hexacyclic derivatives.

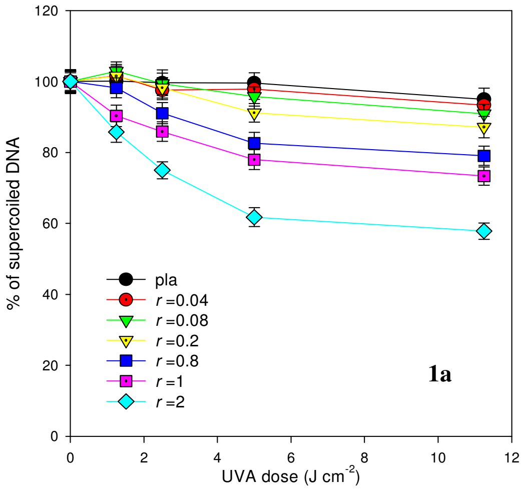

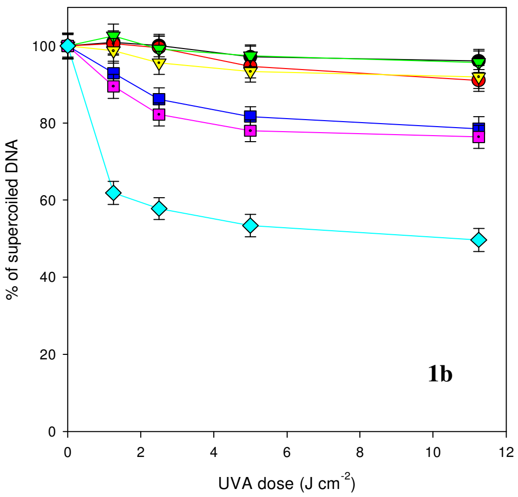

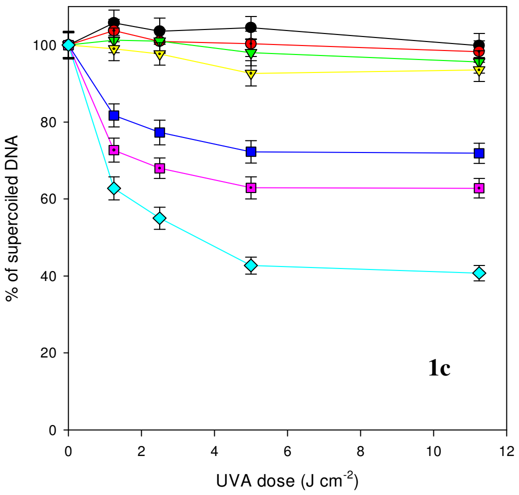

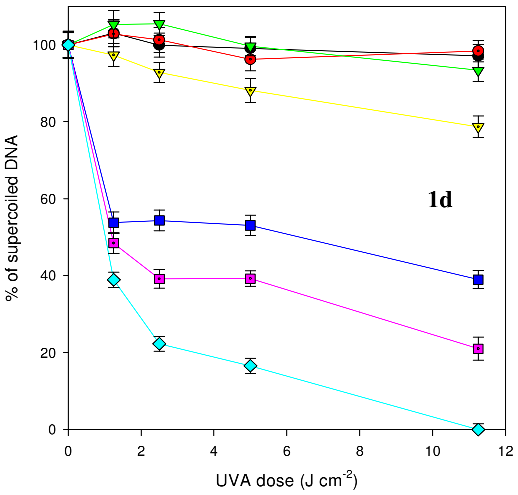

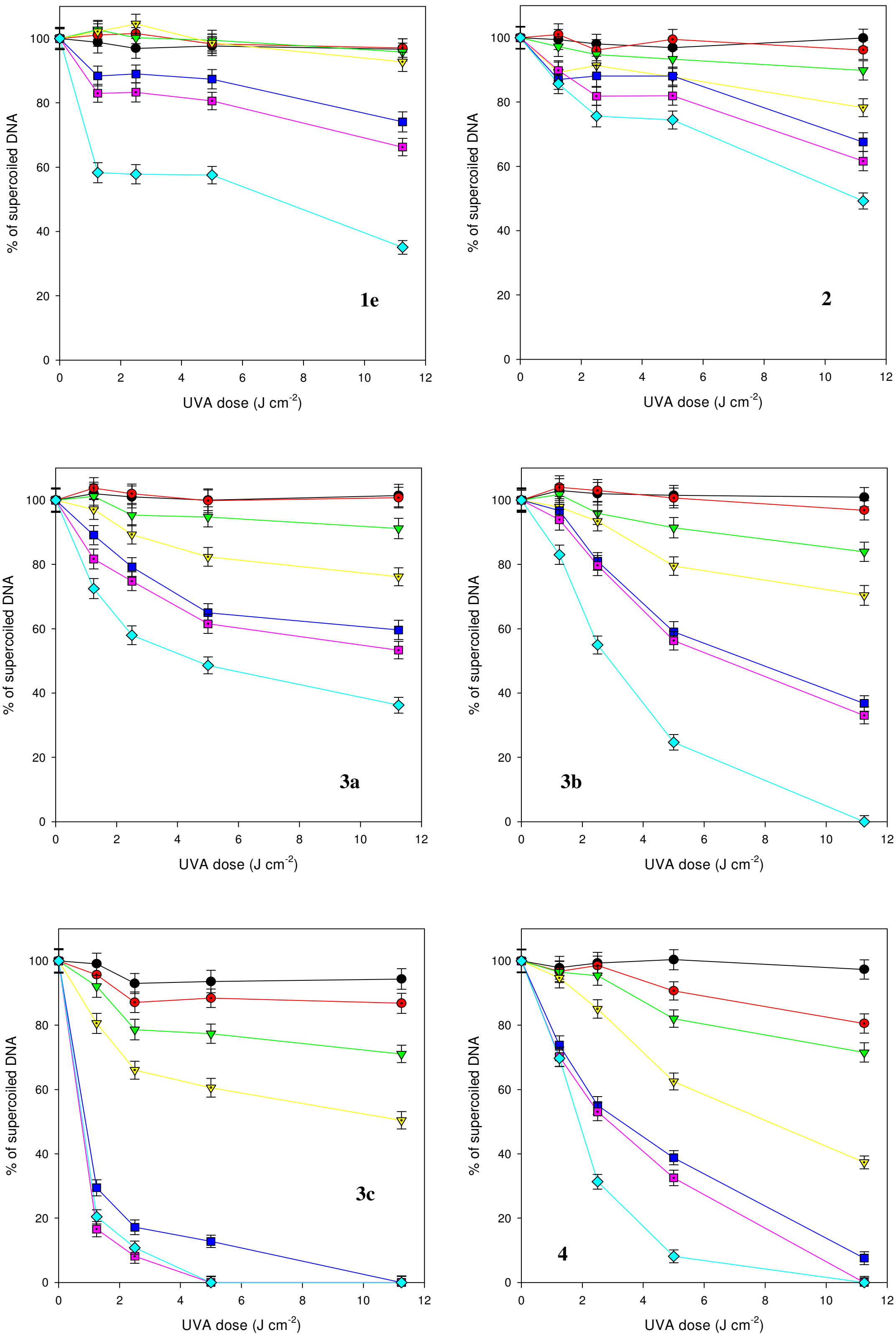

Figure 4.1 Strand breaks of plasmid DNA pBR322 expressed as percentage of form I after UV-A irradiation in the presence of the different compounds at increasing [Dye]/[DNA] ratios (*r* = 0, 0.04, 0.08, 0.2, 0.8, 1 and 2).

4.2 DETERMINATION OF OXIDATIVE DAMAGES

Photocleavage of nucleic acids typically involves an initial oxidative reaction of either a nucleobase or a sugar residue. The damaged nucleotide then degraded either spontaneously (frank strand breaks) or after treatment of the DNA with hot piperidine (alkali labile sites) or with base excision repair enzymes Fpg (Formamido pyrimidin glycosilase) or Endo III (Endonuclease III). The latter reactions yield shorter DNA strands and small molecule by products such as sugar fragments or nucleobase [160, 161].

After irradiation of DNA in the presence of the penta- and hexacyclic derivatives, were determined the DNA modifications sensitive to the following repair enzymes, as Fpg protein, which recognizes 8-hydroxyguanine, purines whose imidazole ring is open (Fapy residues) and sites of base loss (apurinic sites), and Endo III, which recognizes 5,6-dihydropirimidines derivatives in addition to apurinic sites. Damage base release is followed by a β-δ reaction or β-elimination step, resulting in DNA cleavage.

Notably, the treatment of pBR322 with the two base excision repair enzyme, after UV-A irradiation in the presence of the selected compounds, does not significantly increase the number of single-strand breaks. These data indicate that frank strand breaks are induced upon irradiation of DNA in the presence of the derivatives (Fig. 4.2).

1a

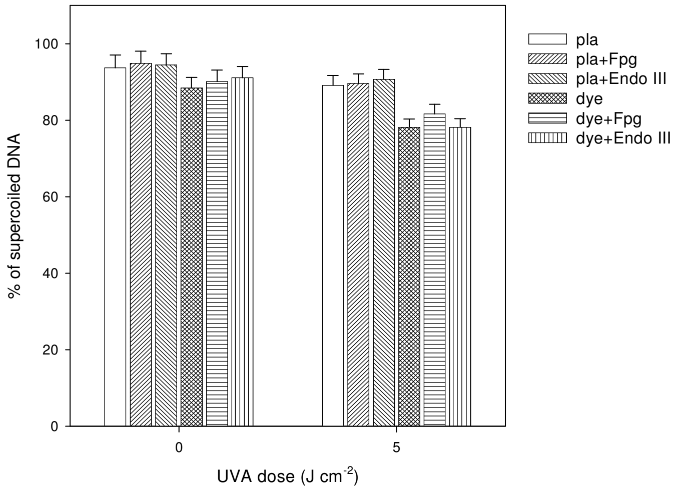

1b

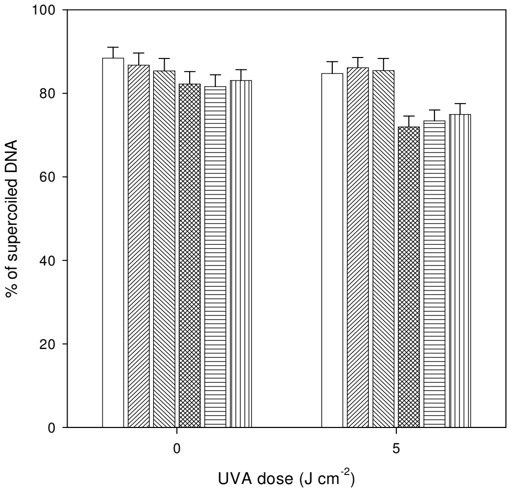

1c

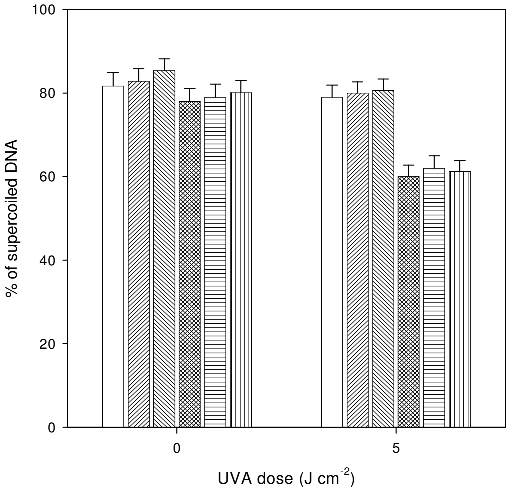

1d

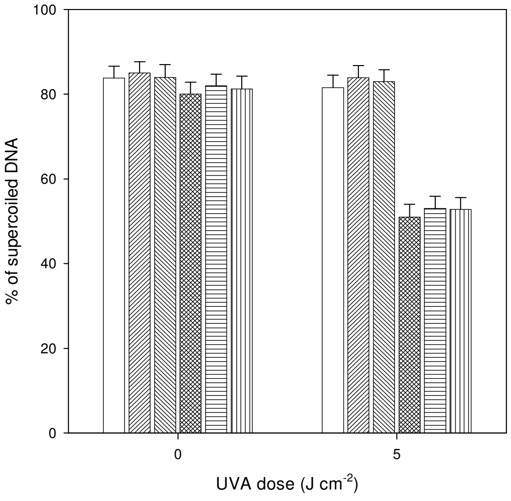

1e

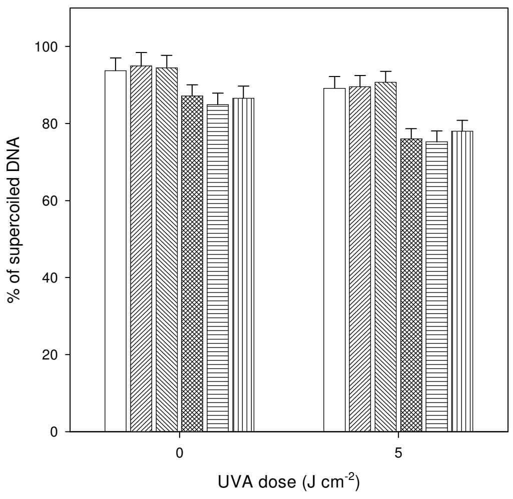

2

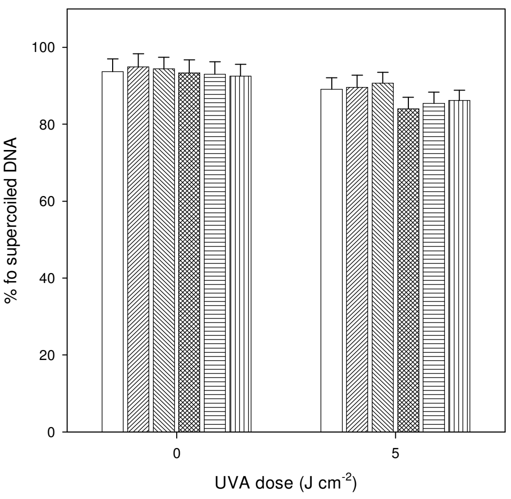

3a

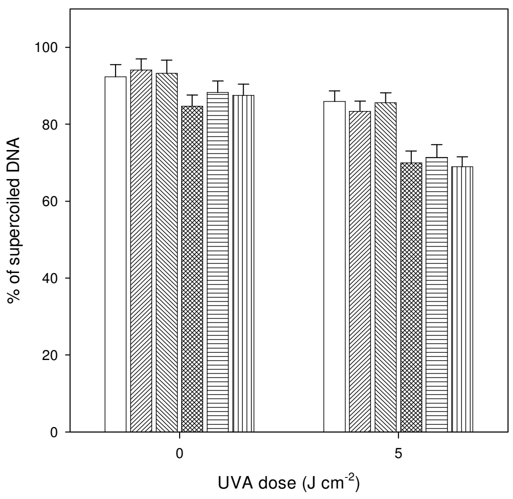

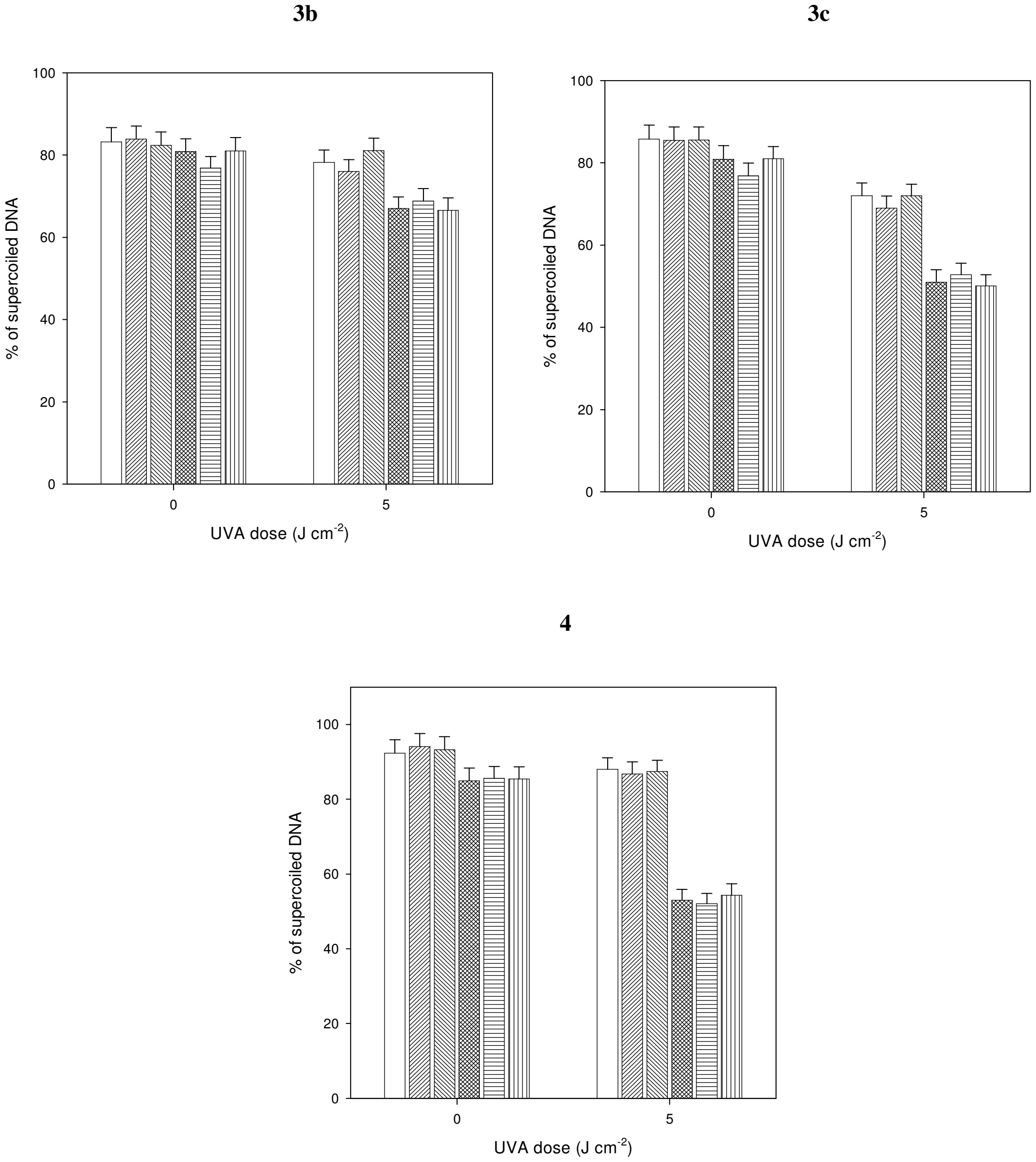

Figure 4.2 DNA strand breaks photoinduced by the compounds expressed as percentage of form I obtained after densitometric analysis of the gel. pBR322 supercoiled circular DNA was irradiated at 5 J/cm^2. [Penta]/[DNA]= 0.8; [Hexa]/[DNA]= 0.2. Then the samples were treated as described in the Experimental procedures. Pla= plasmid pBR322 alone.

4.3 DETERMINATION OF THE PROTECTION INDUCED BY SCAVENGERS

To further evaluate the influence of reactive oxygen species in the photocleavage of the plasmid DNA, a series of experiments were carried out using appropriate scavengers.

The scavengers used were NaN_3 (sodium azide) and DABCO (1,4 diazabicyclo [2,2,2] octane) a $^1O_2$ scavengers; GSH (glutathione reduced form) and BHA (2,6-ditert-butylhydroxyanisole) as radical scavengers; Man (mannitol), DMTU (N-N'-dimethyl thiourea) and t-BuOH which scavenge hydroxyl radicals; SOD (superoxide dismutase) and CAT (catalase) which scavenge O_2-• and H_2O_2, respectively. The reactions were carried out also in deuterated water, in which the lifetime of singlet oxygen is increased by a factor of ca. 14, relative to the one in water.

The compounds tested were the pentacycle **1c** and the hexacycles **3b**, **3c** and **4** at dye-to-DNA ratio of 1, irradiated with an UV-A dose of 5 J/cm^2.

No significant protection on DNA induced photocleavage was observed with GSH and BHA, Man, DMTU and t-BuOH, SOD and CAT indicating that free radicals may not be involved in the mechanism of DNA cleavage. Notably, a marked increase in the formation of single-strand breaks was observed in the presence of NaN_3 and DABCO, which trap singlet oxygen (Fig. 4.3). Furthermore, when the aqueous solution was replaced by D_2O, a dramatic increase of the formation of single strand breaks was detected, confirming the involvement of the singlet oxygen in the mechanism of photocleavage of DNA.

1c

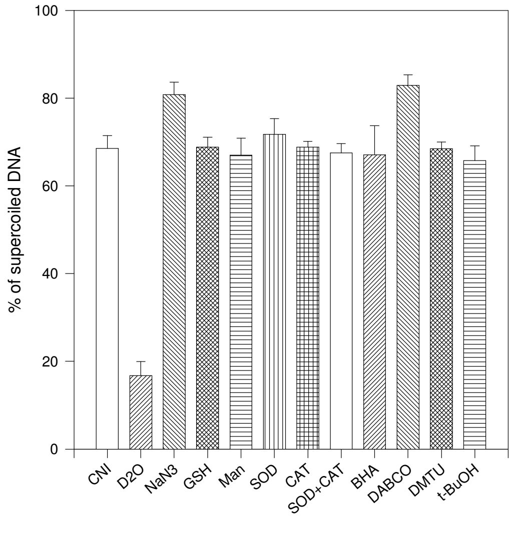

3b

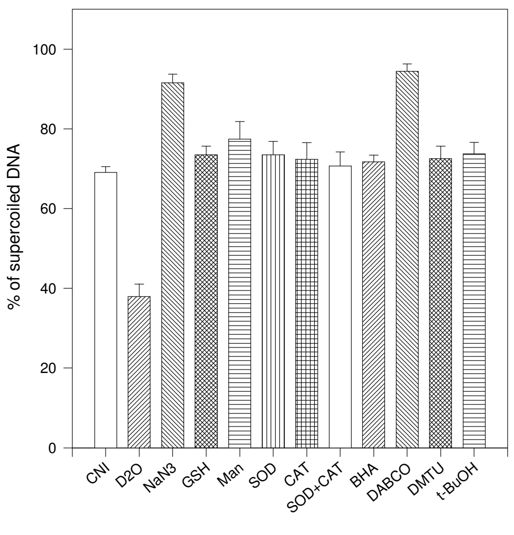

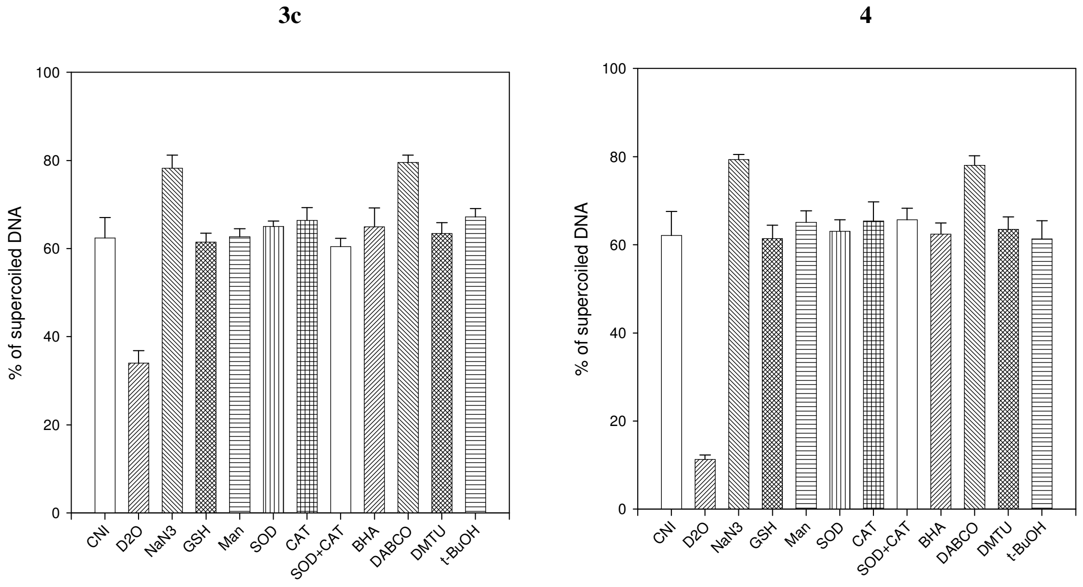

Figure 4.3 DNA strand breaks photoinduced by the compounds at [Dye]/[DNA] ratio of 1. The data are expressed as percentage of form I obtained after densitometric analysis of the gel. CNI = control cells not irradiated.

4.4 DNA-SEQUENCING

DNA-sequencing is a technique that allows to recognize the site of breakage induced by a photosensitizer after UV-A irradiation. As ^{32}P-radiolabeled DNA was used the 236-bp Hind III restriction fragment from plasmid pUC 18, rich in guanine and cytosine, because the high affinity demonstrated in footprinting experiments. The mixture of radiolabeled plasmid and the selected compound **3b** was irradiated with two different UV-A dose (En= 1 and 1.2 J/cm^2). The reactions were stopped in dry ice and then the samples were separated by gel electrophoresis on a denaturing acrylamide gel.

The autoradiogram shows that after irradiation there are five sites of damage, and all sites containing the sequence XGG (Fig. 4.4).

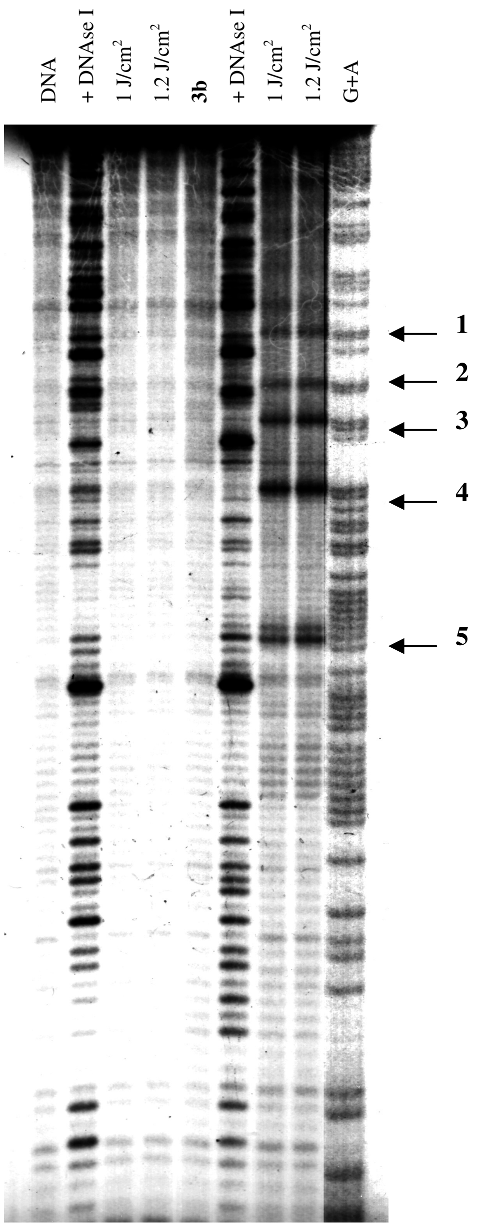

Site 1
5’-^{99}AGGCCA^{104}-3’
3’- TC**CGG**T -5’

Site 2
5’-^{110}AGGCCA^{115}-3’
3’- TC**CGG**T -5’

Site 3
5’-^{117}GAACCG^{122}-3’
3’- CT**TGG**C -5’

Site 4
5’-^{128}AGGCCG^{133}-3’
3’- TC**CGG**C -5’

Site 5
5’-^{147}TTTCCA^{152}-3’
3’- AA**AGG**T -5’

Figure 4.4 Left panel: DNA sequencing of **3b** on the 236-bp Hind III restriction fragment of plasmid pUC 18. [**3b**]= 15 µM. The products obtained after UVA irradiation (En= 1 and 1.2 J cm^{-2}) were resolved on a 10% polyacrylamide gel containing 8 M urea. DNA lane: fragment alone; +Dnase I lane: fragment of DNA digested with the enzyme without compound. G+A lane: marker specific for guanines and adenines obtained after treatment with piperidine (Maxam and Gilbert techniques) [159]. Righ panel: sequence of binding sites from 1 to 5.

These data confirm the results of previous experiments conducted with the scavengers. It is also important to underline that the sites 1 and 3 correspond to sites 1 and 3 found with footprinting, while site 2 is closed to the footprinting site 2, so **3b** causes damage both in the site-sequences of affinity and in other GC rich regions. Sites 1, 2 and 3 have a weaker intensity than site 4 and 5. It will be conclude that probably the damage induced at sites 4 and 5 is due to an externally bound to the DNA. These hypothesis is in agreement with the result obtained from DNA photocleavage.

4.5 CONCLUSIONS ON DNA-PHOTOCLEAVAGING PROPERTIES

The DNA-cleavage may not be exclusively initiated by the intercalated molecules and it may therefore be assumed that a favourable position for dye to initiate this reaction is at the backbone rather than inside DNA. Thus, excited molecules that approach the DNA backbone by collision or the few molecules that bind to minor groove may react more efficiently than the intercalated ones. All the derivatives may lead to photoinduced DNA damages, which depends on the reaction time and on the dye concentration. The damages induce on DNA, after irradiation, are a direct breakages, it means they are due to a frank strand breaks, and they do not involve oxidative damages at purinic or pyrimidinic bases. The use of suitable scavengers indicates the formation of singlet oxygen as reactive oxygen species involved in the mechanism of DNA-photocleavage (type II mechanism). It seems that no other radical could be imply.

After UV-A irradiation, the molecule provokes damages at XGG sequence, and it is known from literature that singlet oxygen (type II mechanism) induce oxidation of every guanine residues, while damage through electron transfer (type I mechanism) cause damage at the underline G of 5’-$\underline{G}$G or 5’-G$\underline{G}$G. So, at the present stage, a definite mechanism for photoinduced DNA damage in the presence of the different compounds cannot be presented, since experimental results are not in agreement.

5. BIOLOGICAL ACTIVITY

5.1 CELLULAR CYTOTOXICITY

For the experiments of cellular viability, other than the penta- and hexacyclic derivatives of quinolozinium ion, were tested also tri- and tetracycle and indolo derivatives (Fig. 5.1), whose DNA-binding and DNA-photocleavaging properties were already been studied [37, 43-47], but whose biological features were not yet analyzed.

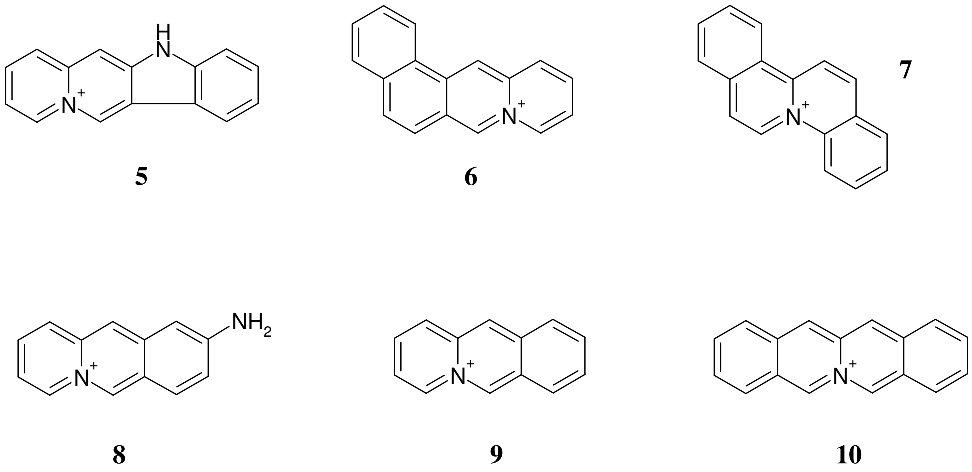

Figure 5.1 Chemical structure of tri- and tetracyclic and indolo derivatives.

Various human tumor cell lines were tested, both leukemic and solid tumors, as: Jurkat are human lymphoblastoid cells; K-562 are chronic myelogenous leukemia; HL-60 are promyelocytic leukemia cells; CEM are human T lymphoblastoid cells; A-549 are human lung carcinoma cells; LoVo are human colon adenocarcinoma; MCF-7 are human breast adenocarcinoma cells; MCF-7 mdr are human breast adenocarcinoma resistant to doxorubicin and NCTC-2544 are human immortalized keratinocytes (not tumoral lines).

The cells were treated with increasing concentrations of the derivatives (1,5625 μM, 3,125 μM, 6,25 μM, 12,5 μM, 25 μM and 50 μM) and cytotoxicity was evaluated, after 72 h of incubation, by MTT test [159]. MTT is a yellow dye that can be absorbed by viable cell and reduced by mitochondrial dehydrogenises, producing insoluble blue crystals. After incubation, crystals were solubilized and the absorbance was detected at λ = 570 nm (see Experimental procedures for more details). As reference compounds were used the two protoberberine derivatives berberine and coralyne, because their structure similarity with the quinolizinium derivatives, and whose cytotoxicity is known in literature.

Otherwise the structural characteristics, it means the presence of the double positive charge, the shape and the absence of hydrophobic group, the compounds are able to permeate the cellular membrane, and for all them were calculated a micromolar GI_{50} values (Table 3). There are no differences between the various derivatives and the leukemic or solid tumor lines. It is important to notice the high GI_{50} values against the line MCF 7-mdr, in some cases at concentration over 50 μM; these data demonstrate that the derivatives are not able to overcome the resistance induced in this tumor line. Only the tricycle **8** and **9**, the tetracycle **10** and the pentacycle **2** have shown no activity. From these results it is very difficult to deduce a structure-activity relationship (SAR), because either the position of the double positive charge as the shape of the various derivatives seem to have no influences on the growth inhibition.

Table 3 Cytotoxicity of the tested compounds against different human tumor cell lines.

IC$_{50}$ (μM)[a]				
Compounds	**Jurkat**	**K-562**	**HL-60**	**CEM**
1a	4.88±0.6	11.84±1.2	6.87±0.9	12.10±1.3
1b	4.50±0.8	4.60±0.6	4.10±0.6	6.90±0.9
1c	3.16±0.3	4.30±0.2	6.83±0.7	2.90±0.1
1d	15.33±1.8	16.87±1.4	12.38±1.6	10.84±1.5
1e	4.11±0.3	6.85±0.5	4.60±0.3	5.52±0.6
2	n.d.	n.d.	n.d.	n.d.
3a	3.25±0.5	8.71±0.9	3.79±0.5	5.00±0.4
3b	5.26±0.7	7.50±0.3	4.60±0.3	5.52±0.6
3c	4.90±0.9	6.20±0.7	7.86±0.7	5.30±0.3
4	7.01±0.7	5.2±0.3	6.92±0.9	2.35±0.6
5	2.33±0.3	3.09±0.4	4.40±0.5	2.60±0.3
6	4.98±0.2	13.47±1.5	6.53±0.7	4.80±0.5
7	5.54±0.6	3.95±0.8	2.63±0.3	4.46±0.3
Coralyne	4.89±0.7	9.5±0.5	3.95±0.3	7.00±0.9
Berberine	4.30±0.4	11.10±1.2	3.44±0.5	4.71±0.5
8	n.d.	n.d.	n.d.	n.d.
9	n.d.	n.d.	n.d.	n.d.
10	n.d.	n.d.	n.d.	n.d.
Eto[b]	250.00±30.0nM	137.50±15.1nM	464.22±42.9nM	48.50±4.1nM
Amsa[b]	65.30±11.2nM	87.62±10.4nM	49.18±4.2 nM	104.00±11.8nM
Campto[b]	12.50±3.0nM	6.16±0.7nM	7.25±0.9 nM	2.00±0.8nM
Doxo[b]	6.60±1.2nM	11.23±0.9nM	16.83±1.3 nM	9.50±1.1nM

n.d.= not determinable (>20 or 50 μM). [a] Concentration of compound required to inhibit the cell growth by 50% after 72 h of exposure as determined by MTT assay [159]. [b] Eto= Etoposide, Amsa= Amsacrine, Campto= Camptothecin, Doxo= Doxorubicin. These molecules are used as reference drugs known in literature.

Table 3 Cytotoxicity of the tested compounds against different human tumor cell lines.

IC_{50} (µM)[a]					
Compounds	**A-549**	**LoVo**	**MCF-7 wt**	**MCF-7mdr**	**NCTC**
1a	2.44±0.6	25.00±2.4	15.00±1.7	n.d.	17.37±1.9
1b	2.39±0.8	23.57±2.5	7.36±0.8	n.d.	6.80±0.7
1c	2.89±0.5	20.43±2.1	7.10±0.7	n.d.	7.20±0.6
1d	13.19±1.1	20.29±2.2	19.53±1.8	n.d.	9.00±0.3
1e	6.79±0.9	14.00±1.2	7.78±0.6	32.8±3.9	4.86±0.3
2	n.d.	n.d.	n.d.	n.d.	n.d.
3a	4.89±0.9	20.41±2.3	8.00±0.6	n.d.	16.55±1.1
3b	4.10±0.7	21.91±2.4	8.60±0.9	n.d.	6.22±05
3c	4.50±0.8	23.80±2.5	16.04±1.7	n.d.	5.49±0.7
4	14.1±1.2	21.85±2.2	17.61±1.9	n.d.	16.46±1.1
5	2.62±0.1	13.16±1.4	2.98±0.4	22.60±2.8	6.74±0.8
6	1.71±0.2	19.71±1.7	4.40±0.6	29.33±3.1	3.75±0.6
7	1.30±0.2	22.00±2.1	5.60±0.7	34.03±3.4	4.62±0.4
Coralyne	8.41±0.9	16.98±1.9	14.04±1.6	35.64±4.1	9.80±0.8
Berberine	7.95±0.3	19.88±1.8	13.00±1.1	28.3±3.5	7.53±0.5
8	n.d.	n.d.	n.d.	n.d.	n.d.
9	n.d.	n.d.	n.d.	n.d.	n.d.
10	n.d.	n.d.	n.d.	n.d.	n.d.
Eto[b]	-	290.00± 27.4nM	2.50±0.6 µM	-	-
Amsa[b]	-	114.00± 12.6nM	3.80±1.2 µM	-	-
Campto[b]	-	35.25±3.3nM	134.70± 18.3nM	-	-
Doxo[b]	-	31.02±2.5nM	58.06±4.7nM	-	-

n.d.= not determinable (<20 or 50 µM). [a] Concentration of compound required to inhibit the cell growth by 50% after 72 h of exposure as determined by MTT assay [159]. [b] Eto= Etoposide, Amsa= Amsacrine, Campto= Camptothecin, Doxo= Doxorubicin. These molecules are used as reference drugs known in literature.

5.2 STABILITY OF THE COMPOUNDS AFTER UV-A IRRADIATION

Before to evaluate the photocytotoxicity against different human tumor cell lines, the photostability of the compounds was checked in order to determine the possible influence due to the action of the photoproducts formed after UV-A irradiation.

Spectra of all compounds, solubilized in DMSO at a final concentration of 20 μM, were recorded at increasing UV-A doses (Fig. 5.2). All penta- and hexacyclic derivatives are characterized by a decrease of the absorption maximum, but without red shift. Almost every of them present an isosbestic point which reveal the presence of two species in solution, the original compound (non-degradated) and photoproducts (Table 4). Similar considerations could be done also for the indolo derivative. The compound **2** shows a different behaviour: at increasing UV-A doses correspond the growth of a new peak whereas the original one disappeared. The formation of these photoproducts could influence the phototoxic activity. The spectra of both tetracyclic derivatives **6** and **7** reveal either the absence of isosbestic points or a very low decreasing of the maximum of absorption, it means they are stable during UV-A irradiation. Finally, the spectra of reference compounds have no isosbestic points, but while coralyne present a constant and weak decrease of the maximum, berberine shows a first low decrease of the absorbance but it is stable at the increasing energy values of UV-A.

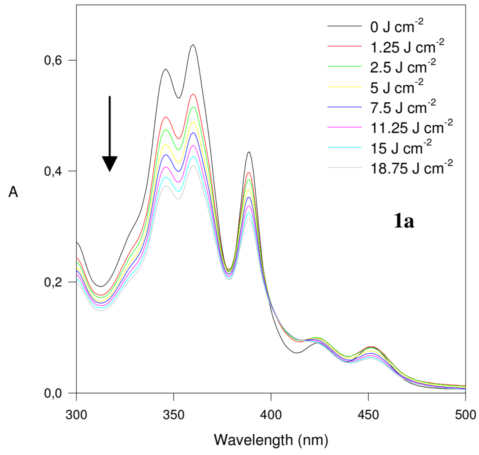

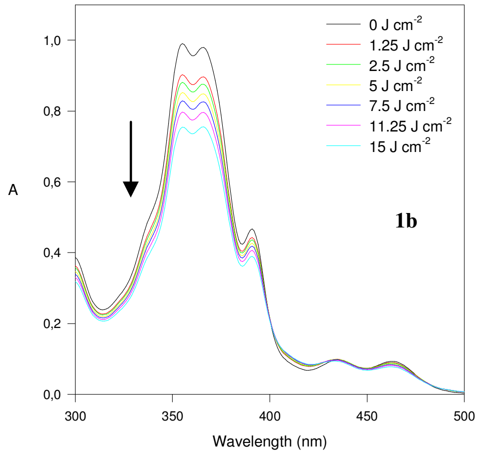

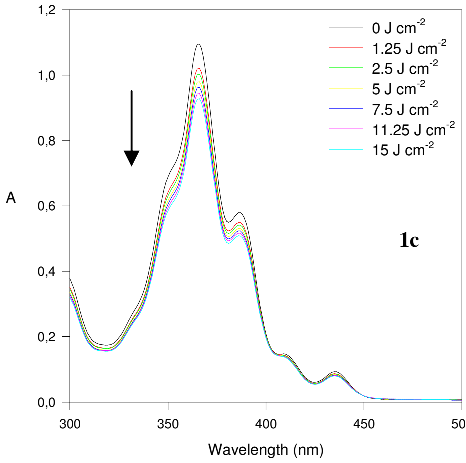
1c
A
Wavelength (nm)
0 J cm^{-2}
1.25 J cm^{-2}
2.5 J cm^{-2}
5 J cm^{-2}
7.5 J cm^{-2}
11.25 J cm^{-2}
15 J cm^{-2}
0,0
0,2
0,4
0,6
0,8
1,0
1,2
300
350
400
450
500

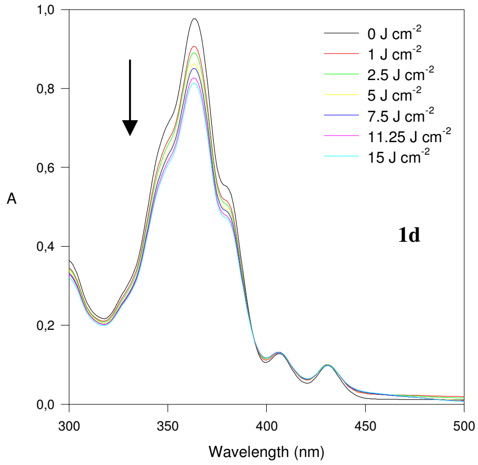
1d
A
Wavelength (nm)
0 J cm^{-2}
1 J cm^{-2}
2.5 J cm^{-2}
5 J cm^{-2}
7.5 J cm^{-2}
11.25 J cm^{-2}
15 J cm^{-2}
0,0
0,2
0,4
0,6
0,8
1,0
300
350
400
450
500

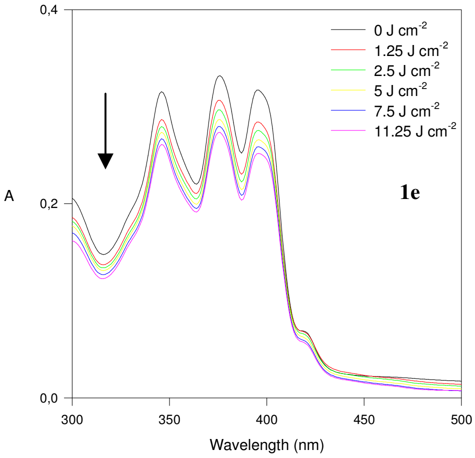
1e
A
Wavelength (nm)
0 J cm^{-2}
1.25 J cm^{-2}
2.5 J cm^{-2}
5 J cm^{-2}
7.5 J cm^{-2}
11.25 J cm^{-2}
0,0
0,2
0,4
300
350
400
450
500

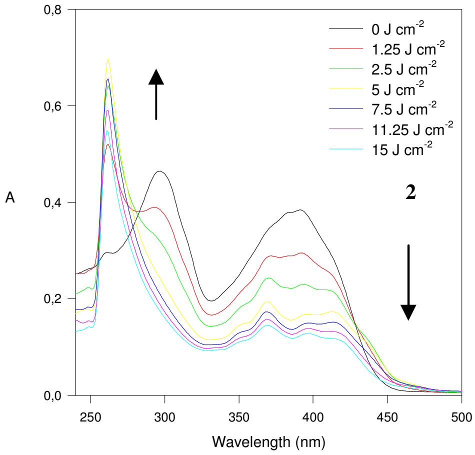
2
A
Wavelength (nm)
0 J cm^{-2}
1.25 J cm^{-2}
2.5 J cm^{-2}
5 J cm^{-2}
7.5 J cm^{-2}
11.25 J cm^{-2}
15 J cm^{-2}
0,0
0,2
0,4
0,6
0,8
250
300
350
400
450
500

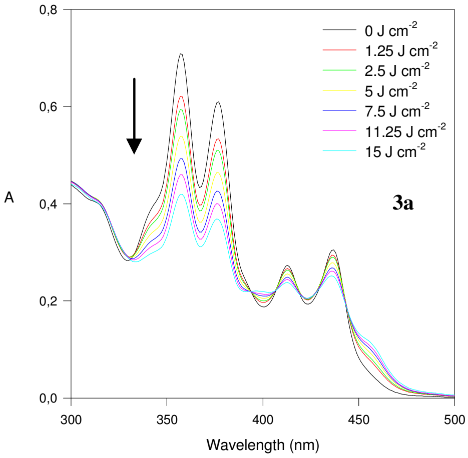
3a
A
Wavelength (nm)
0 J cm^{-2}
1.25 J cm^{-2}
2.5 J cm^{-2}
5 J cm^{-2}
7.5 J cm^{-2}
11.25 J cm^{-2}
15 J cm^{-2}
0,0
0,2
0,4
0,6
0,8
300
350
400
450
500

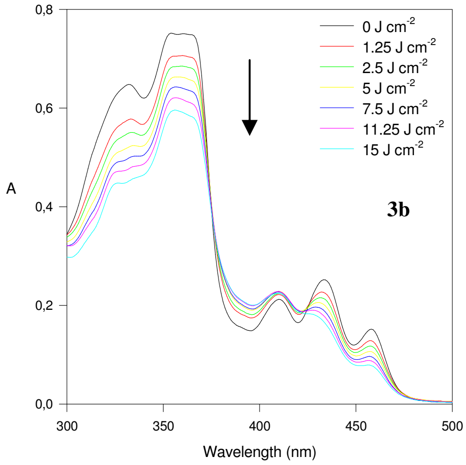
3b
A
Wavelength (nm)
0 J cm^{-2}
1.25 J cm^{-2}
2.5 J cm^{-2}
5 J cm^{-2}
7.5 J cm^{-2}
11.25 J cm^{-2}
15 J cm^{-2}
0,0
0,2
0,4
0,6
0,8
300
350
400
450
500

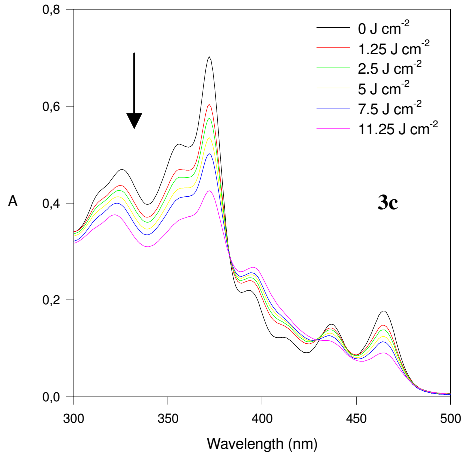
0,8
0,6
0,4
0,2
0,0
A
300
350
400
450
500
Wavelength (nm)
0 J cm-2
1.25 J cm-2
2.5 J cm-2
5 J cm-2
7.5 J cm-2
11.25 J cm-2
3c

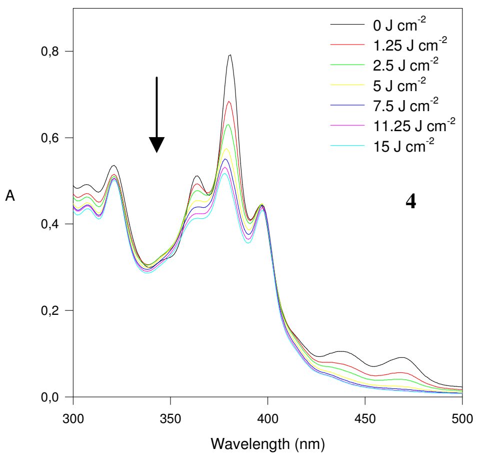
0,8
0,6
0,4
0,2
0,0
A
300
350
400
450
500
Wavelength (nm)
0 J cm-2
1.25 J cm-2
2.5 J cm-2
5 J cm-2
7.5 J cm-2
11.25 J cm-2
15 J cm-2
4

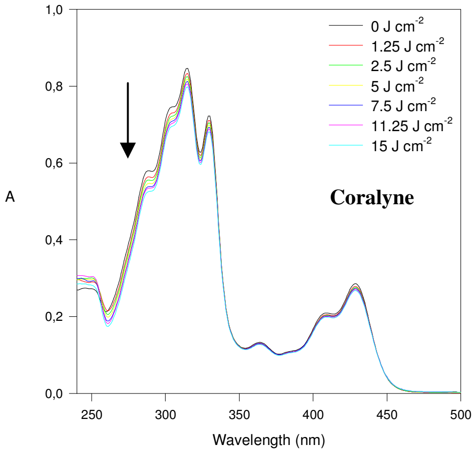
1,0
0,8
0,6
0,4
0,2
0,0
A
250
300
350
400
450
500
Wavelength (nm)
0 J cm-2
1.25 J cm-2
2.5 J cm-2
5 J cm-2
7.5 J cm-2
11.25 J cm-2
15 J cm-2
Coralyne

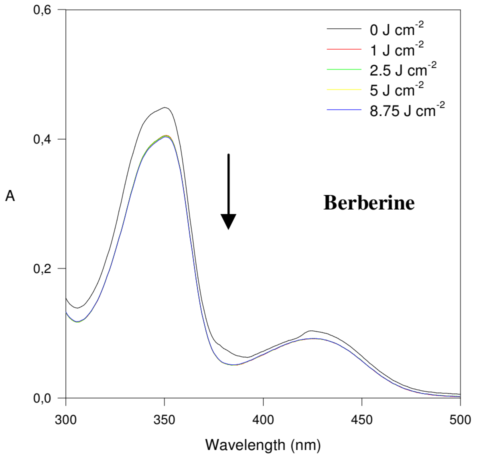
0,6
0,4
0,2
0,0
A
300
350
400
450
500
Wavelength (nm)
0 J cm-2
1 J cm-2
2.5 J cm-2
5 J cm-2
8.75 J cm-2
Berberine

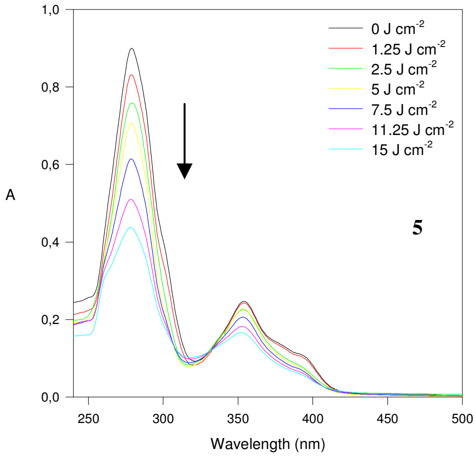
1,0
0,8
0,6
0,4
0,2
0,0
A
250
300
350
400
450
500
Wavelength (nm)
0 J cm-2
1.25 J cm-2
2.5 J cm-2
5 J cm-2
7.5 J cm-2
11.25 J cm-2
15 J cm-2
5

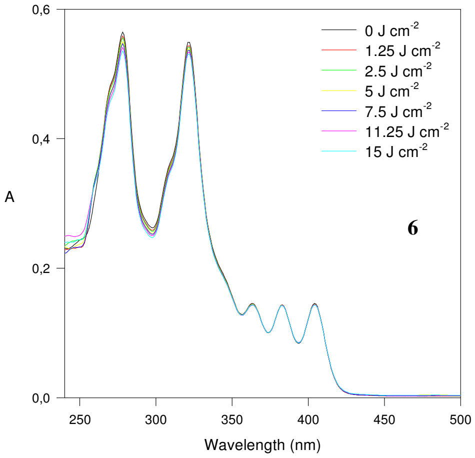
0,6
0,4
0,2
0,0
A
250
300
350
400
450
500
Wavelength (nm)
0 J cm-2
1.25 J cm-2
2.5 J cm-2
5 J cm-2
7.5 J cm-2
11.25 J cm-2
15 J cm-2
6

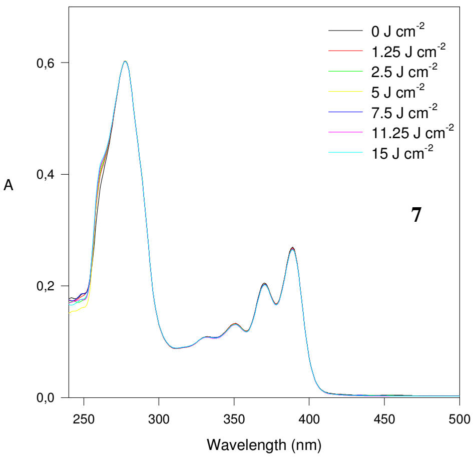

Figure 5.2 Photodegradation spectra of the compounds, at a concentration of 20 µM in DMSO, recorded at increasing UV-A doses (Energy, J/cm^2).

Table 4 Photodegradation spectra: values of λ_{max} of absorbance and isosbestic points.

compounds	λ_{MAX}	**Isosbestic points**
1a	360 nm	n.d.
1b	355 nm	400 nm
1c	365.6 nm	450 nm
1d	363 nm	393 nm
1e	375.6 nm	n.d.
2	296,3 nm	n.d.
3a	357.4 nm	394 nm
3b	354 nm	375 nm
3c	372 nm	383 nm
4	380 nm	397 nm
Coralyne	314.6 nm	n.d.
Berberine	350 nm	n.d.
5	278.6 nm	331 nm
6	278 nm	n.d.
7	277.3 nm	n.d.

5.3 CELLULAR PHOTOCYTOTOXICITY

For the experiments of cellular phototoxicity, a non tumoral line and five different human tumor cell lines were tested, as: NCTC-2544, MCF-7 wt, LoVo, Jurkat, HL-60 and K-562.The cells were treated with increasing concentration of the compounds, solubilized in HBSS aqueous buffer, at two UV-A doses (En= 2.50 J/cm^2 and 3.75 J/cm^2) (Table 5).

Table 5 Photocytotoxicity of the tested compounds against different human tumor cell lines.

IC$_{50}$ (μM)[a]				
Compounds	**NCTC-2544**		**MCF-7 wt**	
	2.50 J/cm^2[b]	**3.75 J/cm^2**	**2.50 J/cm^2**	**3.75 J/cm^2**
1a	n.d.	n.d.	n.d.	n.d.
1b	n.d.	n.d.	n.d.	n.d.
1c	n.d.	n.d.	n.d.	n.d.
1d	7.53±0.5	1.70±0.3	n.d.	9.46±0.8
1e	1.44±0.2	0.6±0.07	3.68±0.4	1.24±0.2
2	n.d.	n.d.	n.d.	n.d.
3a	n.d.	n.d.	n.d.	n.d.
3b	n.d.	n.d.	n.d.	n.d.
3c	n.d.	n.d.	n.d.	n.d.
4	n.d.	8.57±0.9	n.d.	n.d.
5	n.d.	n.d.	n.d.	n.d.
6	n.d.	n.d.	n.d.	n.d.
7	n.d.	n.d.	n.d.	n.d.
Coralyne	n.d.	6.67±0.8	n.d.	n.d.
Berberine	n.d.	4.14±0.3	10.4±1.2	4.6±0.3
8	n.d.	n.d.	n.d.	n.d.
9	n.d.	n.d.	n.d.	n.d.
10	n.d.	n.d.	n.d.	n.d.

n.d.= not determinable or GI$_{50}$ values comparable with ones calculated in “dark condition”

[a] Concentration of compound required to inhibit the cell growth by 50% after 72 h of exposure as determined by MTT assay [159]. [b] UVA dose expressed in J/cm^2 as measured at 365 nm with a Cole-Parmer radiometer.

Table 5 Photocytotoxicity of the tested compounds against different human tumor cell lines.

IC_{50} (µM)[a]				
Compounds	**LoVo**		**Jurkat**	
	2.50 J/cm^{2}[b]	**3.75 J/cm^{2}**	**2.50 J/cm^{2}**	**3.75 J/cm^{2}**
1a	n.d.	n.d.	n.d.	n.d.
1b	n.d.	n.d.	n.d.	n.d.
1c	n.d.	n.d.	n.d.	n.d.
1d	n.d.	12.48±1.3	5.75±0.3	1.91±0.08
1e	7.54±0.6	3.42±0.1	1.99±0.09	598.00± 49.8nM
2	n.d.	n.d.	n.d.	n.d.
3a	n.d.	n.d.	n.d.	n.d.
3b	n.d.	n.d.	n.d.	n.d.
3c	n.d.	n.d.	n.d.	n.d.
4	n.d.	n.d.	n.d.	n.d.
5	8.33±0.7	6.54±0.5	n.d.	n.d.
6	n.d.	n.d.	n.d.	n.d.
7	n.d.	12.05±1.3	n.d.	n.d.
Coralyne	n.d.	n.d.	n.d.	n.d.
Berberine	13.07±1.2	8.30±0.9	3.75±0.2	1.66±0.07
8	n.d.	n.d.	n.d.	n.d.
9	n.d.	n.d.	n.d.	n.d.
10	n.d.	n.d.	n.d.	n.d.
8-MOP	1.1±0.4	0.7±0.1	-	-
Angelicin	1.6±0.2	0.9±0.1	-	-

n.d.= not determinable or GI_{50} values comparable with ones calculated in “dark condition”
[a] Concentration of compound required to inhibit the cell growth by 50% after 72 h of exposure as determined by MTT assay [159]. [b] UVA dose expressed in J/cm^2 as measured at 365 nm with a Cole-Parmer radiometer.

Table 5 Photocytotoxicity of the tested compounds against different human tumor cell lines.

IC$_{50}$ (µM)[a]				
Compounds	**HL-60**		**K-562**	
	2.50 J/cm^{2b}	**3.75 J/cm^2**	**2.50 J/cm^2**	**3.75 J/cm^2**
1a	n.d.	n.d.	n.d.	n.d.
1b	n.d.	n.d.	n.d.	n.d.
1c	n.d.	n.d.	n.d.	n.d.
1d	6.45±0.5	1.41±0.05	n.d.	n.d.
1e	1.43±0.04	652.00± 58.4nM	n.d.	n.d.
2	n.d.	n.d.	n.d.	n.d.
3a	n.d.	n.d.	n.d.	n.d.
3b	n.d.	n.d.	n.d.	n.d.
3c	n.d.	n.d.	n.d.	n.d.
4	n.d.	n.d.	n.d.	n.d.
5	n.d.	n.d.	n.d.	n.d.
6	n.d.	n.d.	n.d.	n.d.
7	n.d.	n.d.	n.d.	n.d.
Coralyne	n.d.	n.d.	5.01±0.7	3.12±0.2
Berberine	2.11±0.1	890.00± 82.3nM	6.65±0.5	3.94±0.4
8	n.d.	n.d.	n.d.	n.d.
9	n.d.	n.d.	n.d.	n.d.
10	n.d.	n.d.	n.d.	n.d.
8-MOP	1.4±0.2	1.2±0.4	-	-
Angelicin	1.5±0.2	0.6±0.1	-	-

n.d.= not determinable or GI$_{50}$ values comparable with ones calculated in "dark condition"
[a] Concentration of compound required to inhibit the cell growth by 50% after 72 h of exposure as determined by MTT assay [159]. [b] UVA dose expressed in J/cm^2 as measured at 365 nm with a Cole-Parmer radiometer.

The photocytotoxicity was evaluated, after 72 h of incubation, by MTT test, as previously described. As reference compounds were also used 8-MOP and angelicin, whose validity in PUVA therapy is amply demonstrated [88, 160, 161].

Only the pentacycle **1d** and **1e** and the reference compound berberine are active after UV-A irradiation in almost every cells lines tested. The GI_{50} are half-reduced compared with the ones calculated in "dark conditions" for these molecules. In the cases of the leukemic lines was found nanomolar values, which are comparable with the ones of the reference drugs 8-MOP and angelicin. Finally, berberine and coralyne are the only molecules active against the leukemic line K-562. A general consideration has be done about the inactive compounds. In fact, they present similar GI_{50} values both in "dark conditions" and after irradiation, so UV-A does not increase their antiproliferative activity. From a structure–activity relationship point of view the following considerations can be done: only pentacycle derivatives are active, so it is necessary a diazoniapentaphenes ring, the absence of substituents on the aromatic rings, and, finally, the presence of one of the double positive charge in position 12a to induce phototoxicity.

Anyway, only the original compounds were tested but not the mixture of drugs-photoproducts, so , at the moment, it is not possible to determine if the phototoxic action is due to the derivatives or the photoproducts.

5.3.1 DETERMINATION OF THE PROTECTION INDUCED BY SCAVENGERS

In order to evaluate the involvement of particular reactive oxygen species in the mechanism of photocytoxicity, some experiments are carried out with appropriate scavengers. The scavengers used were BHA (2,6-diterbutylhydroxy anisole) and GSH (glutathione reduced form), two radical scavengers ($R^{\bullet}$); NaN_3 (sodium azide) and DABCO (1,4-diazabicyclo[2,2,2]octane), two singlet oxygen scavengers ($^1O_2$); DMTU (N,N'-dimethyl thiourea) and Man (mannitol), which scavenge hydroxyl radicals ($OH^{\bullet}$); SOD (superoxide dismutase) and CAT (catalase), which scavenge $O_2^{-\bullet}$ and H_2O_2 respectively. The concentration of the compounds and UV-A doses (En= 3.75 J/cm^2)

were chosen on the base of the results determined by photocytotoxicity. The molecules used for this experiment are **1d**, at a concentration of 2 μM, and berberine, at a concentration of 5 μM, against the cell line NCTC-2544. The GI_{50} values are calculated, after 72 h from irradiation with the selected compounds and the scavengers, as describe before (for more details see Experimental procedures).

Scavengers alone did not have any effect on cell viability before and during UV-A exposure. A significant protection from both **1d** and berberine induced phototoxicity was observed with NaN_3 and DABCO, whereas with the other scavengers used no effects were observed, probably due to their low inherent phototoxic protection. These data indicate that the tested compounds are able to induce toxicity through the formation of singlet oxygen (Fig. 5.3).

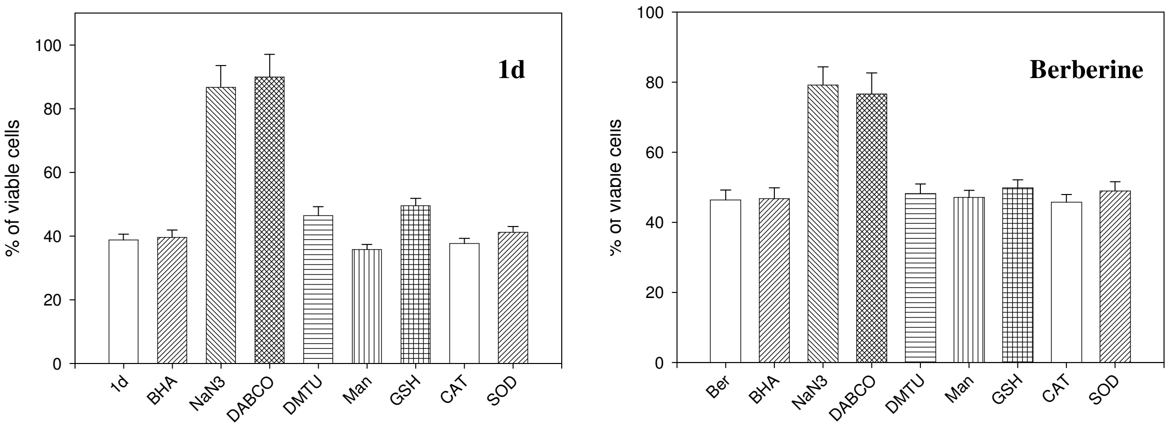

Figure 5.3 Effect of different scavengers on the phototoxicity induced by **1d** (left panel) and berberine (right panel) in NCTC-2544 cells. Cell viability was assayed by MTT test after 72 h from the irradiation in the presence of the compounds and the scavengers.

5.3.2 EVALUATION OF LIPIDIC PEROXIDATION

Oxidative degradation of cell membrane lipids in the presence of molecular oxygen, a sensitizing agent and exciting light is define as photodynamic lipid peroxidation, that is detrimental to membrane structure and function, and could play a role in the toxic effects of the photoreaction. So, photosensitized lipid peroxidation requires molecular oxygen, a sensitizing dye and an exciting light. The absorption of a photon could induce two different pathways of lipid degradation (Fig. 5.4).

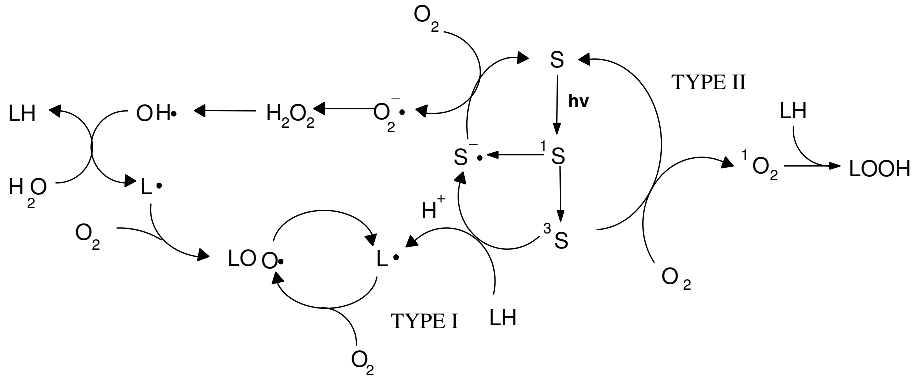

Figure 5.4 General reaction scheme of photosensitized peroxidation. Type I initiation is exemplified by hydrogen transfer from LH to $OH^{\bullet}$ or from LH to ^3S. Type II reactions are depicted by $^1O_2$ addition to LH.

In Type I mechanism free radical intermediates and ground state oxygen are involved and the reaction is initiated by electron or hydrogen atom transfer from a substrate to ^3S, or some cases vice-versa. On the contrary, Type II reaction involves activated oxygen in the singlet excited state.

Thiobarbituric reactive substances (TBARS) are significantly produced when the cells are exposed to the compounds and UVA both in the supernatant and in the cell extract. Aldehydes, such as malondialdehyde (MDA) are meta-stable end-products of lipid peroxidation. During this process the breakdown of the fatty acids occurs and small molecular weight products, such as aldehydes, emerge. Among these, the primary product is malondialdehyde, which was proposed as a diagnostic marker of *in vivo* lipid peroxidation (Fig. 5.5) [162].

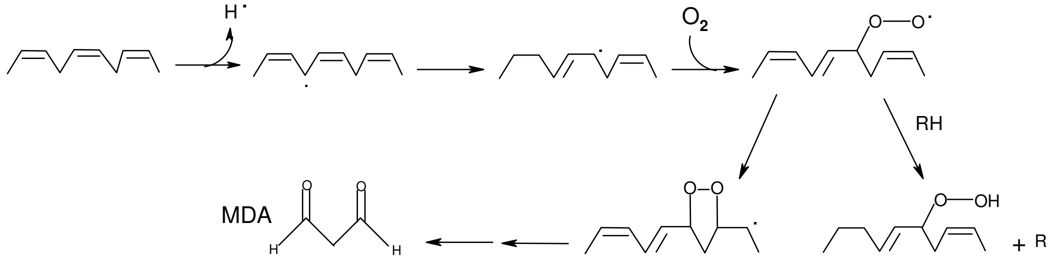

Figure 5.5 Reaction scheme of lipidic peroxidation which induced the formation of MDA as final product.

The thiobarbituric assay (TBARS test) was used in order to determine whether lipid peroxidation occurs upon UV-A irradiation (En= 2.50 J/cm^2 and 3.75 J/cm^2) of Jurkat cells incubated in the presence of **1d**, at a concentration of 8 μM and 20 μM, and berberine, at a concentration of 4 μM and 20 μM (Fig. 5.6). The TBARS test was performed on the supernatants medium and in the cell homogenates, as described in the Experimental procedures [163].

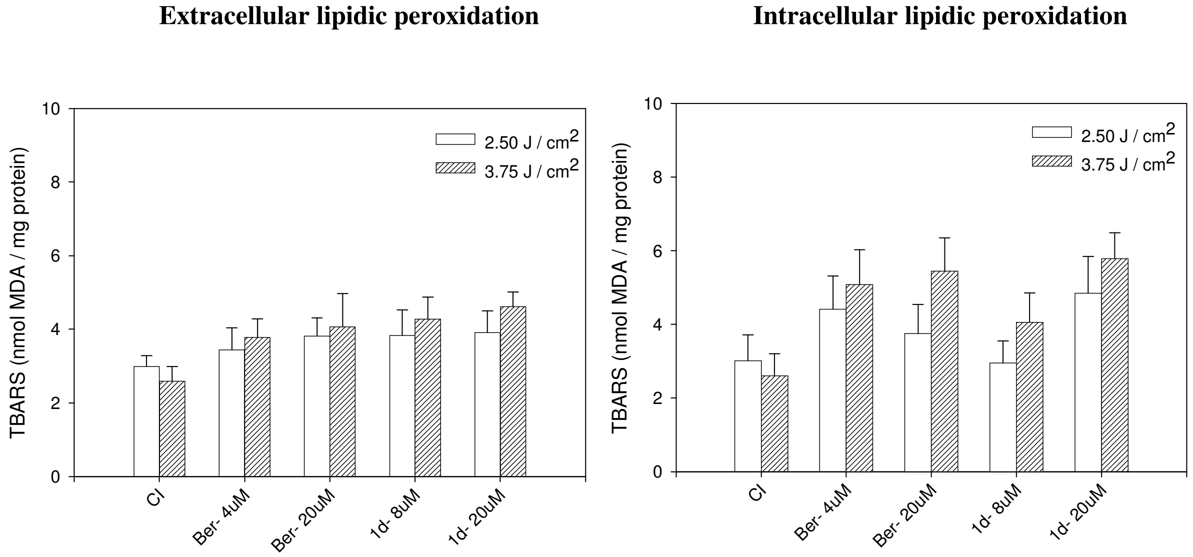
Extracellular lipidic peroxidation

Intracellular lipidic peroxidation

Figure 5.6 Formation of thiobarbituric acid reactive substances (TBARS) in Jurkat cells, following UV-A irradiation in the presence of **1d** (8 μM and 20 μM) and berberine (4 μM and 20 μM). Left panel: extracellular lipidic peroxidation; right panel: intracellular lipidic peroxidation. CI= control cells irradiated.

The results reveal that there are the absence of both extracellular and intracellular lipidic peroxidation, however the increasing both concentration and energy of UV-A irradiation. Otherwise, these data could be predicted because the hydrophilic character of the tested compounds which makes difficult an eventual localization in cellular and subcellular membranes.

5.4 INTRACELLULAR LOCALIZATION

The cellular localization of the compounds is important to check the distribution of molecules inside cells and to evaluate the eventual cellular structure involved in the cytotoxic action. The subcellular localization of a drugs is due to its physicochemical properties such as hydrophobicity, charge, etc. In order to investigate the intracellular localization of quinolizinium derivatives through confocal microscopy (see Experimental procedures for more details), were used two fluorescent probes: JC-1, a lipophilic cation commonly used for the assessment of the mitochondrial potential, and acridine orange (AO), which staine lysosomes [120, 164]. These markers fluoresce in the visible region (λ_{em} = 520 nm), if excited at 488 nm, while the tested compounds emit in the blue region (λ_{exc} = 405 nm). The two fluorescences can be easily separated using suitable band-pass optical filters. After 3 h of incubation in NCTC-2544 cells, the compounds **3b**, at a concentration of 50 μM (Fig. 5.7), and **4**, at the same concentration (Fig. 5.8), were found to both incorporate into the cell with a general diffusion in the cytoplasmatic compartment.

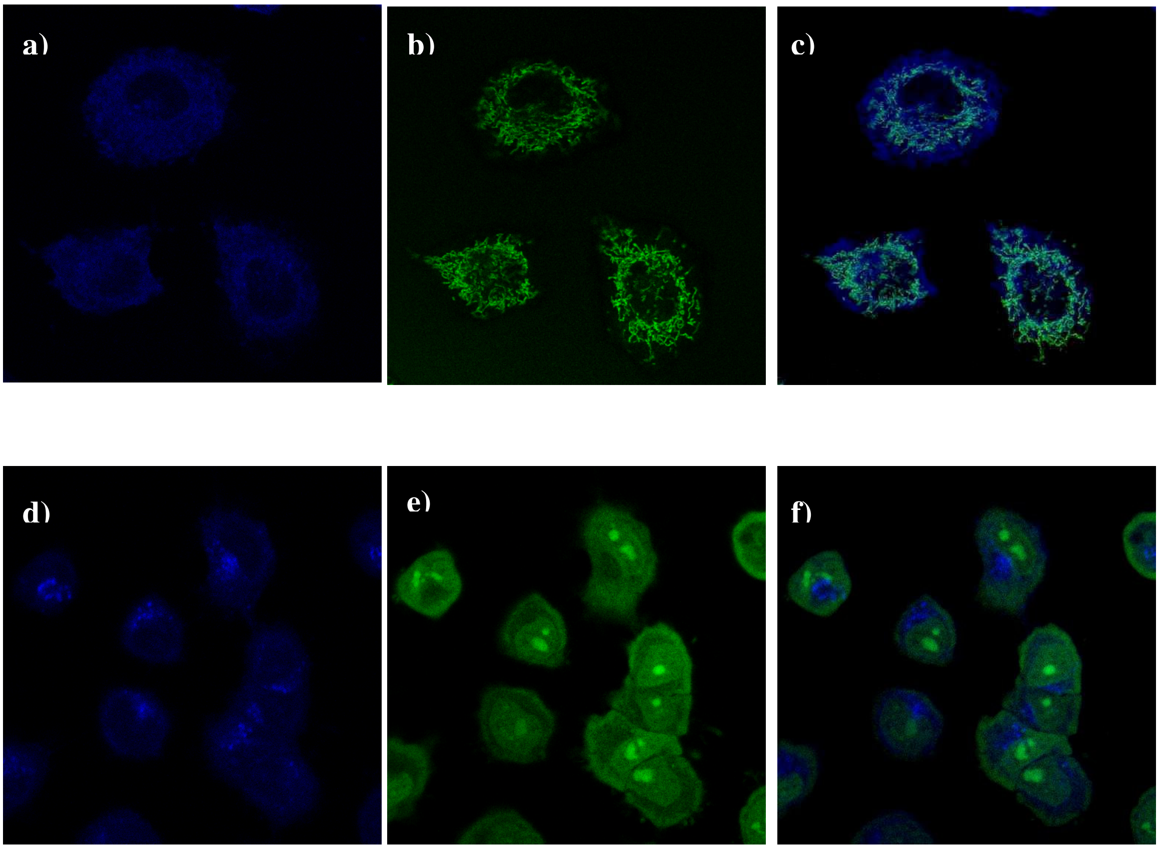

Figure 5.7 Fluorescence micrographs showing the intracellular localization of **3b** in Jurkat cells in the presence of JC-1 (panels b and c) and AO (panels e and f). The cells were treated as described in Experimental procedures. a) fluorescence image of **3b**; b) fluorescence image of JC-1; c) overlay image of **3b** localization generated by transferring the blue colour of the compound seen in panel a onto the corresponding fluorescence image of panel b. d) fluorescence image of **3b**; e) fluorescence image of AO; f) overlay image of **3b** localization generated by transferring the blue colour of the compound seen in panel d onto the corresponding fluorescence image panel e.

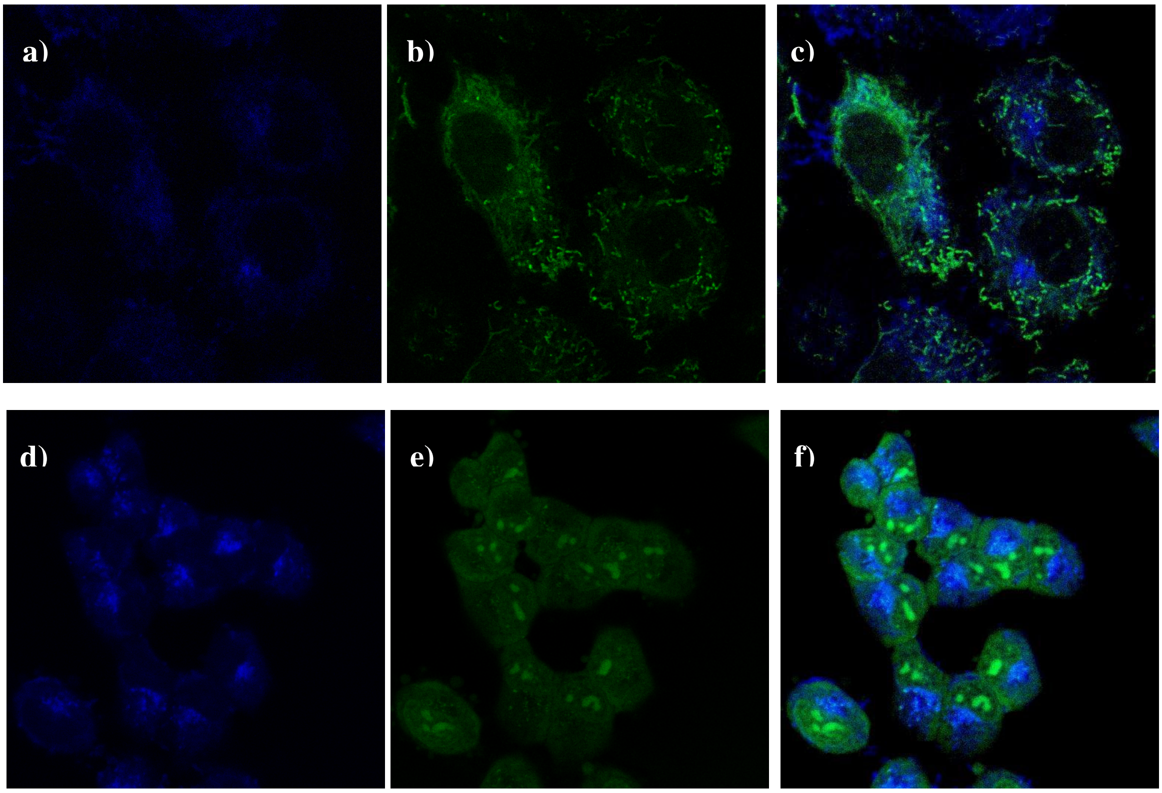

Figure 5.8 Fluorescence micrographs showing the intracellular localization of **4** in Jurkat cells in the presence of JC-1 (panels b and c) and AO (panels e and f). The cells were treated as described in Experimental procedures. a) fluorescence image of **4**; b) fluorescence image of JC-1; c) overlay image of **4** localization generated by transferring the blue colour of the compound seen in panel a onto the corresponding fluorescence image of panel b. d) fluorescence image of **4**; e) fluorescence image of AO; f) overlay image of **4** localization generated by transferring the blue colour of the compound seen in panel d onto the corresponding fluorescence image panel e.

It can be observed that any molecules co-localized with JC-1 or AO, so they do not accumulate into mitochondria or lysosomes. Otherwise, there is an evident localization near the nucleus, probably into the RE (endoplasmatic reticulum), which could be the site of cytotoxic action for this class of compounds.

5.5 DETERMINATION OF MECHANISM OF CELLULAR DEATH

In the early stage of apoptosis, changes occur at the cell surface. One of these plasma membrane alteration is the translocation of phosphatidylserine (PS) from the inner part of the plasma membrane to the external surface of the cell. The translocation of PS precedes other apoptotic processes such as loss of plasma membrane integrity, DNA fragmentation, and chromatin condensation. These modifications are specifically recognized by some cells as macrophages with consequent phagocytosis of the apoptotic cells and bodies [165-167]. This mechanism protects the cells from the exposure to cellular compounds leading to inflammation, which mostly accompanies necrosis. Annexin-V is a Ca^{2+}-dependent phospholipids-binding protein with high affinity for PS. This protein can hence be used as a sensitive probe for PS exposure upon the outer leaflet of the cell membrane and it is therefore suited to detect apoptotic cells in a cell population when conjugated with the fluorescent probe FITC (Fluorescein isothiocyanate). Since necrotic cells also expose PS according to the loss of membrane integrity, apoptotic cells have to be differentiated from these necrotic cells. The simultaneous application of DNA stain which is used for dye exclusion tests as PI (Propidium iodide) allows the discrimination of necrotic cells from the Annexin-V positively stained cluster (Fig. 5.9)

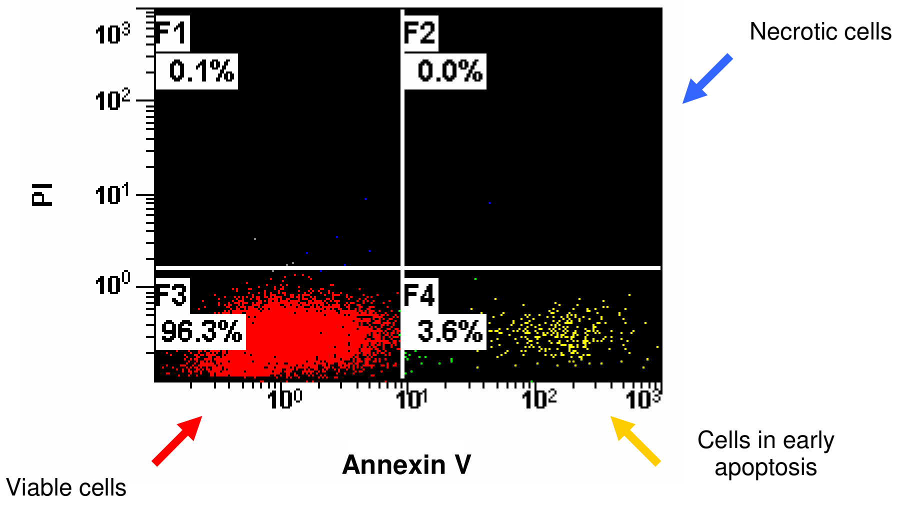

Figure 5.9 Representative bidimensional plot of cytofluorimetric analysis of Jurkat cells. Fluorescence intensities (annexin and PI) are shown as log scale.

The compounds used are **3b** (10 and 20µM), **5** (10 and 20µM), **4** (10 and 20µM) all in "dark conditions", and **1d** (10 and 20µM) after UV-A irradiation (En= 2.50 J/cm^2). After 24 h of incubation of Jurkat cells with the selected derivatives, the cells were labeled with the two fluorescent probes described before, and the resulting red fluorescence due to PI (λ_{exc}=488 nm and λ_{em}=620nm), and green fluorescence due to Annexin-V-FITC (λ_{exc}=488 nm and λ_{em}=520 nm) were monitored by flow cytometer. No induction of apoptosis can be observed neither in "dark conditions" or after UV-A irradiation (Fig. 5.10).

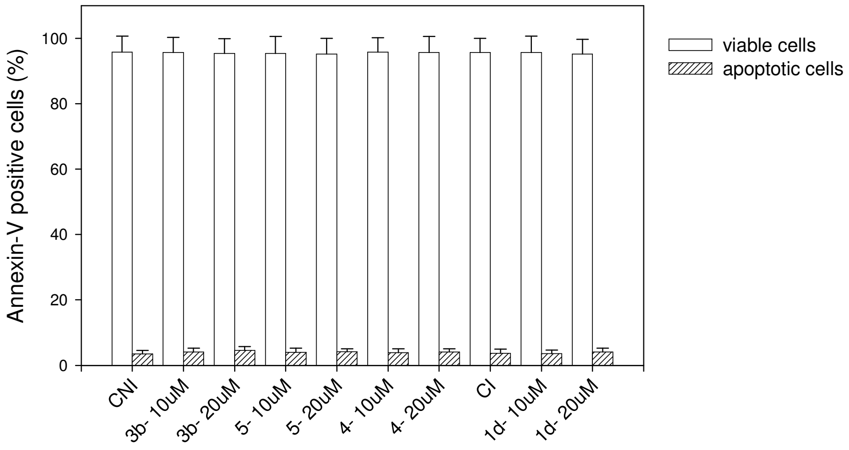

Figure 5.10 Percentage of Annexin-V positive cells after treatment of Jurkat cells with the selected compounds, in "dark conditions" or after UV-A irradiation. CNI= control cells not irradiated; CI=control cells irradiated.

5.6 INVOLVEMENT OF MITOCHONDRIA IN CELL DEATH

Mitochondria play a central role in the integration and propagation of death signals, so they are a key organelles for the cell survival, it means they are implicated in programmed cell death. Most apoptosis-inducing conditions involve the disruption of the mitochondrial inner transmembrane potential ($\Delta\psi$) as well as the so-called permeability transition (PT), a sudden increase of the inner mitochondrial membrane permeability to solutes. Concomitantly, osmotic mitochondrial swelling has been observed by influx of water into the matrix with eventual rupture of the outer mitochondrial membrane, resulting in the release of proapoptotic proteins from the mitochondrial intermembrane space into the cytoplasm, as cytochrome c, which activates the apoptosome and therefore the caspase cascade, but also other factors [168, 169]. The mitochondrial membrane potential (ΔΨ) was measured with the lipophilic cation JC-1, that exhibit potential-dependent accumulation in mitochondria, indicated by a fluorescence emission shift from green (λ ~ 530 nm) to orange (λ ~ 590 nm). Consequently, mitochondrial depolarization, in the early stage of apoptosis, is indicated by a decrease in the orange/green fluorescence intensity ratio. The potential-sensitive fluorescence shift is due to concentration-dependent formation of orange fluorescent J-aggregates, typical of high ΔΨ, toward green fluorescent J-monomers, whose formation is due to a low ΔΨ.

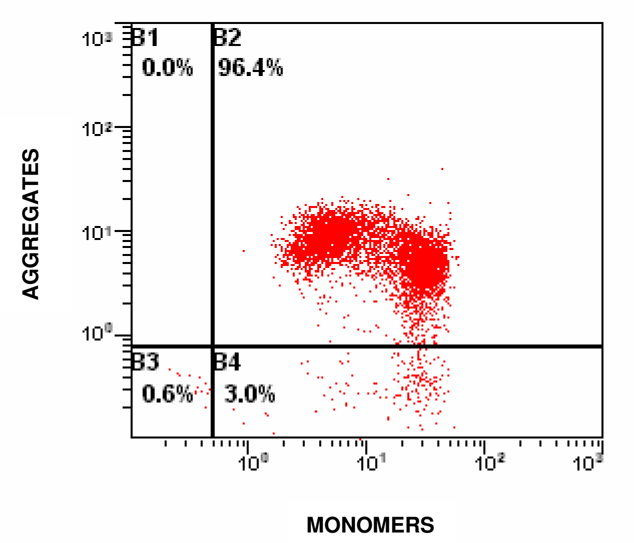

Figure 5.11 Bidimensional plot of Jurkat cells. Fluorescence intensities (aggregates and monomers) are shown as log scale.

In Figure 5.12 were shown the results obtained from cytofluorimetric analysis, after 24 h of incubation of Jurakt cells. The compounds tested are **3b** (10 and 20 µM), **4** (15 and 30 µM), **5** (5 and 10 µM), coralyne (10 and 20 µM) and berberine (10 and 20 µM), in “dark conditions”, and **1d** (5 and 10 µM) after UV-A irradiation (En= 3.75 J/cm^2). The data reveal that there are no changes in the mitochondrial potential neither in “dark conditions” or after UV-A irradiation.

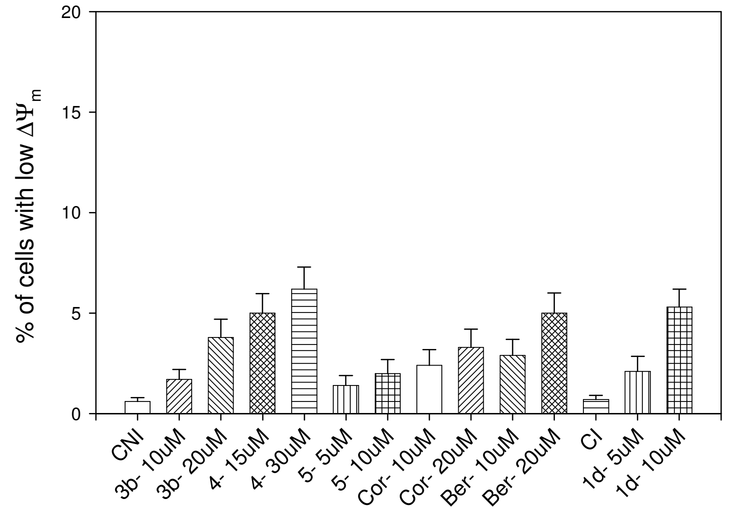

Figure 5.12 Induction of loss of mitochondrial membrane potential after treatment with selected compounds. CNI= control cells not irradiated; CI=control cells irradiated.

5.7 DETERMINATION OF CASPASE ACTIVATION

Many studies have demonstrated that programmed cell death is associated with the activation of the large family of caspase (**C**istein-**Asp**artic acid prote**ases**) as key elements involved in the sequence of events that lead to cell death. In particular, caspase-3, an effector protease, is essential for the propagation of the apoptotic signal after exposure to many DNA-damaging agents, as anticancer drugs. This protease can be activated both through extrinsic pathway by initiator caspase-8, and through intrinsic pathway involving the initiator caspase-9. Once activated it can specifically cleaves most of caspase related substrate known to date, including many key proteins such as the nuclear enzyme poly(ADP-ribose)polymerase (PARP), the inhibitor of caspase-activated deoxyribonuclease (ICAD) and other proteins involved in apoptosis regulation. This cleavage is part of mechanism leading to cell death. In addition, caspase-3 plays a central role in mediating nuclear apoptosis including chromatin condensation and DNA fragmentation as well as cell blebbing [170, 171]. So, it is therefore interesting to evaluate the effect of the compounds on its activity.

The colorimetric assay is based on the hydrolysis of the peptide substrate acetyl-Asp-Glu-Val-Asp p-nitroanilide (Ac-DEVD-pNA) by caspase-3, resulting in the release of the p-NA moiety, which has a high absorbance at 405 nm. So the concentration of the p-NA released from the substrate is calculated from the absorbance values.

Jurkat cells were incubated for 24 h with **3b** (10 and 20 μM), in "dark conditions", and **1d** (5 and 10 μM) and berberine (5 and 10 μM), after UV-A irradiation (En= 3.75 J/cm^2). The results obtained (Fig 5.13) indicate that there is no activation of caspase-3 neither after treatment in "dark conditions" or after UV-A irradiation.

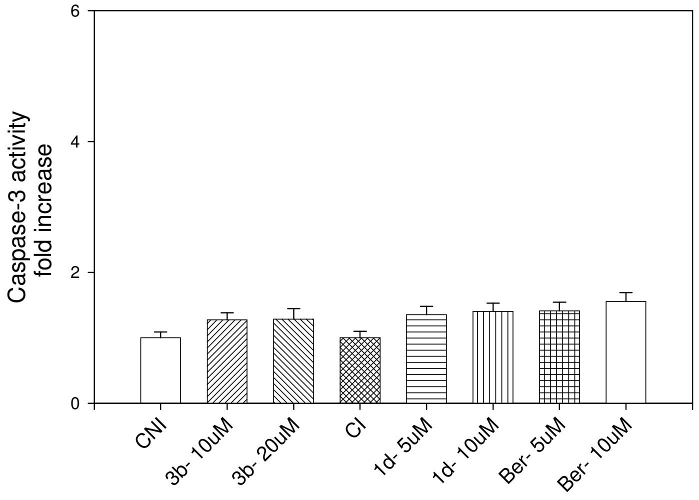

Figure 5.12 Caspase-3 induced activity. Data are represented as fold increase of activity of the enzyme in comparison to non-irradiated and irradiated controls. CNI= control cells not irradiated; CI=control cells irradiated.

5.8 ANALYSIS OF CELL CYCLE

Many antiproliferative drugs could affect cell cycle by blocking one particular phase (G1, S or G2/M phases). Then the cells can repair the damage induced by the exogenous molecules and they return into the cycle (from G0 to G1), or if is a permanent damage they can undergo to apoptosis or necrosis. The analysis of cell cycle was conducted through flow cytometry and the test is based on the different content of DNA presents in each phase. Typical diagram of growing cultures displays a first peak corresponding to G1 phase, a second peak characteristic of G2/M phase with an intermediate area that are the S phase (Fig. 5.14). When DNA is fragmented, as in apoptotic cells, a so-called hypodiploid peak (subG1) becomes apparent on the left of G1 area [172].

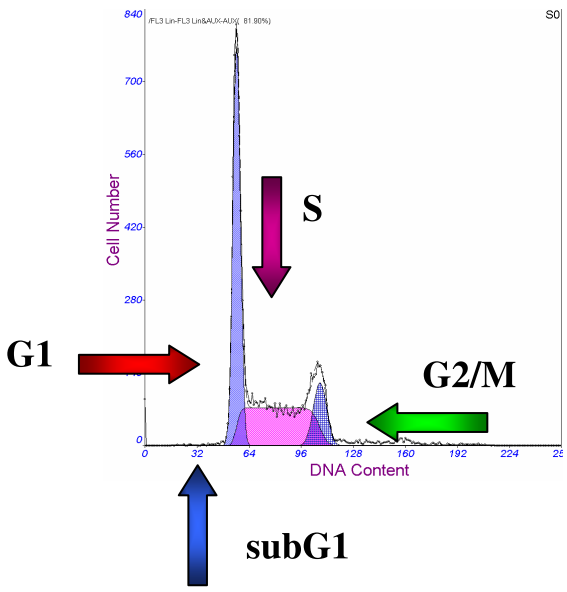

Figure 5.14 Representation of cell cycle distribution.

Jurkat cells were treated with the compounds **3b** (10 and 20 μM), **4** (10 and 20 μM) and **5** (5 and 10 μM) in “dark conditions”. After 24 h of incubation the cells were labeled with PI, a dye that intercalated into DNA and fluoresces in the red (620 nm) if it is excited at 488 nm (Fig. 5.15).

The data reveal that there are no changes in cell cycle after the incubation with the selected compounds (Fig. 5.16).

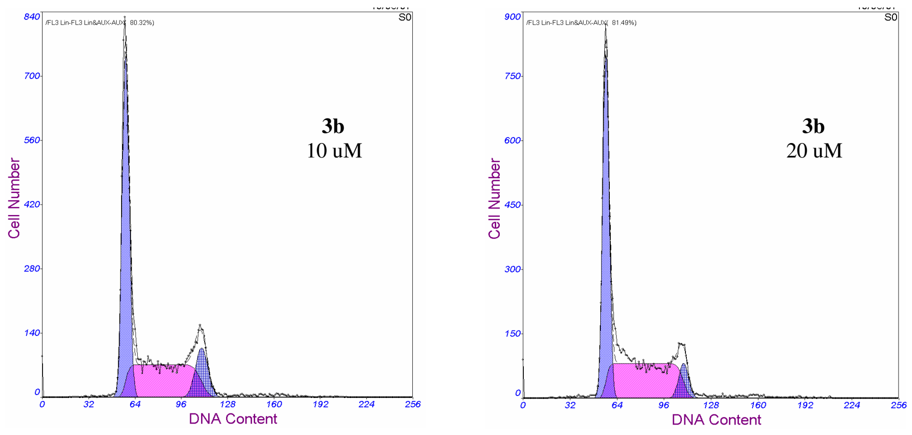

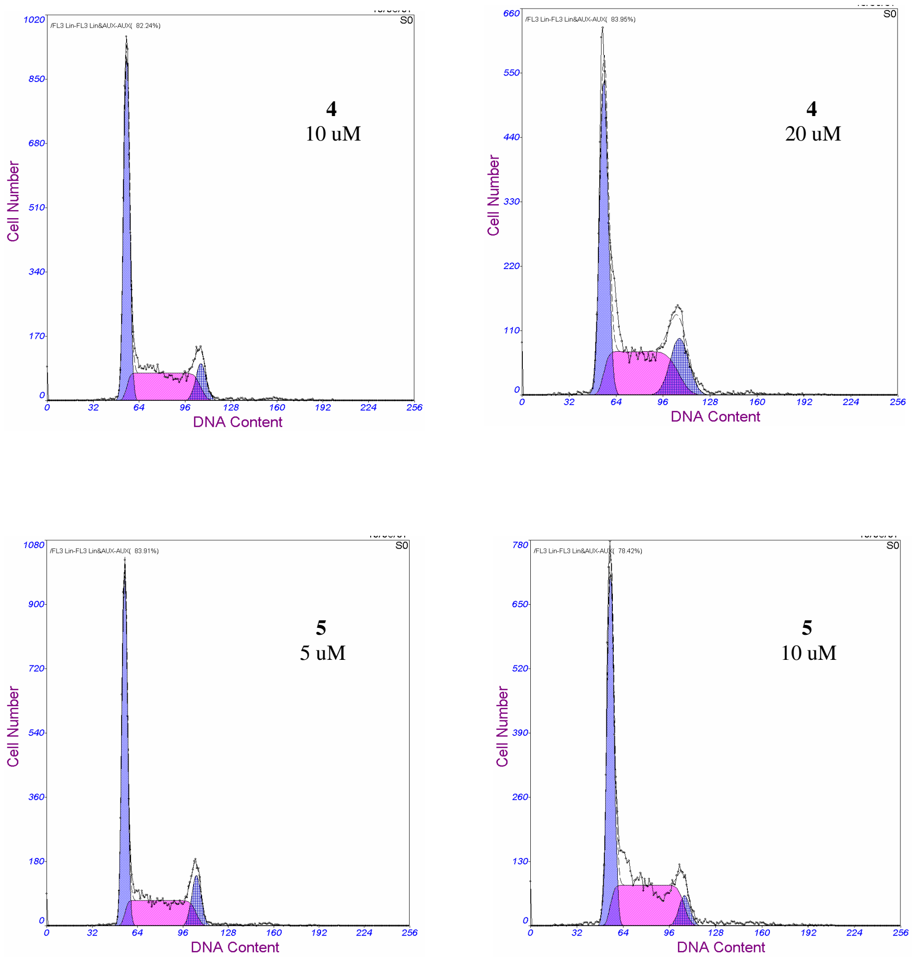

Figure 5.15 Cell cycle analysis of Jurkat cells in the presence of the increasing concentrations of the selected compounds in "dark conditions".

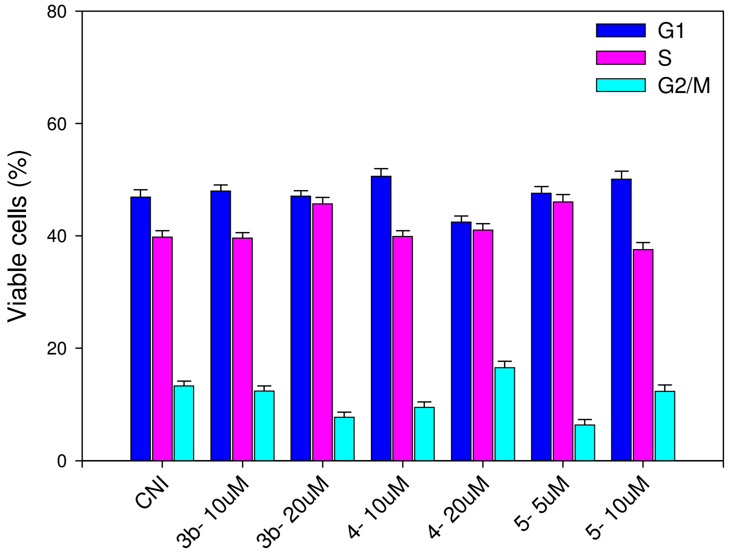

Figure 5.16 Percentage of Jurkat cells in the different phases of the cell cycle. CNI= control cells not irradiated.

5.9 TOPOISOMERASE I AND II ASSAY

Topoisomerases (topos) are essential enzymes that resolve topological problems in DNA, such as overwinding, underwinding and catenation, which normally arise during replication, transcription and perhaps other DNA processes. Two major topoisomerases, types I and II, have been identified in all eukaryotic cells. These enzymes function by forming enzyme-bridged strand-breaks that act as transient gates for the passage of other DNA strands. Topoisomerase I breaks one strand duplex DNA whereas topoisomerase II breaks both strands of the double helix.

Topoisomerase-targeting drugs appear to interfere with the breakage-reunion of DNA, so an aborted reaction intermediate, termed “cleavable complex”, accumulates. As a result of this action, drugs “poison” topos and convert them to a potent cellular toxin that generate breaks in the genetic material of treated cells. The identification of the cleavable complex as the cytotoxic lesion of topoisomerase-targeting drugs readily explains many of the cellular effects of these anticancer molecules. The reversibility of this novel DNA damage suggests that its interaction with certain DNA metabolic machinery may trigger cell death.

5.9.1 INHIBITION OF TOPOISOMERASE I

The ability of the antitumor agent coralyne to stabilize the cleavable complex between topoisomerase I and DNA was amply demonstrated [141], so coralyne was chosen as reference compound because its structural analogy with quinolizinium derivatives. Firstly was analyzed the ability of these molecules to act as catalytic inhibitor and , in second time, if they could be also a poison against the enzyme. The selected compounds are the pentacycle **1c**, the hexacycles **3b**, **3c** and **4** and the indolo-derivative **5**. They were incubated at increasing concentrations, from 0.5 to 200 µM with supercoiled plasmid pBR322 and human topoisomerase I.

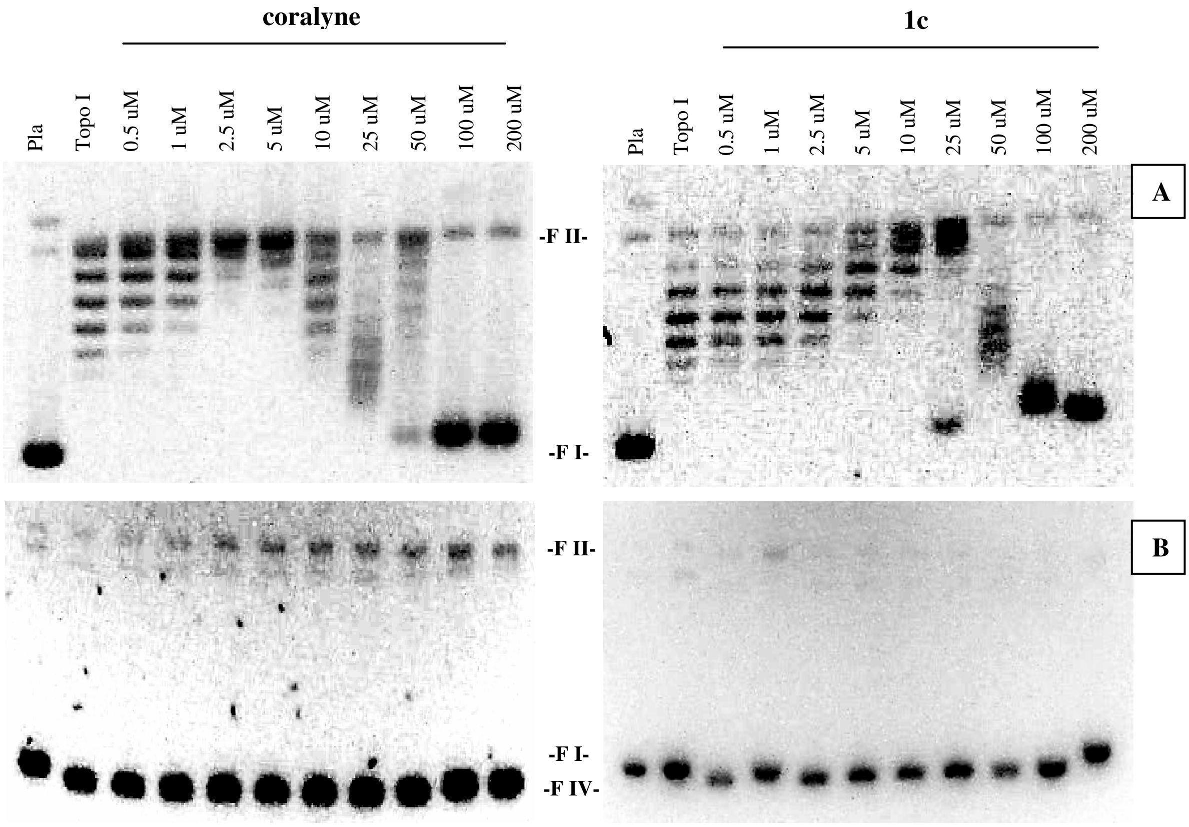
coralyne
1c
Pla
Topo I
0.5 uM
1 uM
2.5 uM
5 uM
10 uM
25 uM
50 uM
100 uM
200 uM
A
B
-F II-
-F I-
-F IV-

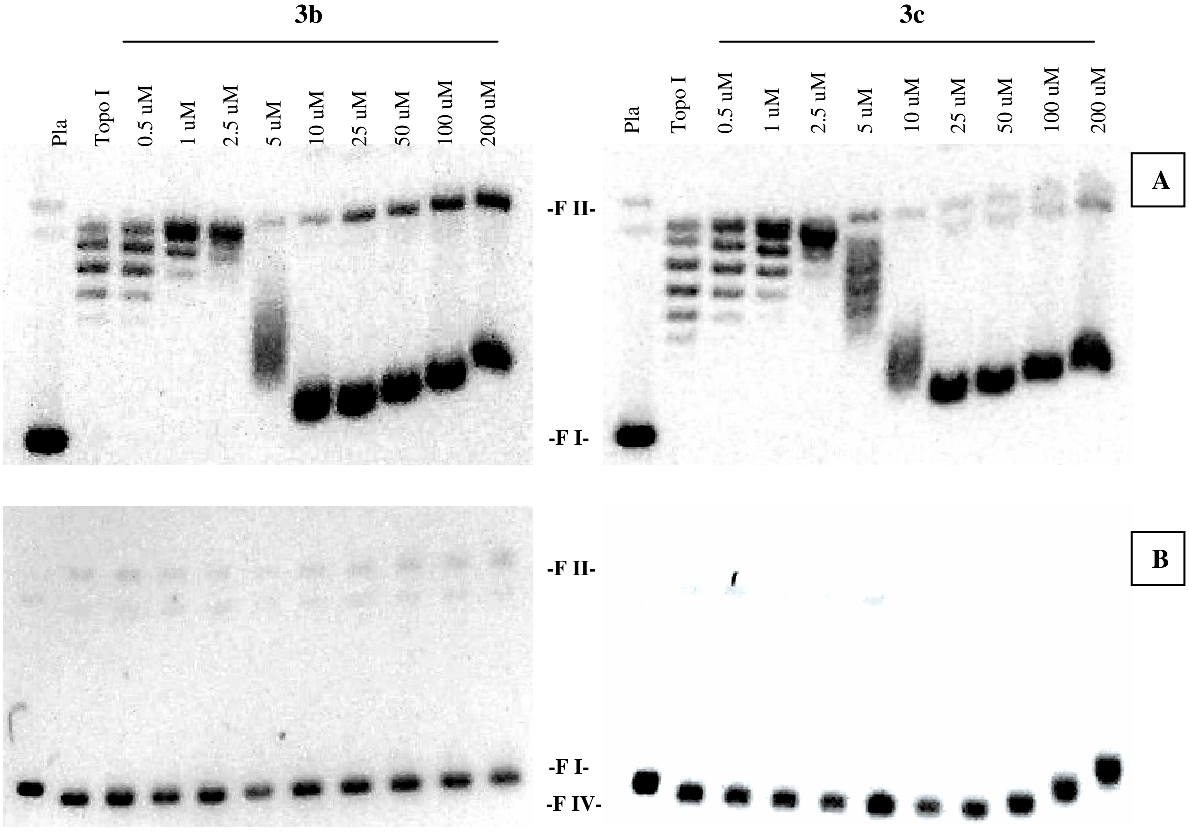
3b
3c
Pla
Topo I
0.5 uM
1 uM
2.5 uM
5 uM
10 uM
25 uM
50 uM
100 uM
200 uM
A
B
-F II-
-F I-
-F IV-

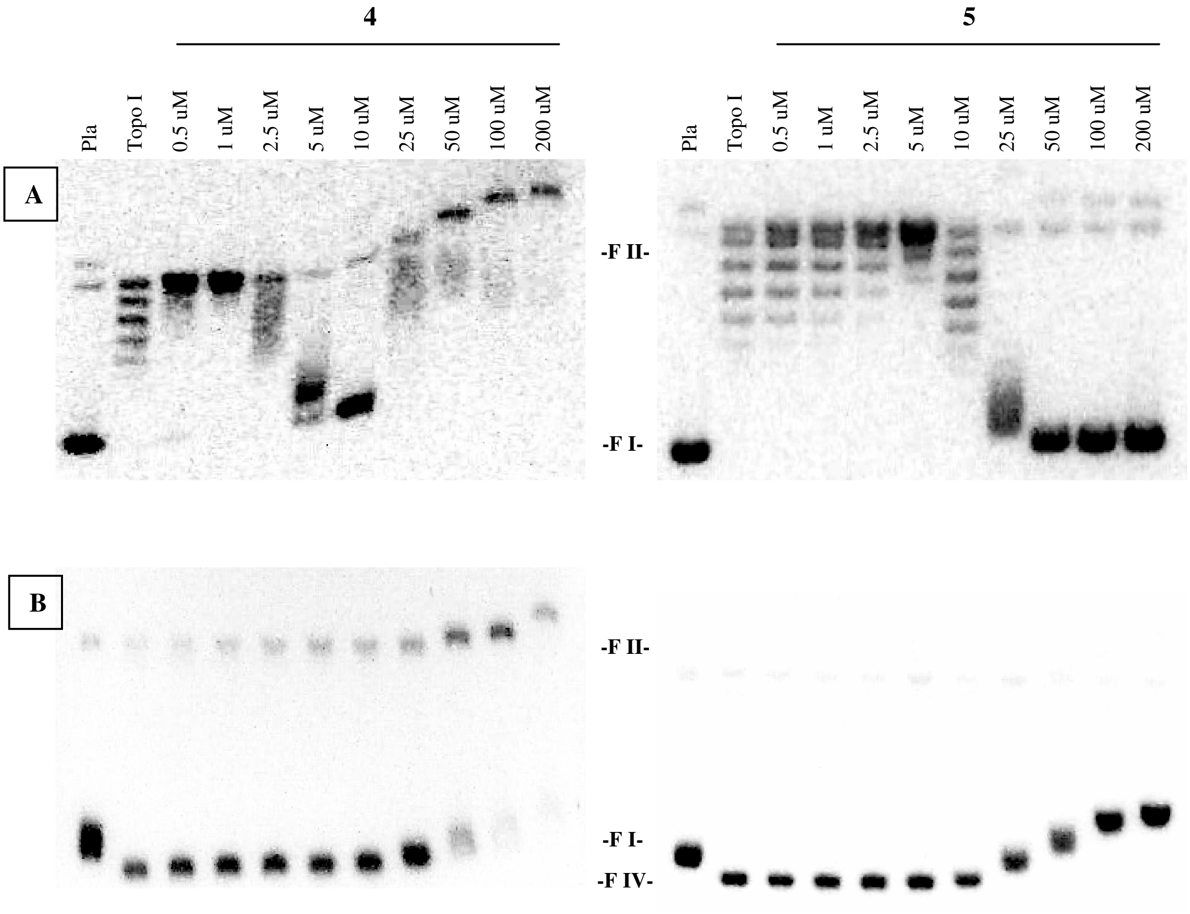

Figure 5.17 Effect of increasing concentrations of the selected compounds on toposiomerase I. Panel A: relaxation assay. Native supercoiled plasmid pBR322 (0.25 μg) (lane pla) was incubated with 10 units of topoisomerase I in the absence (lane topo I) and in the presence of drugs at the indicated concentrations. Reactions were stopped with SDS and treatment with proteinase K. DNA samples were separated by electrophoresis on agarose gel and then stained with a solution containing ethidium bromide. F I= form I, supercoiled; F II= form II, nicked-open circular. Panel B: cleavable complex assay. Native supercoiled plasmid pBR322 (0.25 μg) (lane pla) was incubated with 10 units of topoisomerase I in the absence (lane topo I) and in the presence of drugs at the indicated concentrations. Reactions were stopped with SDS and treatment with proteinase K. DNA samples were separated by electrophoresis on agarose gel containing ethidium bromide. F I= form I, supercoiled; F II= form II, nicked-open circular; F IV= form IV, relaxed.

All the tested compounds act as catalytic inhibitor toward topoisomearse I, but a different concentrations (Fig. 5.17). The pentacycle **1c** inhibits the enzyme at a concentration of 25 μM that is higher than GI_{50} calculated by MTT test. The hexacycle **3b** inhibits topoisomerase at 5 μM as the derivative **3c** and **4**. All these values are comparable with GI_{50} calculated, so topoisomerase I can be a possible target of the haxacyclic derivatives. The indolo quinolizinium **5** has the same behaviour of the pentacycle **1c**. The data suggest that it is necessary a diazoniaanthra[1,2-a]anthracenes or a diazoniahaxephene rings as essential structures to block the action of the enzyme, also due to the ability of these derivatives to intercalate into DNA, so to compete with topoisomerase to the binding sites along DNA.

It is interesting to note that only the hexacycle **4** acts as poison toward the enzyme. The bands corresponding to nicked DNA (F II) could be clearly identify, attesting to the fact that the compound inhibited the relegation of DNA once the strand had been cleaved by the enzyme. Otherwise the induction of the cleavable complex is observed but at high concentration (~ 50 μM) that is not comparable with GI_{50} values. Otherwise, these compounds could constitute a promising platform for the future synthesis of new molecules targeting topoisomerase I.

5.9.2 INHIBITION OF TOPOISOMERASE II

Some experiments are carried out in order to verify an eventual interaction also with topoisomerase II , because it is known from literature that there are molecules that inhibit both enzyme. As reference compound was chosen etoposide [144]. Only the hexacycle **3b** was tested.

For the relaxation assay, supercoiled plasmid pBR322 was incubated with human topoisomerase II and concentration of **3b** ranging from 0.5 to 50 μM. The gel shown in Fig. 5.18 (panel A) indicates that at a concentration of 5 μM the relaxation of DNA was inhibited, most likely as a result of the intercalation of the hexacycle into DNA, as previously observed for topoisomerase I. The gel of the cleavable complex assay (Fig. 5.18, panel B) reveals that **3b** does not induce permanently breakage, as it can been observed for etoposide. Finally, the hexacyclic derivatives acts as a catalytic inhibitor due to its ability to intercalate into DNA.

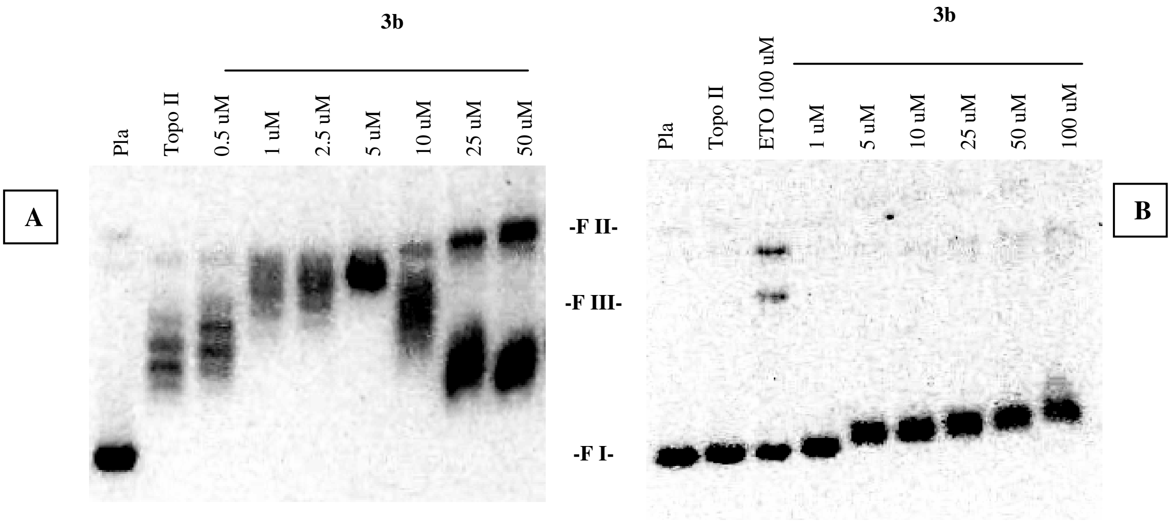

Figure 5.18 Effect of increasing concentrations of **3b** on toposiomerase II. Panel A: relaxation assay. Native supercoiled plasmid pBR322 (0.125 μg) (lane pla) was incubated with 2 units of topoisomerase II in the absence (lane topo I) and in the presence of drugs at the indicated concentrations. Reactions were stopped with SDS and treatment with proteinase K. DNA samples were separated by electrophoresis on agarose gel and then stained with a solution containing ethidium bromide. F I= form I, supercoiled; F II= form II, nicked-open circular. Panel B: cleavable complex assay. Native supercoiled plasmid pBR322 (0.10 μg) (lane pla) was incubated with 6 units of topoisomerase II in the absence (lane topo I) and in the presence of drugs at the indicated concentrations. Etoposide (lane ETO) was used at 100 μM. Reactions were stopped with SDS and treatment with proteinase K. DNA samples were separated by electrophoresis on agarose gel containing ethidium bromide. F I= form I, supercoiled; F II= form II, nicked-open circular; F III= form III, linear.

5.10 CONCLUSIONS ON BIOLOGICAL ACTIVITY

The data about citotoxicity obtained on a panel of human tumor cells lines clearly demonstrated that these derivatives have an antiproliferative activity, with micromolar GI_{50} values. Considering the structure, the double positive charge and the lack of a lipophilic group, these are evidences that the molecules permeate inside the cell and are able to induce toxicity. Some structure-activity relationship has to be done: there is no difference between penta- and hexacyclic derivatives and the relative position of the double positive charge; only the partially saturated compound **2** is completely inactive. The tricyclic compounds are not active as the tetracyclic linear derivative, whereas the other angular tetracycles have an antiproliferative activity. Probably it is necessary a minimum planar structure and an “angular” shape to induce cytotoxicity. About the photocytotoxicity, only the pentacyclic derivatives **1d** and **1e** are active after UV-A irradiation, with nanomolar GI_{50} values. These results suggest that probably it is necessary a diazoniapentaphenes rings and one of the positive charge in position 12a to induce phototoxicity, also if it was not clarify if the antiproliferative activity is due to the molecules or the photoproducts or the mixture of them. Otherwise, the mechanism of the phototoxicity involved singlet oxygen as reactive oxygen species. The images obtained from confocal microscopy reveal a general cytoplasmatic diffusion of the compounds and a clearly localization in specific structure close to the nuclei, probably the endoplasmatic reticulum. All the flow cytometry and biochemical experiments performed demonstrate that the quinolizinium derivatives are a cytostatic agents, both in "dark conditions" and after UV-A irradiation. Further studies are necessary to evaluate if they induce toxicity in a long time (48 h or 72 h).

The hexacyclic molecules act as a catalytic inhibitors toward topoisomerase I and II, due to their intercalative binding mode into the double helix of DNA. Also the pentacycle and the indolo derivatives provoke inhibition but at high concentrations. Only the compound **4** induce the stabilization of the ternary complex against topoisomerase I, but at higher concentration than the calculated GI_{50} values. Finally, it seems necessary a diazoniaanthra[1,2-a]anthracenes or a diazoniahexaphene rings to better inhibit the activity of the enzymes.

6. EXPERIMENTAL PROCEDURES

6.1 MATERIALS

6.1.1 COMPOUNDS

All the compounds used in this project were synthesized in the laboratory of Prof. Heiko Ihmels, Department of Organic Chemistry II, University of Siegen, Germany.

- **1a = MK 10** : 4a,8a-Diazoniapentaphene bis(tetrafluoroborate)
- **1b = MK 16** : 6,13-Dimethyl-4a,8a-Diazoniapentaphene bis(tetrafluoroborate)
- **1c = MK 23** : 14-Methyl-4a,12a-Diazoniapentaphene bis(tetrafluoroborate)
- **1d = JPM** : 4a,12a-Diazoniapentaphene bis(tetrafluoroborate)
- **1e = AG 07** : 12a,14a-Diazoniapentaphene bis(tetrafluoroborate)
- **2 = AG 101** : 6,13a-Dimethyl-13,13a-Dihydro-4a,8a-Diazoniapentaphene-13-ol bis (tetrafluoroborate)
- **3a = MK 19** : 14a,16a-Diazoniaanthra[1,2-a]antracene bis(tetrafluoroborate)
- **3b = MK 24** : 4a,10a-Diazoniaanthra[1,2-a]antracene bis(tetrafluoroborate)
- **3c = AG 151** : 4a,14a-Diazoniaanthra[1,2-a]antracene bis(tetrafluoroborate)
- **4 = AG 150** : 13a,16a-Diazoniahexaphene bis(tetrafluoroborate)
- **5 = IQ** : Indolo[2,3-b]quinolizinium tetrafluoroborate
- **6 = Q2** : Naphtho[1,2-b]quinolizinium tetrafluoroborate
- **7 = DBQ** : Dibenzo[a,f]quinolizinium tetrafluoroborate
- **8 = 9-AA** : 9-Aminobenzo[b]quinolizinium tetrafluoroborate
- **9 = AB** : Benzo[b]quinolizinium tetrafluoroborate
- **10 = MONOMERO** : Dibenzo[b,g]quinolizinium tetrafluoroborate

6.1.2 REAGENTS AND SOLVENTS

- FBS (foetal bovine serum), JC-1 (5,5’,6,6’ tetrachlo-1,1’,3,3’-tetraethylbenzimidazol carbocyanine) and T4 polynucleotide kinase were from Invitrogen S.R.L., Milano, Italy.

- Annexin V- Fluos staining kit was purchased from Roche Diagnostic S.p.A., Milano, Italy.
- Plasmid pBR322 was from Fermentas, Milano, Italy.
- Topoisomerase I was from Calbiochem, Italy.
- DNase I, *Taq* polymerase, ultrapure dATP, dTTP, dCTP and dGTP and the restriction endonuclease Hind III were purchased from Promega UK, Southampton, UK.
- Nucleoside triphosphates labeled with ^{32}P (γ-ATP, 6000 Ci/mmol) were obtained from Amersham Biosciences, UK.
- The PCR forward primers: 5'-CTCCAGAAAGCCGGCACTCAG-3', PCR reverse primers: 5'-GTCGGTTAGGAGAGCTCCACTTG-3', the templates IM18: 5'-A TGCTCCAGAAAGCCGGCACTCAGTCTACAAACGCGTCATCCTTGATCATG CATGTTCACAGAAATTTCTCTAGATCTAAGCTAAACTCTAGTACTAGTCT TCAAGCAAGTGGAGCTCTCCTAACCGACTT-3' and IM20: 5'AAAGTC GGTTAGGAGAGCTCCACTTGCTTGAAGACTAGTACTAGAGTTTAGCTTAG ATCTAGAGAAATTTCTGTGAACATGCATGATCAAGATGACGCGTTTGTA GACTGAGTGCCGGCTTTCTGGAGCAT-3' were synthesized by MGW-Biotech, London, UK.
- MERMAID kit was purchased from Q-Biogene, UK.
- DABCO (1,4 diazabicyclo [2,2,2] octane), Berberine hydrochloride and Coralyne hydrochloride were purchased from Acros Organics, Nidderau, Germany.
- Camptotecin and Etoposide were from Alexis Biochemicals, Lausen, Switzerland.
- Ethidium bromide, agarose, TRIS (tris(hydroxymethyl)aminomethane), EDTA, DTT (dithiothreitolo), bromophenol blue, xylene cianol FF, trypan blue, SDS (sodium dodecyl sulphate), proteinase K, BSA (bovine serum albumin), pUC18, stDNA (sodium salt from salmon testes DNA), MTT (3-[4,5-dimetiltiazol-2yl]-2,5-difenil tetrazolium bromide), HBSS (Hank's Balanced Salt Solution), BHA (2,6-di-tert-butylhydroxyanisole), DMTU (N-N' dimethyl thiourea), MAN (Mannitol), GSH (reduced glutation), NaN_3 (sodium azide), CAT (Catalase), SOD (Superoxide dismutase), Trypsin, RPMI-1640 medium, HAM'S (Nutrient Mixture F-12 HAM), DMEM (Dulbecco's Modified Eagle's Medium), penicillin-streptomycin solutions, Amsacrine hydrochloride, Camptothecin, Doxorubicin hydrochloride,

Topoisomerase II, FPG (Formamido pyrimidin glycosilase), Endo III (Endonuclease III) and all other solvents were purchased from Sigma-Aldrich, Milano, Italy.

6.2 METHODS

6.2.1 CIRCULAR DICHROISM SPECTROSCOPY

Circular dichroism is defined to be the differential absorption of right- (A_R) and left-handed (A_L) circularly polarized light. At a given wavelength:

$$\mathrm{CD}(\lambda) = \mathrm{A_R}(\lambda) - \mathrm{A_L}(\lambda)$$

Linearly polarized light is polarized in a certain direction (i.e., the magnitude of its electric field vector oscillates only in one plane, similar to a sine wave). In circularly polarized light the electric field vector has a constant length, but rotates about its propagation direction. Hence, it forms a helix in space while propagating. If this is a left-handed helix the light is referred to as left circularly polarized and vice versa for a right handed helix. The electric field of a light beam causes a linear displacement of charge when interacting with a molecule, whereas the magnetic field of it causes a circulation of charge. These two motions combined result in a helical displacement when light is impinged on a molecule. Since circularly polarized light itself is "chiral", it interacts differently with chiral molecules. That is, one of the two types of circularly polarized light are absorbed to different extents. In a CD experiment, equal amounts of left and right circularly polarized light are radiated into a (chiral) solution. One of the two types is absorbed more than the other one and this wavelength dependent difference of absorption is measured, yielding the CD spectrum of the sample. Due to the interaction with the molecule, the electric field vector of the light traces out an elliptical path while propagating. Generally, the circular dichroism effect is small so the ellipticity values usually are on the order of mdeg [148, 149]. The ellipticity becomes, in radians:

$$\theta_{\mathrm{r}} = \frac{2.303}{4}(\mathrm{A}_{\mathrm{L}} - \mathrm{A}_{\mathrm{R}})[rad]$$

and it could be easily converted into mdeg:

$$\theta_{d} = \frac{2.303}{4}(\mathrm{A}_{\mathrm{L}} - \mathrm{A}_{\mathrm{R}})\frac{180}{\pi}[\mathrm{deg}]$$

Circular dichroism spectra were recorded in 10 mM ETN buffer solution, pH=7.0, in a quartz sample cuvette (pathlength ℓ = 1 cm) at 25°C on a Jasco J810A spectropolarimeter. Concentration of DNA was 30 µM and the measurements were performed at [DNA]/[Dye] = 0.02, 0.04, 0.08, 0.20 and 0.40.

6.2.2 LINEAR DICHROISM SPECTROSCOPY

Linear dichroism is defined as the differential absorption of orthogonal forms of linearly polarized light:

$$\mathrm{LD} = \mathrm{A}_{//} - \mathrm{A}_{\perp}$$

$\mathrm{A}_{//}$ corresponds to the absorbance of the sample when the light is polarized parallel to the orientation of flow, and $\mathrm{A}_{\perp}$ is the perpendicular absorbance. The “reduced” linear dichroism, LD_{r}, reflects the dependence of the LD on the wavelength:

$$\mathrm{LD}_{\mathrm{r}} = \frac{\mathrm{LD}}{\mathrm{A}_{\mathrm{iso}}}$$

Here $\mathrm{A}_{\mathrm{iso}}$ is the absorbance of an isotropic sample, determined by the measurement of absorption spectra of ligand–DNA complexes. The “reduced” linear dichroism may be related to the orientation of DNA (S) and the angle between the respective light-absorbing transition moment and DNA helix axis according to Nordén *et al.*[150].

$$\mathrm{LD_r} = \frac{3}{2} \times \mathrm{S}(3\cos^2\alpha - 1)$$

Assuming a value of α = 90° for the DNA bases for a ligand bound to it, α is given:

$$\alpha_\mathrm{L} = \arccos\sqrt{\frac{\frac{1}{3} - (\mathrm{LD_r})_\mathrm{L}}{3\,(\mathrm{LD_r})_\mathrm{DNA}}}$$

Here $(\mathrm{LD_r})_\mathrm{L}$ is the reduced linear dichroism for the ligand, $(\mathrm{LD_r})_\mathrm{DNA}$ is the reduced LD for DNA and α_L defines the ligand-DNA relative orientation. For an intercalated system, $\alpha_\mathrm{L} \approx 90°$ and $(\mathrm{LD_r})_\mathrm{L} \approx (\mathrm{LD_r})_\mathrm{DNA}$. Linear dichroism spectra of the ligand–nucleic acid complexes were recorded in ETN buffer in a flow cell on a Jasco J500A spectropolarimeter equipped with an IBM PC and a Jasco J interface. Partial alignment of the DNA was provided by a linear-flow device designed by Wada and Kozawa [173] at a shear gradient of approx. 800 RPM (Fig. 6.1). Concentration of DNA in samples for LD spectroscopy constituted approx. 2.72 mM (bp), and ligand-to-DNA ratios r = 0, 0.04, 0.08 and 0.2 were used.

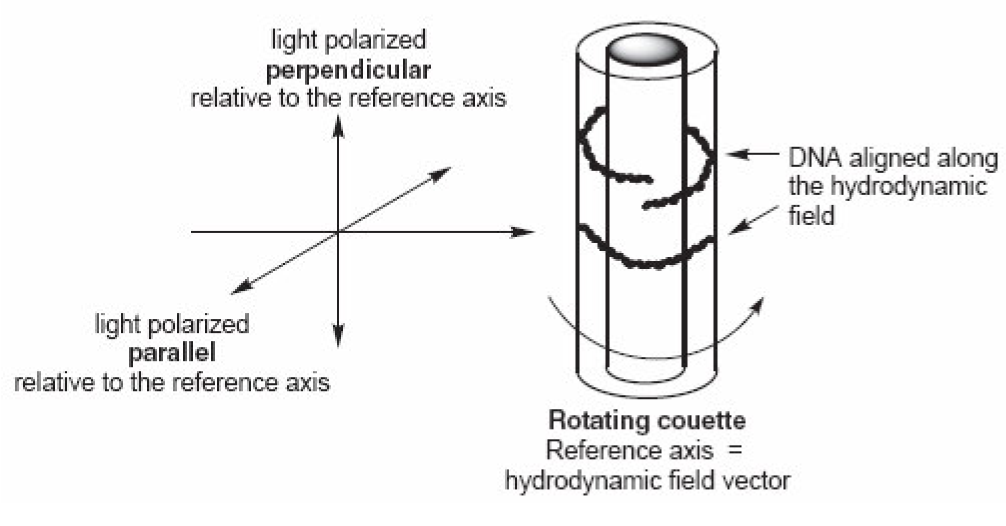
light polarized
perpendicular
relative to the reference axis
DNA aligned along the hydrodynamic field
light polarized
parallel
relative to the reference axis
Rotating couette
Reference axis = hydrodynamic field vector

Figure 6.1 Schematic illustration of the orientation of a cylindrical Couette flow cell relative to the linearly polarized light.

6.2.3 SPECTROPHOTOMETRIC AND SPECTROFLUORIMETRIC TITRATIONS

6.2.3.1 Spectrophotometric titrations

Spectrophotometric titrations of acridizinium salts with stDNA, aimed at the determination of the binding constants, were performed in aqueous ETN buffer, pH=7.0, at a ligand concentration c_L = 20 μM. To avoid dilution of the analyte solutions, the titrant solutions contained stDNA at a concentration c_{DNA} = 4 mM (bp) as well as the ligand at the same concentration as in the titrated solution.

Aliquots (2.5 ml) of the analyte solutions in ETN buffer were placed into quartz spectrophotometric cells and titrated with the titrant solutions in 0.5–2 equivalent intervals.

UV-Vis spectra were recorded on a UV-Vis Perkin-Elmer Lambda 12 double beam spectrophotometer (wavelength range of 300-500 nm). The titrations were finished after no changes were observed in absorption spectra upon addition of at least three two-equivalent portions of the titrant. All spectrophotometric titrations were performed at least three times to ensure the reproducibility.

6.2.3.2 Spectrofluorimetric titrations

Spectrofluorimetric titrations were performed essentially as described for the spectrophotometric titrations. In this case, a ligand concentration c_L = 2 or 5 μM was used. The excitation wavelength for spectrofluorimetric titrations corresponded to one of the isosbestic points, as determined from the spectrophotometric titrations. The spectra were recorded on a Perkin Elmer LS50B fluorimeter (wavelength range 400-600 nm). All fluorimetric titrations were performed at least three times to ensure the reproducibility.

6.2.3.3 Evaluation of binding costants (K) and binding site size (n)

Firstly, the concentration of the ligand bound to the DNA was calculated:

$$c_b = c_L \times \frac{A_f - A}{A_f - A_b}$$

Here c_L is the bulk concentration of the ligand, A_f is the absorbance at a given wavelength (usually absorption maximum of the unbound ligand) in the absence of DNA, A_b is the absorbance of the fully bound ligand, and *A* is the absorbance at a given ligand-to-DNA ratio.

Then, the concentration of the unbound dye (*c*) was calculated:

$$c = c_L - c_b$$

The ratio of bound ligand molecules per DNA base pair (*r*) is:

$$r = \frac{c_b}{c_{DNA}}$$

Again, no error in the DNA concentration is assumed since it is not determined in the course of titration. The data were presented as Scatchard plots [151], i.e., *r*/*c vs. r* values, and numerically fitted to the neighbour exclusion model of McGhee and von Hippel [152], to determine the values of the binding constant (*K*) and the binding site size (*n*). The numerical fitting was performed using non-linear curve fitting algorithm implemented into the Sigma-Plot® software.

$$\frac{r}{c} = K(1 - nr)\left(\frac{1 - nr}{1 - (n-1)r}\right)^{n-1}$$

6.2.4 DNase I FOOTPRINTING

6.2.4.1 Preparation, radiolabeling and purification of DNA fragments

A 132 bp fragment was designed and amplified by PCR. Reverse primer (4 ng) was radioactively labeled by reaction with γ-[^{32}P]-ATP (3 μl) and T4 polynucleotide kinase (1 μl) in 10 μl of forward reaction buffer (70 mM Tris-HCl, pH=7.6, 10 mM $MgCl_2$, 100 mM KCl and 1 mM 2-mercaptoethanol) for 1 h at 37°C. PCR was performed in 50 μl thermophilic DNA poly-buffer containing dNTPs (125 μM), $MgCl_2$ (1mM), *Taq* polymerase (5μM), [^{32}P]-labeled reverse primer (4 ng), forward primer (4 ng) and the templates IM18/IM20 (20 ng). The PCR products were purified by 2% agarose gel electrophoresis. DNA was isolated using MERMAID kit according to the manufacturer's instructions [155, 174]. A 236 bp fragment, obtained from the digestion of the plasmid pUC 18 with *Hind III*, was amplified with PCR as previously described.

6.2.4.2 DNase I footprinting and electrophoresis

For DNAse I experiments, the labeled DNA fragment (2 μl) was added to 4 μl of the appropriate concentration of drug in TN buffer (10 mM Tris-HCl, pH=7.0, 10 mM NaCl) or TN buffer alone and incubated for 3 h at 37°C. The digestion of the samples was then initiated by the addiction of 2 μL of DNase I solution (20 mM NaCl, 2 mM $MgCl_2$ and 2 mM $MnCl_2$, pH=8.0) adjusted to yield a final concentration of about 0.1 U ml^{-1} in the reaction mixture. Thus, the extent of digestion was limited to less than 30% of the starting material so as to minimize the incidence of multiple cut in any strand ("single hit kinetic" conditions). Optimal enzyme diluition was established in preliminary calibration experiments. After 9 min the digestion was stopped by placing the samples on dry ice and then lyophilized. DNA was resuspended in 4 μl of an 80% formamide solution containing tracking dyes (bromophenol blue and cyanol blue) and denaturated by heating the samples at 90°C for 4 min and chilled on ice for 5 min prior to load in a 10% denaturating polyacrylamide gel containing 8 M urea. After electrophoresis (about 3 h at 70 W, 2000 V, 55°C in TBE buffer), the gel was transferred onto Whatman 3 mm paper and dried under vacuum at 80°C for about 2 h and, finally, exposed overnight to X-ray film at -80°C.

6.2.5 IRRADIATION PROCEDURES

HPW 125 Philips lamps, mainly emitting at 365 nm, were used for irradiation experiments. The spectral irradiance of the source was 4.0 mW cm^{-2} as measured, at the sample level, by a Cole-Parmer Instrument Company radiometer (Niles, IL), equipped with a 365-CX sensor.

6.2.6 DNA PHOTOCLEAVAGE

In order to investigate the DNA photocleavage activity, all the compounds were irradiated, under aerobic conditions in ETN buffer, in the presence of supercoiled double strand pBR322 plasmid, which it is a very sensitive tool for damages detection. The irradiation of a photosensitizer could provoke a damage at single or both strands of the plasmid, inducing the formation of different hydrodynamic forms as OC (form II: open circular) and L (form III: linear) (Fig. 6.2). So the reaction mixtures were resolved by agarose electrophoresis and the DNA bands were opportunely detected and quantified.

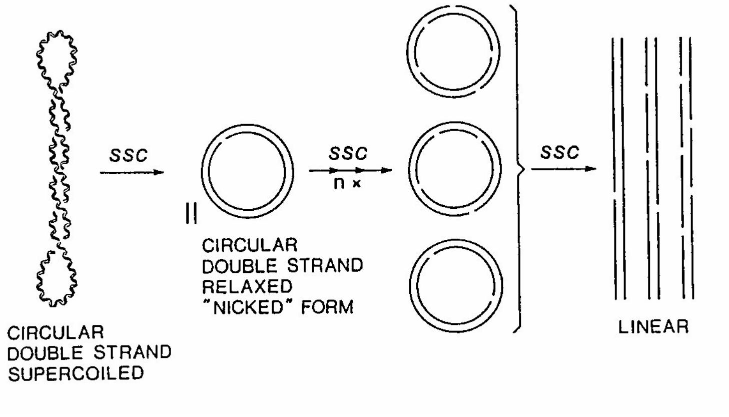
SSC
CIRCULAR DOUBLE STRAND SUPERCOILED
SSC
n ×
CIRCULAR DOUBLE STRAND RELAXED "NICKED" FORM
SSC
LINEAR

Figure 6.2 Representation of the three possible plasmidic DNA forms: supercoiled (SC, Form I); open circular (OC, Form II); linear (L, Form III).

6.2.6.1 ***Determination of strand breaks***

The plasmid solution (20 µl), containing pBR322 (100 ng) and the selected compound at increasing [Drug]/[DNA] ratios, was irradiated with different UVA doses (En= 0, 1.25, 2.5, 5 and 11.25 J/cm^2). After the addition of 4 µl of loading buffer (0.25% bromophenol blue, 0.25% xylene cianol, 30% glycerol in water) the samples were loaded on 1% agarose gel and the run was carried out in TAE buffer (0.04 M Tris-acetate, 1mM EDTA) at 80 V for 2 hours. After staining with ethidium bromide solution (0.5 mg/ml), gel was washed with water and the DNA bands were detected with a UV transilluminator. Photographs were taken by a digital photocamera Kodak DC256 and the quantification of the bands was achieved by image analyzer software Quantity One (BIO-RAD, Milano, Italy). The fractions of supercoiled DNA (Form I) were calculated:

$$\mathrm{sc-DNA} = \frac{\mathrm{Area_{sc}}}{\mathrm{Area_{sc}} + \sum_{i=1}^{n} \mathrm{Area_{cl}}/1.66}$$

Where Area$_{sc}$ is the area of supercoiled DNA (form I) and Area$_{cl}$ is the area of the open circular or linear DNA (form II and III, respectively) obtained by the densitometric analysis of gel. The presence of the coefficient 1,66 in the formula is due to the fact that ethidium bromide bound to the supercolied pBR322 is 1,66 times less than that bound to form. II and III [175]. Each experiment was repeated at least three times.

6.2.6.2 ***Determination of oxidative damages***

The irradiation of the plasmid with a photosensitizing agent can provoke frank strand breaks (i.e., direct cleavage) or oxidative damages at purinic or pyrimidinic bases along DNA. This type of damage was visualized using properly base excision repair enzymes as Fpg (Formamido pyrimidin glycosilase), which recognizes purinic damages, and Endo III (Endonuclease III), which recognizes pyrimidinic ones. The plasmid solution (20 µl), containing pBR322 (100 ng) and the selected compound at [Drug]/[DNA]= 0, 0.04, 0.08 and 0.2, was irradiated with UVA (En= 5 J/cm^2). After irradiation two aliquots of samples were incubated at 37 °C with Fpg and Endo III, respectively, as described by Pflaum *et al.* [160]. The reactions were stopped by addition of 4 µl of loading buffer and the sample loaded into 1% agarose gel as described in the section 6.2.6.1. Each experiment was repeated at least three times.

6.2.6.3 Determination of the protection induced by scavengers

To further evaluate the influence of reactive oxygen species in the photocleavage of plasmid DNA, a series of experiments were carried out using appropriate scavengers.

The scavengers used were: BHA (2,6-ditert-butylhydroxyanisole, 10 µM in ethanol) and GSH (glutathione reduced form, 1 mM in PBS, i.e., phosphate buffer, 10 mM, NaCl 9 g/l, pH=7,2) as radical scavengers (R•); DMTU (N-N'-dimethyl thiourea, 1 mM in ethanol), t-BuOH (0.2%)and Man (Mannitol, 10 mM in phosphate buffer) which scavenge hydroxyl radicals (OH•); SOD (Superoxide dismutase, 1000 UI/ml in phosphate buffer) and CAT (Catalase, 1000 UI/ml in phosphate buffer) which scavenge O_2-• and H_2O_2 respectively; NaN_3 (sodium azide, 10 mM in phosphate buffer) and DABCO (1,4 diazabicyclo [2,2,2] octane, 1 mM in ethanol) a $^1O_2$ scavengers. The reaction was also carried out in deuterated water, in which the lifetime of singlet oxygen is increased by a factor of ca. 14, relative to the one in water.

The plasmid solution, containing pBR322 (100 ng), the selected compounds at drug to DNA ratio of 0 and 1 plus the selected scavengers, was irradiated with UVA (En= 5 J/cm^2). The reactions were stopped and run as described in section 6.2.6.1. All experiments were performed at least three times to ensure the reproducibility.

6.2.7 DNA-SEQUENCING

The preparation, the radiolabeling and purification of DNA fragments were described in section 6.2.4.1.

The method was similar to the DNAse I footprinting [158, 177]. Briefly, after incubation for 3 h at 37°C, the labeled DNA solutions were irradiated with UVA (En= 0, 1 and 1.2 J/cm^2). The reaction was stopped by placing the samples in dry ice and then lyophilized. DNA was resuspended in 4 µl of an 80% formamide solution containing tracking dyes and gel was run as previously described (see section 6.2.4.2)

6.2.8 CELLULAR CYTOTOXICITY AND PHOTOTOXICITY

For experiments of cellular viability, various human cell lines were used: Jurkat, K-562, HL-60, CEM, A-549, MCF-7, MCF-7 mdr, NCTC-2544 and LoVo.

Jurkat are human lymphoblastoid cells; K-562 are chronic myelogenous leukaemia; HL-60 are promyelocytic leukemia cells and CEM are human T lymphoblastoid cells. All the leukemic cells were grown in RPMI-1640 medium supplemented with 115 units/ml of penicillin G, 115 μg/ml streptomycin and 10% heat-inactivated foetal bovine serum (complete RPMI-1640 medium). Cells were kept at 37°C in 5% CO_2 humidified atmosphere and re-seeded into fresh medium three times a week.

A-549 are human lung carcinoma cells; MCF-7 are human breast adenocarcinoma cells; MCF-7 mdr are human breast adenocarcinoma resistant to doxorubicin; NCTC-2544 are human immortalized keratinocytes. All these cells were grown in DMEM medium supplemented with 115 units/ml of penicillin G, 115 μg/ml streptomycin and 10% heat-inactivated foetal bovine serum (complete DMEM medium). Cells were kept at 37°C in 5% CO_2 humidified atmosphere, trypsinized and re-seeded into fresh medium twice a week. LoVo are human intestinal adenocarcinoma; the cells were grown in HAM'S F12 medium supplemented with 115 units/ml of penicillin G, 115 μg/ml streptomycin and 10% heat-inactivated foetal bovine serum (complete HAM'S medium). Cells were kept at 37°C in 5% CO_2 humidified atmosphere, trypsinized and re-seeded into fresh medium twice a week.

Individual wells of a 96-well tissue culture microtiter plate were inoculated with 100 μl of complete medium containing $5x10^3$ cells. The plates were incubated at 37 C° in a humidified 5% CO_2 incubator for 24 hours prior to the cell viability experiments. Drugs were dissolved in DMSO, then were diluted with appropriate complete medium for cytotoxicity assay. After medium removal, 100 μl of the drug solution in different concentration were added to each well and incubated at 37 °C for 72 hours.

In the case of photocytotoxicity the compounds were diluited in Hank's Balanced Salt Solution (HBSS pH=7,2), incubated for 30 minutes at 37°C and then irradiated with UVA (En=2.5 and 3.75 J/cm^2). Finally, the drug solution was replaced with the appropriate complete medium and the plates were incubated for 72 hours.

After the period of incubation, in both cases, the cell viability was evaluated by the MTT [(3-(4,5-dimethylthiazol-2-yl)-2,5 diphenyl tetrazolium bromide)] test [159]. In each well, 10 μl of MTT, 5 mg/ml in PBS, were added and plates were put into the incubator for 3 or 4 hours. MTT is a yellow dye that can be absorbed by viable cell and reduced by mitochondrial dehydrogenises, producing insoluble blue crystals. After incubation, crystals were solubilized adding 100 μl of 0.08 N HCl in isopropanol and plates were detected through microplate BIO-RAD reader at λ=570 nm. The absorbance of each sample was corrected by instrument which subtracted the mean value of blanks, i.e., well in which there were all the components of the medium except cells.

The absorbance is proportional with cellular viability, so the cellular survival was calculated by this equation:

$$\%\ \text{cell survival} = \frac{A_{100\%} - A_{\text{sample}}}{A_{100\%}}$$

$A_{100\%}$ = mean of controls, i.e., cells without drug nor irradiation exposure, which represents 100% of survival.

A_{sample} = absorbance of various samples in which cells were in contact with drug or irradiated in presence of drug.

For every cellular line, GI_{50}, i.e., the drug concentration that induces 50% of inhibition of cell growth of the treated cells, was calculated through SigmaPlot® software. Each experiment was repeated at least three times.

6.2.8.1 Determination of the protection induced by scavengers

In order to evaluate the involvement of reactive oxygen species in the mechanism of phototoxicity, some experiments were carried out with appropriate scavengers as GSH (1mM in PBS), BHA (10 μM in ethanol), DMTU (1 mM in ethanol), Man (10 mM in PBS), DABCO (1 mM in PBS), NaN_3 (1 mM in PBS), SOD (1000 UI/ml in PBS) and CAT (1000 UI/ml in PBS). The microtiter plates are inoculated as previously described with the tested compounds, but the selected scavengers are added into the solutions of compounds prior the incubation of 30 minutes. The GI_{50} values are calculated as described before. Each experiment was repeated at least three times.

6.2.9 EVALUATION OF LIPIDIC PEROXIDATION

Lipidic peroxidation was monitored by Morlière method or TBARS assay [163], which checks the formation of malondialdehyde (MDA), one of the final product of this oxidation process, as it reacts with thiobarbituric acid.

Jurkat cells (500.000 cells/well) were irradiated (En= 2.5 and 3.75 J/cm^2) in the presence of the most active compounds dissolved in HBSS. Then the drug solution was replaced with RPMI-1640 medium and cells were incubated for 24 hours. To check lipidic peroxidation, after cell centrifugation, 900 µl of surnatant were collected and put at -20 °C after having added 90 µl of 2,6-ditert-butyl-*p*-cresol (BHT, 2% in absolute ethanol). Cells were washed, resuspended in 500 µl of water and then 400 µl of cells were lysed by addition of SDS (final concentration, 1% in water) and vortexed. This suspension was divided into two aliquots: in 500 µl were added 50 µl of BHT and 300 µl were used for protein quantification with Peterson method [176]. Lipid peroxidation both in the supernatants and cell extracts was measured using a thiobarbituric acid assay as described by Morlier *et al.*[163]. A standard curve of 1,1,3,3 tetraethoxypropane was used to quantify the amount of produced MDA. Data were expressed in terms of nanomoles of TBARS normalized to the total protein content in an aliquot of the cell extract. All experiments were performed at least three times to ensure the reproducibility.

6.2.10 CONFOCAL MICROSCOPY

Confocal (fluorescence) microscopy is a microscopic technique that provides true three dimensional imaging and resolution. The 3D resolution is attained by designing a microscope in such a way that all the light which is not coming from an in-focus plane is being blocked or removed afterwards. The way to achieve this is by putting a pinhole in front of the detector (Fig. 6.3). The light coming from the laser passes an (excitation) pinhole and is reflected by a dichroic mirror and focused by a microscope objective to a small spot on the sample. To obtain a full image, the image point is moved across the specimen by mirror scanners. The emitted/reflected light passing through the detector pinhole is transformed into electrical signals by a photomultiplier and displayed on a computer monitor screen [166].

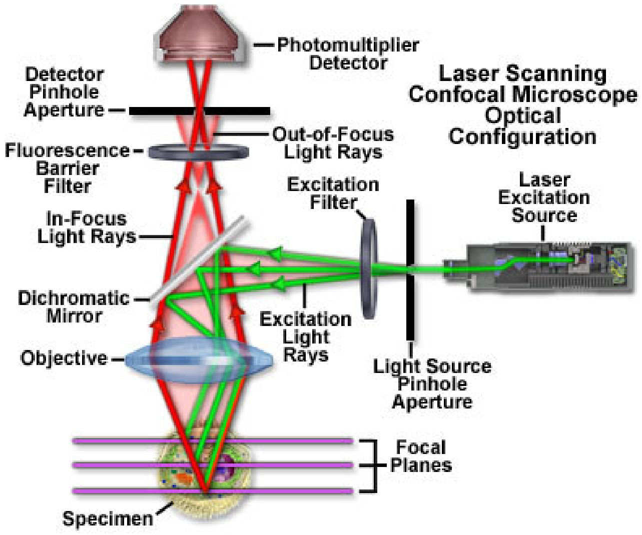
Photomultiplier Detector
Laser Scanning Confocal Microscope Optical Configuration
Detector Pinhole Aperture
Out-of-Focus Light Rays
Fluorescence Barrier Filter
Excitation Filter
Laser Excitation Source
In-Focus Light Rays
Dichromatic Mirror
Excitation Light Rays
Objective
Light Source Pinhole Aperture
Focal Planes
Specimen

Figure 6.3 Schematic representation of confocal microscope.

In a 6-wells/plate, 150.000 NCTC-2544 cells were incubated at 37°C with the presence of the selected compounds for 3 h. Then the medium was removed and replaced with HBSS solution contained the selected fluorescent probes. The first one is JC-1, that enter selectively in the mitochondria, and AO (acridine orange), specific for lysosomes. The fluorescence of the drugs was detected by confocal microscopy using a Leica TCS-SP5 workstation (Leica Microsystem, Germany) with a 63 X / 1.4 NA oil objective, equipped with an argon laser (Lasos 80) and a *diode* laser. The optical sections were obtained in the Z axis and stored on the computer with a scanning mode. The excitation wavelength used for the drugs was λ_{exc}= 405 nm while for the probes was λ_{exc}= 488 nm. Data were collected using Leica FW4000 software and analyzed with Leica Deblur and ImageJ version 1.35

6.2.11 FLOW CYTOMETER

Flow cytometry is a very important technique to obtain cellular characteristics: from the presence of membrane antigens with immunofluorescence methods to cellular volume, from cellular granularity to cellular membrane permeability. This is an instrument that makes statistical analysis in samples of microscopic dispersed particles in liquid suspension, through light diffusion and fluorescence phenomena. The instrument is formed by five components: fluidic system, optical system, electronic system, mechanic system and finally data SW-analysis system (Fig. 6.4). Fluidic system consists of a flow cell, a special capillary, usually in quartz, where an hydrodynamic apparatus allowed to obtain the so-called “hydrodynamic focalization”. In this system, single particles are forced to flow at the centre of this capillary, where ideally they can perform laminar flow. Inside this flow cell, particles are in single line, so the instrument has the possibility to take single measures sequentially. The light source can be a laser or mercury vapour lamp. The optical system lets the light beam arrives in the capillary core where it is focalized to each single cell flowing. Signals from cells are sent to respective photomultipliers.

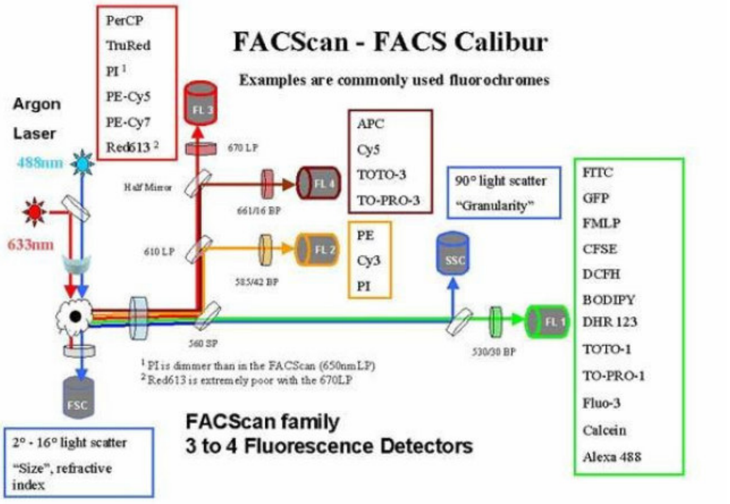
FACScan - FACS Calibur
Examples are commonly used fluorochromes
Argon
Laser
488nm
633nm
PerCP
TruRed
PI 1
PE-Cy5
PE-Cy7
Red613 2
FL 3
670 LP
Half Mirror
661/16 BP
FL 4
APC
Cy5
TOTO-3
TO-PRO-3
90° light scatter
"Granularity"
610 LP
585/42 BP
FL 2
PE
Cy3
PI
SSC
560 SP
530/30 BP
FL 1
FITC
GFP
FMLP
CFSE
DCFH
BODIPY
DHR 123
TOTO-1
TO-PRO-1
Fluo-3
Calcein
Alexa 488
1 PI is dimmer than in the FACScan (650nmLP)
2 Red613 is extremely poor with the 670LP
FSC
2° - 16° light scatter
"Size", refractive index
FACScan family
3 to 4 Fluorescence Detectors

Figure 6.4 Schematic representation of a flow cytofluorimeter.

There is also an optical group parallel and orthogonal to light beam to check side scattering (SS) and forward scattering (FS), respectively. SS gives information about cellular morphology (shape, cytoplasmatic granularity and nucleus/cell rate), while FS about the size of objects. In the SS there are also fluorescent phenomena if fluorochromes are used for analysis (FITC, PE, etc). The emitted light is checked for spectral analysis (separation of wavelength through dichroic spectra) and it is sent to a photomultiplier to amplify signals that are transformed to electric impulses and digitalised. A computer analyses the data and helps their visualization. It is possible to isolate single populations of cell (for example living cells) and to analyse, only in this subpopulation, the parameters (gating).

Flow cytometry presents numerous advantages: the possibility of multiparametric analysis, the reproducibility, the high number of analysed cells (1.000.000 events), the speed of analysis (seconds) and the simplicity of the preparation of samples.

6.2.12 DETERMINATION OF MECHANISM OF CELLULAR DEATH

6.2.12.1 Externalization of phosphatidylserine (PS)

In the early stages of apoptosis, changes occur at the cell surface. One of these modifications is the loss of plasmatic membrane asymmetry, with the translocation of phosphatidylserine (PS) from the inner side of the plasma membrane to the outer layer, by which PS becomes exposed at the external surface of the cell. Annexin-V binds PS selectively and, when conjugated with a fluorophore (FITC, fluorescein isothiocyanate), it can be used as a sensitive probe for PS exposure upon cell membrane. The measurement of Annexin V binding to the cell surface, as indicative for apoptosis, was performed in conjunction with a dye (PI, propidium iodide) exclusion test to establish integrity of the cell membrane (Fig. 6.5) [165, 167].

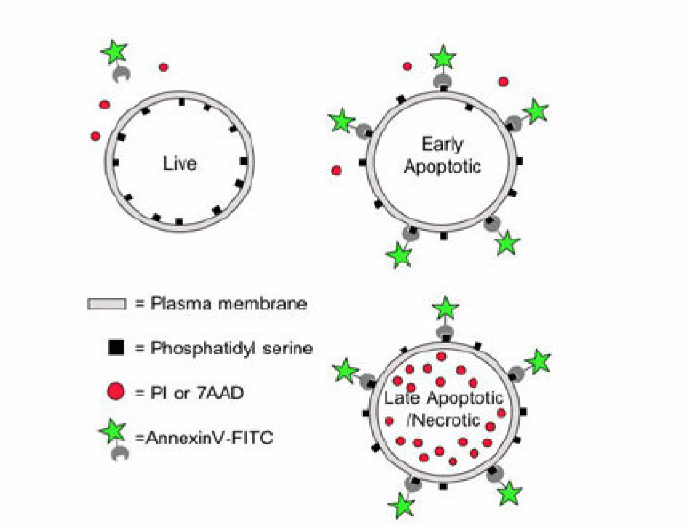

Figure 6.5 Localization of PS and integrity membrane.

100.000 Jurkat cells were treated with different concentrations of selected compounds, in dark conditions or after UVA irradiation. After 24 of incubation, samples were centrifuged and 70 μl of Annexin V-FITC/PI were added. Samples were incubated for 15 minutes in the dark and then were analysed by Coulter Cytomics FC500 (Beckman–Coulter) cytofluorimeter. Both the probes are excited at 488 nm and while FITC emitted at 520 nm (green, FL1), PI fluoresces at 620 nm (red, FL3).

In conclusion, living cells do not show any fluorescence, late apoptosis cells demonstrate both fluorescence, early apoptotic cells present only the FITC one as their plasmatic membrane is still integer, necrotic cells demonstrate PI one.

6.2.13 INVOLVEMENT OF MITOCHONDRIA IN CELL DEATH

6.2.13.1 Determination of mitochondrial potential membrane

One parameter of mitochondrial dysfunction is the loss of mitochondrial membrane potential. The mitochondrial membrane potential was measured with the lipophilic cation 5,5’,6,6’ tetrachlo-1,1’,3,3’-tetraethylbenzimidazol-carbocyanine (JC-1) (Fig. 6.6).

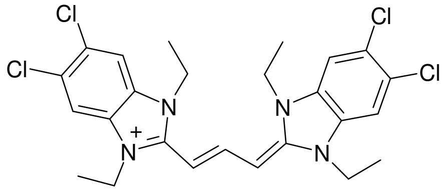

Figure 6.6 Structure of JC-1 (5,5’,6,6’ tetrachlo-1,1’,3,3’-tetraethylbenzimidazol-carbocyanine).

The method is based on the ability of this fluorescent probe to enter selectively into mitochondria and to change reversibly its colour from green to orange as membrane potential increases. This property is due to the reversible formation of JC-1 aggregates upon membrane polarization that causes shift in the emitted light from 530 nm (i.e., emission of JC-1 monomeric form) to 590 nm (emission of J-aggregate) when excited at 488 nm [168, 169]. Briefly, after 24 hours from incubation with the selected compounds, Jurkat cells were collected by centrifugation and resuspended in HBSS containing the JC-1 at the concentration of 2.5 µg/ml. Cells were then incubated for 10 min at 37 °C, centrifuged and resuspended again in HBSS. The cytofluorimetric analysis (Coulter Cytomics FC500) was performed collecting green (FL1) and orange (FL2) fluorescence.

6.2.14 DETERMINATION OF CASPASE ACTIVATION

Caspases are **C**istein-**Asp**artic acid prote**ases** and participate in a cascade that is triggered in response to proapoptotic signals and culminates in cleavage of a set of proteins, resulting in disassembly of the cell [170, 171].

The activation of caspase 3, an executioner caspase, was tested by a colorimetric assay using a caspase-3 assay kit. 1.000.000 Jurkat cells were treated with the selected compounds, in dark conditions or after UVA irradiation, and after 24 h the cells were harvested, washed and resuspended in a lysis buffer. Lysed cells were put in contact with the caspase-3-substate tetrapeptide conjugated with *p*-nitroanilide (*N*-acetyl-Asp-Glu-Val-Asp-pNA, DEVD-*p*NA).

The formation of *p*NA was measured at 405 nm using a microtiter plate reader. Values were normalized to the protein content in cell lysates, obtained by Bradford method [178]. Each experiment was repeated at least three times.

6.2.15 ANALYSIS OF CELL CYCLE

The analysis of cell cycle was conducted through flow cytometry; this test is based in the fact that each phase presents a different content of DNA.

Diagrams of growing cultures display the characteristic x-axis distribution according to the DNA content, the first peak corresponding to the diploid peak, i.e., to cells in the G1 phase, and the second peak to cells with DNA content, i.e., to cells in G2/M phase. Cells with an intermediate DNA content are in the S phase. When DNA is fragmented, as in apoptotic cells, the affinity with the intercalating PI dye is decreased and a so-called hypodiploid peak (or area) becomes apparent to the left of the G1 peak (Fig. 6.8) [172].

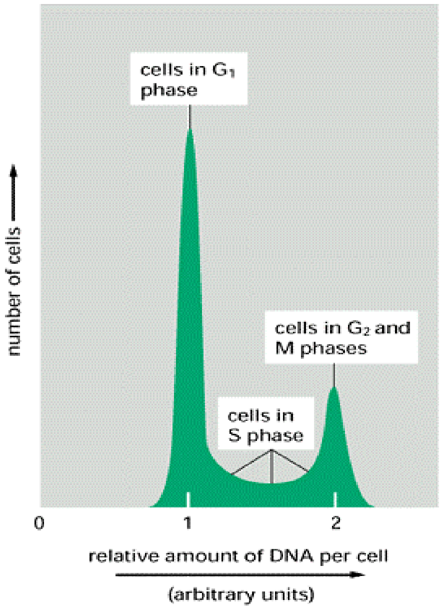

Figure 6.8 Representation of cell cycle distribution.

For flow cytometric analysis of DNA content, $5x10^5$ Jurkat cells in exponentially growth were treated with the selected compounds for 24hours. After the incubation period, cells were centrifuged and fixed with ice-cold ethanol (70%), then treated overnight with PBS buffer containing RNAse (10 KU/ml) and propidium iodide (PI, 10 µg/ml) (Fig. 6.9). When intercalated in DNA, PI fluoresces in the red (620 nm, FL3), if it is excited at 488 nm. Each experiment was repeated three times.

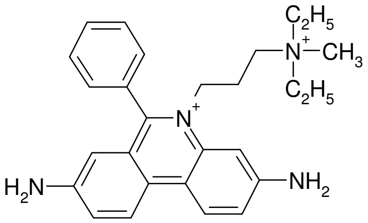

Figure 6.9 Structure of Propidium Iodide (PI).

Samples were analyzed on a Becton Coulter Epics XL-MCL flow cytometer. For cell cycle analysis, results were examined using MultiCycle for Windows (Phoenix Flow Systems, San Diego, CA) [166]. Data were expressed as fractions of cells in the different cycle phases.

6.2.16 TOPOISOMERASE I AND II ASSAY

6.2.16.1 Topoisomerase I relaxation and cleavable complex assay

This assay was adapted from Bridewell *et al.* [179]. Incubation mixtures (20µl) contained 50 mM Tris-HCl (pH=7.5), 50 mM KCl, 10 mM $MgCl_2$, 0.5 mM dithiothreitol (DTT), 0.1 mM EDTA, 30 µg/ml of BSA, 0.25 µg pBR322 supercoiled plasmid DNA and 10 units of human topoisomerase I. Reactions were assembled on ice with drug (0-200 µM) and topoisomerase being added last, incubated at 37°C for 30 min and terminated by the addition of pre-warmed SDS (final concentration 1%) followed by proteinase K treatment (final concentration 50 µg/ml) for an additional digestion at 37°C for 30 min. The reaction was terminated by addition of 2 µl of loading buffer (0.25% bromophenol blue, 50% glycerol). The samples contained the compound were successively extracted with chloroform and isoamyl alchool (CIA 24:1) prior to load. The reaction mixtures were analyzed by electrophoresis on 1% agarose gel in TAE buffer (40 mM Tris-acetate, pH=8.0, 1 mM EDTA) at 20 V overnight and then stained with a solution containing 0.5 µg/ml of ethidium bromide. DNA bands were visualized by UV light and photographed through a digital photocamera Kodak DC256.

For the cleavable complex assay the final reactions mixtures were loaded in a 1% agarose gel contained 0.5 µg/ml of ethidium bromide, run overnight, as previously described, and then washed with distilled water.

6.2.16.2 Topoisomerase II relaxation assay

Assay mixtures (20 µl) contained 125 ng of supercoiled plasmid pBR322, 2 units of human topoisomerase IIα and 0-200 µM of selected compounds in aqueous solution (50 mM Tris-HCl, pH=8.0, 120 mM KCl, 10 mM $MgCl_2$, 0.5 mM DTT and 30 µg of BSA). The reactions were carried out as described in section 6.2.16.1.

6.2.16.3 Topoisomerase II cleavable complex assay

Incubation mixtures (20 µl) contained 100 ng of supercoiled plasmid pBR322, 6 units of human topoisomerase IIα and 0-200 µM of selected compound in aqueous solution (50 mM Tris-HCl, pH=8.0, 120 mM KCl, 10 mM $MgCl_2$, 0.5 mM DTT and 30 µg of BSA). Reactions were assembled on ice with drug and topoisomerase IIα being added at last, incubated at 37°C for 30 min and enzyme-DNA cleavage intermediates were trapped by the addition of pre-warmed SDS (final concentration 0.5%) followed by proteinase K treatment (final concentration 50µg/ml) for 1h at 45°C to digest topoisomerase IIα. Samples were mixed with 2 µl of loading buffer and then subjected to electrophoresis in 1% agarose gel, containing 0.5 µg/ml of ethidium bromide, in TAE buffer (40 mM Tris-acetate, pH=8.0, 1 mM EDTA) at 20 V overnight and then washed with distilled water. DNA bands were visualized by UV light and photographed through a digital photocamera Kodak DC256.

7. REFERENCES

7. REFERENCES

1. Katzung B.G., Basic and clinical pharmacology. *Ed Lange Medical Books,* **1998**.
2. Rang H.P., Dale M.M. and Ritter J.M., Pharmacology. *Harcourt Health Sciences,* **1999**.
3. Tolone G., General oncology. *Medical books,* **2001**.
4. Maraldi N.M., Zini N., Santi S., Scotlandi K., Serra M. and Baldini N., P-glycoprotein subcellular localization and cell morphotype in MDR1 gene-transfected human osteosarcoma cells. *Biol. Cell,* **1999**, 91, 17-28.
5. Gariboldi M.B., Terni F., Ravizza R., Meschini S., Marra M., Condello M., Arancia G. and Monti E., The nitroxide tempol modulates anthracycline resistance in breast cancer cells. *Free Rad. Biol. & Med.,* **2006**, 40, 1409-1418.
6. Foye W.O., Lemke T.L. and Williams D.A., Principles of medicinal chemistry. *Lea & Fabinger Book,* **1995**.
7. Hurley L.H., DNA and its associated process as target for cancer therapy. *Nature,* **2002**, 11, 188-200.
8. Hadfield J.A., Ducki S., Hirst N. and McGrow A.T., Tubulin and microtubules as targets for anticancer drugs. *Prog. Cell Cyc. Res.,* **2003**, 5, 309-325.
9. Jordan M.A. and Wilson L., Microtubules and actin filaments: dynamic targets for cancer chemotherapy. *Curr. Op. Cell Biol.,* **1998**, 10, 123-130.
10. Denny B.J., Whellhouse R.T., Stevens M.F.G., Tsang L.L.H. and Slack J.A., NMR amd molecular modeling investigation of mechanism of action of antitumor drug temozolomide and its interaction with DNA. *Biochemistry,* **1994**, 33, 9045-9051.
11. Diana P., Barraja P., Lauria A., Montalbano A., Almerico A.M., Dattolo G. and Cirrincione G., Pyrrolo[2,1-d][1,2,3,5]tretrazin-4(3H)-ones, a new class of azolotetrazines with potent antitumor activity. *Bioorg. Medic. Chem.,* **2003**, 11, 2371-2380.
12. Goodman L.S., Wintrobe M.M., Dameshek W., Goodman J.J. and Gilman A., Nitrogen mustard therapy. Use of methyl-bis(β-chloroethylamine hydrochloride) and tris(β-chloroethyl)amine hydrochloride for Hodgkin's disease, lymphosarcoma, leukaemia and certain allied and miscellaneous disorders. *JAMA,* **1946**, 132, 126-132.

13. Muller W. and Crothers D.M., Studies of the binding of actinomycin and related compounds to DNA. *J. Mol. Biol.,* **1968**, 35, 251-290.
14. Zimmer C. and Wahnert U., Non-intercalating DNA-binding ligands: specificity of the interaction and their use as tools in biophysical, biochemical and biological investigations of the genetic material. *Prog. Biophys. Mol. Biol.,* **1986**, 47, 31-112.
15. Thuong N. and Helene C., Sequence specific recognition and modification of double helical DNA by oligonucleotides. *Angew. Chem. Int. Ed. Engl.,* **1993**, 32, 666-690.
16. Han H. and Hurley L.H., G-quadruplex DNA: a potential target for anti-cancer drug design. *Trends Pharmacol. Sci.,* **2000**, 21, 136-142.
17. Sun D et al., Inhibition of human telomerase by a G-quadruplex-interactive compound. *J. Med. Chem.,* **1997**, 40, 2113-2116.
18. Broggini M. and D'Incalci M., Modulation of transcription factor-DNA interactions by anticancer drugs. *Anticancer Drug Des.,* **1994**, 9, 373-387.
19. Wang J.C., DNA topoisomerases. *Annu. Rev. Biochem.,* **1996**, 65, 635-692.
20. Pourquier P. and Pommier Y., Topoisomerase I-mediated DNA damage. *Adv. Cancer Res.,* **2001**, 80, 189-216.
21. Ihmels H., Faulhaber K. and Viola G., Evaluation of the DNA-binding properties of cationic dyes by absorption and emission spectroscopy. *Highlights in Bioorg. Chem. Meth. and Appl.,* Ed. by Carsten Schmuck and Helma Wennemers, **2004**.
22. a) Haq I and Ladbury J., Drug-DNA recognition: energetics and implications for design. *J. Mol. Recognit.,* 2000, 13, 188-197. b) Wemmer D.E. and Dervan P.B., Targeting the minor groove of DNA. *Curr. Opin. Struct. Biol.,* **1997**, 7, 355-361. c) Hurley L.H., DNA and associated targets for drug design. *J. Med. Chem.,* **1989**, 32, 2027-2033.
23. Probst C.L. and Perun T.L., Nucleic acid targeted drug design. *Ed. Marcell Dekker, New York,* **1992**.
24. Demeunynck M., Bailly C. and Wilson W.D., DNA and RNA binders, *Ed. Wiley-VCH, Weinheim,* **2002**.
25. Wilson W.D., Blackburn G.M. and Gait M.J., Nucleic acids in chemistry and biology. *Ed. IRL Press, Oxford, UK,* **1996**.
26. Gottesfeld J.M,. Neely L., Trauger J.W., Baird E.E. and Dervan P.B., Regulation of gene expression by small molecules. *Nature,* **1997**, 387, 202-205.

27. Takahashi T., Tanaka H., Matsuda A., Doi T., Yamada H., Matsumoto T., Sasaki D. and Sugiura Y., DNA cleaving activities of 9-membered masked enediyne analogues possessing DNA intercalator and sugar moieties. *Bioorg. Med. Chem. Lett.,* **1998**, 8, 3303-3306.
28. Odom D.T., Parker C.S. and Barton J.K., Site-specific inhibition of transcription factor binding to DNA by a metallointercalator. *Biochemistry*, **1999**, 38, 5155-5163.
29. Wagenknecht H.A., Stemp E.D.and Barton J.K., DNA-Bound peptide radicals generated through DNA-mediated electron transport. *J. Am. Chem. Soc.,* **2000**, 39, 5483-5491.
30. Lerman L.S., Structural considerations in the interaction of DNA and acridines. *J. Mol. Biol.*, **1961**, 3, 18-30.
31. Armstrong R.W., Kurucsev T. and Strauss U.P., The interaction between acridine dyes and deoxyribonucleic acid. *J. Am. Chem. Soc.*, **1970**, 92, 3174-3181.
32. Tuite E. and Norden B., Intercalative interactions of ethidium dyes with triplex structures. *Bioorg. Med. Chem.,* **1995**, 3, 701-711.
33. LePecq J.B. and Paoletti C., A fluorescent complex between ethidium bromide and nucleic acids. Physical-chemical characterization. *J. Mol. Biol.,* **1967**, 27, 87-106.
34. Rye H.S., Yue S., Wemmer D.E., Quesada M.A., Haugland R.P., Mathies R.A. and Glazer A.N., Stable fluorescent complexes of double-stranded DNA with bis-intercalating asymmetric cyanine dyes: properties and applications. *Nucleic Acids Res.,* **1992**, 20, 2803-2812.
35. Breslin D.T., Yu C., Ly D. and Schuster G.B., Structural modification changes the DNA binding mode of cation-substituted anthraquinone photonucleases: association by intercalation or minor groove binding determines the DNA cleavage efficiency. *Biochemistry,* **1997**, 36, 10463-10473.
36. Molina A., Vaquero J.J., Garcia-Navio J.L., de Pascal-Teresa B., Gado F. and Rodrigo M.M., Novel DNA intercalators based on the pyridazino[1’,6’:1,2]pyrido[4,3-b]indol-5-inium system. *J. Org. Chem.,* **1999**, 64, 3907-3915.
37. Ihmels H., Faulhaber K., Sturm C., Bringmann G., Messer K., Gabellini N., Vedaldi D. and Viola G., Acridizinium salts as novel class of DNA-binding and

site-selective DNA-photodamaging chromophores. *Photochem. Photobiol.,* **2001**, 74, 505-512.

38. Pilch D.S., Yu C., Makhey D., LaVoie E.J., Srinivasan A.R., Olson W.K., Sauers R.S., Breslauer K.J., Geacintov N.E. and Liu L.F., Minor groove-directed and intercalative ligand-DNA Interactions in the poisoning of human DNA topoisomerase I by protoberberine analogs. *Biochemistry,* **1997**, 36, 12542-12553.
39. Pjura P.E., Grzeskowiak K. and Dickerson R.E., Binding of Hoechst 33258 to the minor groove of B-DNA. *J Mol Biol.*, **1987**, 197, 257-271.
40. Bailly C. and Chaires J.B., Sequence-specific DNA minor groove binders. Design and synthesis of netropsin and distamycin analogues. *Bioconjug. Chem.,* **1998**, 9, 513-538.
41. Lerman L.S., The structure of the DNA-acridine complex. *Proc. Natl. Acad. Sc.i USA.,* **1963**, 49, 94-102.
42. Wilson W.D., Gough A.N., Doyle J.J. and Davidson M.W., Intercalation with DNA as a possible mechanism of antileukemic action. *J. Med. Chem.,* **1976**, 19, 1261-1263.
43. Viola G., Bressanini M., Gabellini N., Vedaldi D., Dall'Acqua F. and Ihlmes H., Naphtoquinolizinium derivatives as a novel platform for DNA-binding and DNA-photodamaging chromophores. *Photochem. Photobiol. Sci.,* **2002**, 1, 882-889.
44. Viola G., Dall'Acqua F., Gabellini N., Moro S., Vedaldi D. and Ihmels H., Indolo[2,3-b]-quinolizinium bromide: an efficient intercalator with DNA-photodamaging properties. *ChemBioChem,* **2002**, 3, 550-558.
45. Viola G., Ihmels H., Krauber H., Vedaldi D. and Dall'Acqua F., DNA-binding and DNA-photocleavaging properties of 12a,14a-diazoniapentaphene. *ARKIVOC,* **2004**, 219-230.
46. Ihmels H., Faulhaber K., Vedaldi D., Dall'Acqua F. and Viola G., Intercalation of organic dye molecules in to double-stranded DNA. Part 2: the annelated quinolizinium ion as a structural motif in DNA intercalators. *Photochem. Photobiol.,* **2005**, 81, 1107-1115.
47. Ihmels H., Otto D., Dall'Acqua F., Faccio A., Moro S. and Viola G., Comparative studies on the DNA-binding properties of linear and angular dibenzoquinolizinium ions. *J. Org. Chem.,* **2006**, 71, 8401-8411.

48. Martinez R. and Chacon-Garcia L., The search of DNA-intercalators as antitumoral drugs: what it worked and what did not work. *Curr. Med. Chem.,* **2005**, 12, 127-151.
49. Cotter T.G., Lennon S.V., Glynn J.G. and Martin S.J., Cell death via apoptosis and its relationship to growth, development and differentiation of both tumor and normal cells. *Anticancer Res.,* **1990**, 10, 1153-1159.
50. Calabresi P. and Chabner B.A., In Goodman and Gilman's The pharmacological basis of therapeutics. *9th ed., Hardman J.G., Goodman Gilman A., Limbird L.E., Eds., Mc. Graw Hill,* **1996**, 1225-1232.
51. Solary E., Bertrand R. and Pommier Y., Apoptosis induced by DNAtopoisomerase I and II inhibitors in human leukemic HL-60 cells. *Leuk. Lymphoma,* **1994**, 15, 21-32.
52. Watson J.D., and Crick F.H.C., Molecular structure of nucleic acids: a structure for deoxyribose nucleic acid. *Nature,* **1953**, 171, 737-738.
53. Maiti M. and Kumar G.S., Molecular aspects on the interaction of protoberberine, benzophenanthridine, and aristolochia group of alkaloids with nucleic acid structures and biological perspectives. *Medic. Res. Rev.,* **2006**.
54. Blackburn G.M. and Gait N.J., Nucleic acids in chemistry and biology. *Oxford: IRL Press,* **1990**.
55. Saenger W., Principles of nucleic acids structure. *New York: Springer-Verlag*, **1984**.
56. Pohl F.M. and Jovin T.M., Salt-induced co-operative conformational change of a synthetic DNA: Equilibrium and kinetic studies with poly (dG-dC). *J. Mol. Biol.,* **1972**, 67, 375–396.
57. Wang A.H., Quigley G.J., Kolpak F.J., Crawford J.L., van Boom J.H., van der Marel G. and Rich A., Molecular structure of a left-handed double helical DNA fragment at atomic resolution. *Nature*, **1979**, 282, 680–686.
58. Ivanov V.I., Minchenkova L.E., Schyolkina A.K. and Poletayev A.I., Different conformations of double-stranded nucleic acid in solution as revealed by circular dichroism. *Biopolymers,* **1973**, 12, 89–110.
59. Wang A.J., Quigley G.J., Kolpak F.J., van der Marel G., van Boom J.H. and Rich A., Left-handed double helical DNA: Variations in the backbone conformation. *Science*, **1981**, 211, 171 176.

60. Reddy S.Y., Leclerc F. and Karplus M., DNA polymorphism: A comparison of force fields for nucleic acids. *Biophys. J.,* **2003**, 84, 1421–1449.
61. Felsenfeld G., Davies D.R. and Rich A., Formation of a three-stranded polynucleotide molecule. *J. Am. Chem. Soc.,* **1957**, 79, 2023–2024.
62. Feigon J., A new DNA quadruplex. *Curr. Biol.,* **1993**, 3, 611–613.
63. Brown D.M. and Todd A.R., Nucleic acids. *Annu. Rev. Biochem.,* **1955**, 24, 311-338.
64. Chargaff E. Some recent studies on the composition and structure of nucleic acids. *J. Cell. Physiol.,* **1951**, 38, 41-59.
65. Foloppe N. and MacKerell A.D.J., Intrinsic conformational properties of deoxyribonucleosides: implicated role for cytosine in the equilibrium among the A, B, and Z forms of DNA. *Biophys. J.,* **1999**, 76, 3206-3218.
66. Behe M. and Felsenfeld G., Effects of methylation on a synthetic polynucleotide: The B–Z transition in poly(dG-m5dC).poly(dG-m5dC). *Proc. Natl. Acad. Sci. USA.,* **1981**, 78, 1619 1623.
67. Rich A., Nordheim A. and Wang A.H., The chemistry and biology of left-handed Z-DNA. *Annu. Rev. Biochem.,* **1984**, 53, 791–846.
68. Jovin T.M., Soumpasis D.M. and McIntosh L.P., The transition between B-DNA and Z-DNA. *Annu. Rev. Phys. Chem.,* **1987**, 38, 521–558.
69. Jagger J., Introduction to research in ultraviolet photobiology. In *Prentice-Hall, Englewood Cliffs,* **1967**.
70. Coohill T.P., Action spectroscopy: ultraviolet radiation. In *Handbook of organic photochemistry and photobiology, CRC Press, Inc.,* **1995**.
71. Sutherland J.C. and Griffin K.P., Absorption spectrum of DNA for wavelength greater than 300 nm. *Radiat. Res.,* **1981**, 41, 339-348.
72. Coohill T.P., Peak M.J. and Peak J.G., The effects of ultraviolet wavelength present in sunlight on human cells *in vitro*. *Photochem. Photobiol.,* **1987**, 46, 1043-1051.
73. Painter R.B., The role of DNA damage and repair in cell killing induced by ionizing radiation. In *Radiation Biology in Cancer Research, Ed. Raven Press,* **1980**.

74. Peak M.J., Peak J.G. and Carnes B.A., Induction of direct and indirect single-strand breaks in human cell DNA by far- and near-ultraviolet radiations: action spectrum and mechanism. *Photochem. Photobiol.,***1987**, 45, 381-390.
75. Peak M.J., Peak J.G. and Jones C.A., Different (direct and indirect) mechanism for the induction of DNA-protein crosslinks in human cells by far- and near-ultraviolet radiation (290 and 405 nm). *Photochem. Photobiol.,* **1985**, 42, 141-149.
76. Peak J.G., Peak M.J. and MacCoss M., DNA breakage caused by 334-nm ultraviolet light is enhanced by naturally occurring nucleic acid components and nucleotide coenzymes. *Photochem. Photobiol.,* **1984**, 39, 713-721.
77. Parrish J.A., Fitzpatrick T.B., Tanembaum L. and Pathak M.A., Photochemotherapy of psoriasis with oral methoxalen and long wave ultraviolet light. *New Eng. J. Med.,* **1974**, 291, 1207-1220.
78. Kochevar I.E., Basic concepts in photobiology. *Photoimmunology, Ed. Plenum Press,* **1983**.
79. Pouget J.P., Douki T., Richard M.J. and Cadet J., DNA damage induced in cells by gamma and UV-A radiation as measured by HPLC/GC-MS and HPLC-EC and Comet assay. *Chem. Res. Toxicol.,* **2000**, 13, 541-549.
80. Misiaszek R., Crean C., Joffe A., Geacintov N.E. and Shafirovich V., Oxidative DNA damage associated with combination of guanine and superoxide radicals and repair mechanism *via* radical trapping. *J. Biol. Chem.,* **2004**, 279, 32106-32115.
81. Hiraku Y., Ito K., Hirakawa K. and Kawanishi S., Photosensitized DNA damage and its protection *via* a novel mechanism. *Photochem. Photobiol.,* **2007**, 83, 205-212.
82. Ravanat J.L., Di Mascio P., Martinez G.R., Medeiros M.H. and Cadet J., Singlet oxygen induces oxidation of cellular DNA. *J. Biol. Chem.,* **2000**, 275, 40601-40604.
83. Celander D.W. and Cech T.R., Iron(II)-ethylenediaminetetraacetic acid catalyzed cleavage of RNA and DNA oligonucleotides: similar reactivity toward single- and double-stranded forms. *Biochemistry,* **1990**, 29, 1355-1361.
84. Yamamoto K. and Kawanishi S., Hydroxyl free radical is not the main active species in site-specific DNA damage induced by copper(II) ion and hydrogen peroxide. *J. Biol. Chem.,* **1989**, 264, 15435-15440.

85. Vargas F., Rivas C. and Drosos J.C., Clinical application of phototherapy. In *Advances in biomedical applications of photochemistry & photobiology,* **2002**.
86. Krumann J. and Morita A., Mechanism of ultraviolet (UV)B and UVA phototherapy. *J. Invest. Dermatol.,* **1999**, 4, 70-76.
87. Beijersbergen van Henegouwen G.M.J., Medicinal photochemistry: phototoxic and phototherapeutic aspects of drugs. In *Advances in drug research, Academic Press Limited,* **1997**.
88. Dall'Acqua F. and Rodighiero G., Biological and medicinal aspects of furocoumarins (psoralens and angelicins). In *Primary photo-processes in biological medicine, Ed. Plenum Press,* **1985**.
89. Parrish J.A., Stern R.S., Pathak M.A. and Fitzpatrick T.B., Photochemotherapy of skin diseases. In *The science of photomedicine, Ed. Plenum Press,* **1982**.
90. Gasparro F.P., Psoralen Photochemistry. In *Extracorporeal photochemotherapy: clinical spects and the molecular basis for efficacy, Ed. CRC Press,* **1994**.
91. Chang T.Y., Heinrich L.A., Schultz M.D., Reizner G.T., Kumm R.C. and Cripps D.J., PUVA and skin cancer. A historical cohort study on 492 patients. *J. Am. Acad. Dermatol.,* **1992**, 26, 173-177.
92. Stern R.S. and Laird S., The carcinogenic risk of treatment for severe psoriasis. *Cancer,* **1994**, 73, 2759-2764.
93. Friedman P.S., Effects of ultraviolet radiation on immune responses of skin. *Abstracts of book of first European congress of photobiology,* **1986**.
94. Moor A.C. and Gasparro F.P., Biochemical aspects of psoralen photochemotherapy. *Clin. Dermatol.,* **1996**, 14, 353-365.
95. Edelson R., Berger C., Gasparro F.P., Jegasothy B., Heald P., Wintroub B., Vonderheid E., Knobler R., Wolff K., Plewig G., McKiernan G., Christiansen I., Oster M., Honigsmann H., Wilford H., Kokoschka E., Rehle T., Perez M., Stingl G. and Laroche L., Treatment of cutaneous T-cell lymphoma by extracorporeal photochemotherapy. *New Engl. J. Med.,* **1987**, 316, 297-303.
96. Heald P.W. and Edelson R.L., Photopheresis for T-cell mediated diseases. *Adv. Dermatol.,* **1989**, 3, 25-40.
97. Edelson R.L., Photopheresis: present and future aspects. *J. Photochem. Photobiol. B: Biol.,* **1991**, 10, 165-174.

98. Heald P., Rook A., Perez M., Wintroub B., Knobler R., Jegasothy B., Gasparro F.P., Berger C. and Edelson R., Treatment of erythrodermic cutaneous T-cell lymphoma with extracorporeal photochemotherapy. *J. Am. Acad. Dermatol.,* **1992**, 27, 427-433.
99. Jori G., Molecular and cellular mechanisms in photodmedicine: porphyrins in cancer treatment. In *Primary photo-processes in biology and medicine, Ed Plenum Press,* **1985**.
100. Moan J., Porphyrin photosensitization and phototherapy. *Photochem. Photobiol.,* **1986**, 43, 681-690.
101. Stables G.I. and Ash D.V., Antitumour treatment: photodynamic therapy. *Cancer Treat. Rev.,* **1989**, 21, 311-323.
102. Lockshin R.A. and Zakeri Z., Programmed cell death and apoptosis: origin of the theory. *Nat. Rev. Cell. Biol.,* **2001**, 2, 545-550.
103. Kerr J.F., Wyllie A.H. and Currie A.R., Apoptosis is a basic biological phenomenon with wide-ranging implications in tissue kinetics. *Br. J. Cancer,* **1972**, 26, 239-257.
104. Leist M. and Jaattela M., Four deaths and a funeral: from caspases to alternative mechanisms. *Nat. Rev. Mol. Cell Biol.,* **2001**, 2, 589-598.
105. Meier P., Finch A. and Evan G., Apoptosis in development. *Nature*, **2000**, 407, 796-801.
106. Fadeel B., Gleiss B., Hogstrand K., Chandra J., Wiedmer T., Sims P.J., Henter J.I., Orrenius S. and Samali A., Phosphatidylserine exposure during apoptosis is a cell-type-specific event and does not correlate with plasma membrane phospholipid scramblase expression. *Biochem. Biophys. Res. Commun.,* **1999**, 266, 504-511.
107. Saraste A. and Pulkki K., Morphologic and biochemical hallmarks of apoptosis. *Cardiovasc. Res.,* **2000**, 45, 528-537.
108. Ishizaki Y., Cheng L., Mudge A.W. and Raff M.C., Programmed cell death by default in embryonic cells, fibroblasts, and cancer cells. *Mol. Biol. Cell.,* **1995**, 6, 1443-1458.
109. Weil M., Jacobson M.D., Coles H.S., Davies T.J., Gardner R.L., Raff K.D. and Raff M.C., Constitutive expression of the machinery for programmed cell death. *J. Cell. Biol.,* **1996**, 133, 1053-1059.

110. Bratton S.B., MacFarlane M., Cain K. and Cohen G.M., Protein complexes activate distinct caspase cascades in death receptor and stress-induced apoptosis. *Exp. Cell. Res.,* **2000**, 256, 27-33.

111. Denault J.B. and Salvesen G.S., Caspases: keys in the ignition of cell death. *Chem. Rev.,* **2002**, 102, 4489-4500.

112. Earnshaw W.C., Martins L.M. and Kaufmann S.H., Mammalian caspases: structure, activation, substrates, and functions during apoptosis. *Annu. Rev. Biochem.,* **1999**, 68, 383-424.

113. Naismith J.H. and Sprang S.R., Modularity in the TNF-receptor family. *Trends Biochem. Sci.,* **1998**, 23, 74-79.

114. Scaffidi C., Fulda S., Srinivasan A., Friesen C., Li F., Tomaselli K.J., Debatin K.M., Krammer P.H. and Peter M.E., Two CD95 (APO-1/Fas) signaling pathways. *Embo J.,* **1998**, 17, 1675-1687.

115. Luo X., Budihardjo I., Zou H., Slaughter C. and Wang X., Bid, a Bcl2 interacting protein, mediates cytochrome c release from mitochondria in response to activation of cell surface death receptors. *Cell,* **1998**, 94, 481-490.

116. Slee E.A., Harte M.T., Kluck R.M., Wolf B.B., Casiano C,A,, Newmeyer D.D., Wang H.G., Reed J.C., Nicholson D.W., Alnemri E.S., Green D.R. and Martin S.J., Ordering the cytochrome c-initiated caspase cascade: hierarchical activation of caspases-2, -3, -6, -7, -8, and -10 in a caspase-9-dependent manner. *J. Cell. Biol.,* **1999**, 144, 281-292.

117. Salvesen G.S. and Renatus M., Apoptosome: the seven-spoked death machine. *Dev. Cell.,* **2002**, 2, 256-257.

118. Hengartner M.O., The biochemistry of apoptosis. *Nature,* **2000**, 407, 770-776.

119. Wang X., The expanding role of mitochondria in apoptosis. *Genes Dev.,* **2001**, 15, 2922-2933.

120. Bernardi P., Scorrano L., Colonna R., Petronilli V. and Di Lisa F., Mitochondria and cell death. Mechanistic aspects and methodological issues. *Eur. J. Biochem.,* **1999**, 264, 687-701.

121. Kroemer G. and Reed J.C., Mitochondrial control of cell death. *Nat. Med.,* **2000**, 6, 513-519.

122. Beutner G., Ruck A., Riede B. and Brdiczka D., Complexes between porin, hexokinase, mitochondrial creatine kinase and adenylate translocator display

properties of the permeability transition pore. Implication for regulation of permeability transition by the kinases. *Biochim. Biophys. Acta,* **1998**, 1368, 7-18.

123. Reed J.C., Apoptosis-based therapies. *Nat. Rev. Drug Discov.,* **2002**, 1, 111-121.
124. Wang X.W., Role of p53 and apoptosis in carcinogenesis. *Anticancer Res.,* **1999**, 19, 4759-4771.
125. Wolfe L.S., Biology of the cell. *Ed. Wadsworth Publishing Company, Inc.,* **1981**.
126. Alberts B., Johnson A., Lewis J., Raff M., Roberts K. and Walter P., Molecular Biology of the Cell. *Garland Science: New York,* **2003**.
127. Elledge S.J., Cell Cycle Checkpoints: Preventing an Identity Crisis. *Science*, **1996**, 274, 1664-1672.
128. Morgan D.O., The Cell Cycle: Principles of Control. *New Science Press*, **2007**.
129. Osheroff N., DNA topoisomerases. *Biochim. Biophys. Acta,* **1998**, 1400, 1-2.
130. Palumbo M., Gatto B., Moro S., Sissi C. and Zagotto G., Sequenze-specific interactions of drugs interfering with the topoisomerase-DNA cleavage complex. *Biochim. Biophys. Acta,* **2002**, 1587, 145-154.
131. Pommier Y., Pourquier P., Fan Y. and Strumberg D., Mechanism of action of eukaryotic DNA topoisomerase I and drugs targeted to the enzyme. *Biochim. Biophys. Acta,* **1998**, 1400, 83-106.
132. D’Arpa P. and Liu L.F., Topoisomerase-targeting antitumor drugs. *Biochim. Biophys. Acta,* **1989**, 989, 163-177.
133. Nitiss J.L., Investigating the biological functions of DNA topoisomerases in eukaryotic cells. *Biochim. Biophys. Acta,* **1998**, 1400, 63-81.
134. Berger J.M., Structure of DNA topoisomerases. *Biochim. Biophys. Acta,* **1998**, 1400, 3-18.
135. Wang J.C., DNA topoisomerases. *Annu. Rev. Biochem.,* **1996**, 65, 635-692.
136. Kaufmann S.H., Cell death induced by topoisomerase-targeted drugs: more questions than answers. *Biochim. Biophys. Acta,* **1998**, 1400, 195-211.
137. Pommier Y., Pourquier P., Fan Y. and Strumberg D., Mechanism of action of eukaryotic DNA topoisomerase I and drugs targeted to the enzyme. *Biochim. Biophys. Acta,* **1998**, 1400, 83-106.
138. Pourquier P. and Pommier Y., Topoisomerase I-mediated DNA damage. *Adv. Cancer Res.,* **2001**, 80, 189, 216.

139. Bailly C., Topoisomerase I poisons and suppressors as anticancer drugs. *Curr. Med. Chem.,* **2000**, 7, 39-58.
140. Marco E., Laine W., Tardy C., Lansiaux A., Iwao M., Ishibashi F., Bailly C. and Gago F., Molecular determinants of topoisomerase I poisoning by Lamellarins: comparison with camptothecin and structure-activity relationship. *J. Med. Chem.,* **2005**, 48, 3796-3807.
141. Wang L.K., Rogers B.D. and Hecht S.M., Inhibition of topoisomerase I function by coralyne and 5,6-dyhyrocoralyne. *Chem. Res. Toxicol.,* **1996**, 9, 75-83.
142. McCledon A.K. and Osheroff N., DNA toposiomerase II, genotoxicity, and cancer. *Mut. Res.,* **2007**, 623, 83-97.
143. Burden D.A. and Osheroff N., Mechanism of action of eukaryotic topoisomerase II and drugs targeted to the enzyme. *Biochim. Biophys. Acta,* **1998**, 1400, 139-154.
144. Baldwin E.L. and Osheroff N., Etoposide, topoisomerase II and cancer. *Curr. Med. Chem.,* **2005**, 5, 363-372.
145. Fortune J.M. and Osheroff N., Merbarone inhibits the catalytic activity of human topoisomerase IIα by blocking DNA cleavage. *J. Biol. Chem.,* **1998**, 273, 17643-17650.
146. Felix C.A., Kolaris C.P. and Osheroff N., Topoisomerase II and the etiology of chromosomal translocations. *DNA Repair,* **2006**, 5, 1093-1108.
147. Dassonneville L., Wattez N., baldeyrou B., Mahieu C., Lansiaux A., Banaigs B., Bonnard I. and Bailly C., Inhibition of topoisomerase II by the marine alkaloid ascididemin and induction of apoptosis in leukaemia cells. *Biochem. Phamacol.,* **2000**, 60, 527-537.
148. Norden B. and Kurucsev T., Analysing DNA complexes by circular and linear dichroism. *J. Mol. Recognit.,* **1994**, 7, 141-156.
149. Lyng R., Hard T. and Norden B., Induced circular dichroism of DNA intercalators: electric dipole allowed transitions. *Biopolymers,* **1987**, 26, 1327-1345.
150. Norden B., Kubista M. and Kurucsev T., Linear dichroism spectroscopy of nucleic acids. *Q. Rev. Biophys.,* **1992**, 25, 51-170.
151. Scatchard G., The attraction of proteins for small molecules and ions. *Ann. N. Y. Acad. Sci.,* **1949**, 51, 660-672.

152. McGhee D. and vonHippelk P.H., Theoretical aspects of DNA-protein interactions: co-operative and non-co-operative binding of large ligands to a one-dimentional homogeneous lattice. *J. Mol. Biol.,* **1974**, 86, 469-489.
153. Bailly C., Tardy C., Wang L., Armitage B., Hopkins K., Kumar A., Schuster G.B., Boykin D.W. and Wilson W.D., Recognition of ATGA sequences by the unfused aromatic dication DB293 forming stacked dimmers in the DNA minor groove. *Biochemistry,* **2001**, 40, 9770-9779.
154. Crow S.D.G., Bailly C., Garbay-Jaureguiberry C., Roques B., Ramsay-Shaw B. and Waring M.J., DNA sequence recognition by the antitumor drug ditercalium.*Biochemistry,* **2002**, 41, 8672-8682.
155. Martin C., Ellis T., McGurk C.J., Jenkins T.C., Hartley J.A., Waring M.J. and Thurston D.E., Sequence-selective interaction of the minor-groove interstrand cross-linking agent SJG-136 with naked and cellular DNA: footprinting and enzyme inhibition studies. *Biochemistry,* **2005**, 4, 4135-4147.
156. Maxam A.M. and Gilbert W., Sequencing end-labeled DNA with base-specific chemical cleavages. *Methods Enzymol.,* **1980**, 65, 499-560.
157. Pflaum M., Haring M., Hegler J., Raudiger H.; Use of repair endonucleases to characterize DNA damage induced by reactive oxygen species in cellular and cell – free systems. *Toxicol. Lett*., **1993**, 67, 57-72.
158. Cadet J., Bourdat A.G., D'Ham C., Duarte V., Gasparutto D., Romieu A. and Ravanat J.L., Oxidative base damage to DNA: specificity of base excision repair enzymes. *Mutation Res.,* **2000**, 462, 121-128.
159. Mosmann T., Rapid colorimetric assay for cellular growth and survival: application to proliferation and cytotoxic assay. *J. Immunol. Meth.,* **1983**, 65, 55-63.
160. Potapenko A.Y., Mechanisms of photodynamic effects of furocoumarins, *Photochem. Photobiol.*, **1991**, 9, 1-33.
161. Pathak M.A., Fitzpatrick T.B., The evolution of photochemotherapy with psoralens and UVA (PUVA): 2000 BC to 1992 AD, *Photochem. Photobiol.*, **1992**, 14, 3-22.
162. Girotti A.W., Photodynamic lipid peroxidation in biological systems. *Photochem. Photobiol.,* **1990**, 51, 497-509.
163. Morlière P., Moysan A., Santus R., Hüppe G., Mazière J., Dubertret L., UVA-indeced lipid peroxidation in cultured human fibroblasts. *Biochem. Biophys. Acta,* **1991**, 1084, 261-268.

164. Kessel D., Luo Y., Mathieu P. and Reiners J.J.Jr., Determinants of the apoptotic response to lysosomal photodamage. *Photochem. Photobiol.,* **2000**, 71, 196-200.

165. Vermes I., Haanen C., Steffens-Nakken H. and Reutelingsperger C. A novel assay for apoptosis. Flow cytometric detection of phosphatidylserine expression on early apoptotic cells using fluorescein labelled Annexin V. *J. Immun. Method.,* **1995**, 184, 39-51.

166. Kluza J., Lansiaux A., Wattez N., Hildebrand M.P., Lèonce S., Pierrè A., Hickman J.A. and Bailly C. Induction of apoptosis in HL-60 leukemia and b-16 melanoma cells by the acronycine derivative S23906-1. *Biochem. Pharmacol.,* **2002**, 63, 1443-1452.

167. Verhoven B., Schlegel R.A. and Williamson P., Mechanisms of phosphatidylserine exposure, a phagocyte recognition signal, on apoptotic T lymphocytes. *J. Exp.Med.,* **1995**, 182, 1597-1601.

168. Salvioli S., Ardizzoni A., Franceschi C and Cossarizza A. JC-1, but not $DiOC_6(3)$ or rhodamine 123, is a reliable fluorescent probe to assess $\Delta\psi$ changes in intact cells: implications for studies on mitochondrial functionality during apoptosis. *FEBS Letters,* **1997**, 411, 77-82.

169. Cossarizza A., Baccarani Contri M., Kalashnikova G. and Franceschi C., A new method for the cytofluorimetric analysis of mitochondria membrane potential using the J-aggregate forming cation 5,5’,6,6’-tetrachloro-1,1’,3,3’-tetraethylbenzimidazolcarbocyanine iodide (JC-1). *Biochem. Biophys. Res. Comun.,* **1993**, 197, 40-45.

170. Thornberry N.A. and Lazebnik Y., Caspases: enemies within. *Science,* **1998**, 281, 1312-1316.

171. Kohler C., Orrenius S. and Zhivotovsky B. Evaluation of caspase activity in apoptotic cells. *J. Immunol. Meth.,* **2002**, 265, 97-110.

172. Fabbri F., Carloni S., Brigliadori G., Zoli W., Lapalombella R. and Marini M. Sequential events of apoptosis involving docetaxel, a microtubule-interfering agent: a cytometric study. *BMC Cell Biol.,* **2006**, 7:6.

173. Wada A. and Kozawa S., Instrument for studies of differential flow dichroism of polymer solutions. *J. Polym. Sci.: Part A,* **1964**, 2, 853-864.

174. Brown T., Taherbhai Z., Sexton J., Sutterfied A., Turlington M., Jones J., Stallings L., Stewart M., Buchnueller K., Mackay H., O’Hare C., Kluza J., Nguyen B.,

Wilson D., Lee M. And Hartley J.A. Synthesis and biophysical evaluation of minor-groove binding C-terminus modified pyrrole and imidazole triamide analogs of distamycin. *Bioorg. Med. Chem.,* **2007,** 15, 474-483.

175. Ciulla T.A., Van Camp J.R., Rosenfeld E., Kochevar I.E., Photosensitization of single-strand breaks in pBR322 DNA by rose Bengal. *Photochem. and Photobiol.*, **1989**, 49, 293-298.
176. Peterson G.L., A simplification of the protein assay method of Lowry et al. which is more generally applicable. *Analyt. Biochem.,* **1977**, 83, 346-356.
177. Lansiaux A., Tanious F., Mishal Z., Dassonneville L., Kumar A., Stephens C.E., Hu Q., Wilson W.D., Boykin D.W. and and Bailly C. Distribution of furamidine analogues in tumor cells: targeting of the nucleus or mitochondria depending on the amidine substitution. *Cancer Res.,* **2002**, 62, 7219–7229.
178. Bradford M.M., A rapid and sensitive method for the quantification of microgram quantities of protein-dye binding. *Anal. Biochem.,* **1976**, 72, 248-254.
179. Bridwell D.J.A., Finlay G.J. and Baguley B.C., Mechanism of cytotoxicity of N-[2-(dimethylamino)ethyl] acridine-4-carboxamide and of its 7-chloro derivative: the roles of topoisomerases I and II. *Cancer Chemother. Pharmacol.,* **1999**, 43, 302-308.

8. ACKOWNLEDGEMENTS

- Department of Pharmaceutical Science, University of Padova, Italy:

  Prof. Francesco Dall'Acqua
  Prof.ssa Daniela Vedaldi
  Dott.ssa Alessia Salvador

- Department of Pediatrics, University of Padova, Italy:

  Prof. Giuseppe Basso
  Dott.ssa Elena Fortunato

- Department of Organic Chemistry II, University of Siegen, Germany:

  Prof. Heiko Imhels
  Dott. Anton Granzhan

- Department of Oncology, Cancer Research UK Drug-DNA Interaction Research Group, Royal Free and University College Medical School, UCL, UK:

  Prof. John A. Hartley
  Dott. Jerome Kluza